

การสังเคราะห์และการตรึงพอลิเอไมด์นิวคลีอิกแอซิดบนผิวทอง



นางสาวจิรภรณ์ อนันต์ธนวัฒน์

สถาบันวิทยบริการ

จุฬาลงกรณ์มหาวิทยาลัย

วิทยานิพนธ์นี้เป็นส่วนหนึ่งของการศึกษาตามหลักสูตรปริญญาวิทยาศาสตรมหาบัณฑิต

สาขาปิโตรเคมีและวิทยาศาสตร์พอลิเมอร์

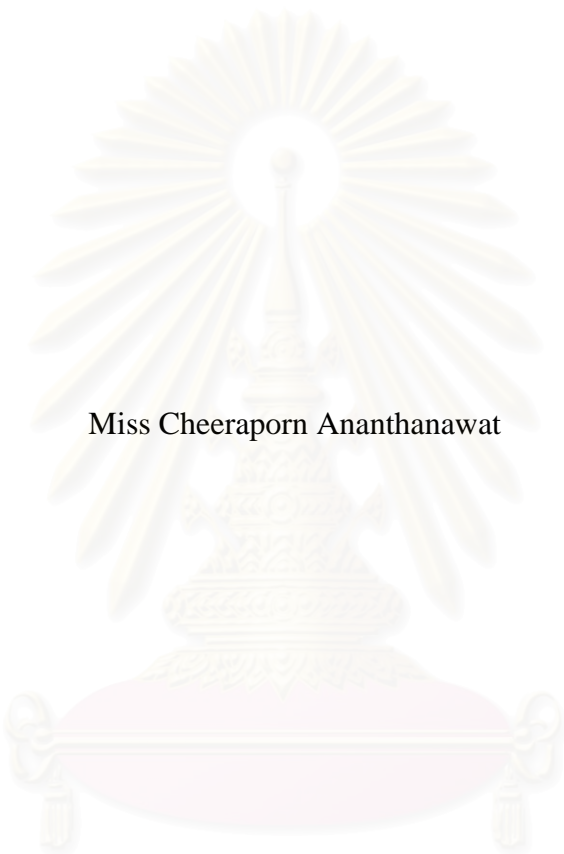
คณะวิทยาศาสตร์ จุฬาลงกรณ์มหาวิทยาลัย

ปีการศึกษา 2548

ISBN 974-14-2077-3

ลิขสิทธิ์ของจุฬาลงกรณ์มหาวิทยาลัย

SYNTHESIS AND ATTACHMENT OF POLYAMIDE NUCLEIC ACID  
ON GOLD SURFACE



Miss Cheeraporn Ananthanawat

สถาบันวิทยบริการ  
จุฬาลงกรณ์มหาวิทยาลัย

A Thesis Submitted in Partial Fulfillment of the Requirements

for the Degree of Master of Science Program in Petrochemistry and Polymer Science

Faculty of Science

Chulalongkorn University


Academic Year 2005

ISBN 974-14-2077-3

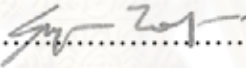
Thesis Title           SYNTHESIS AND ATTACHMENT OF POLYAMIDE  
                                  NUCLEIC ACID ON GOLD SURFACE  
By                         Miss Cheeraporn Ananthanawat  
Field of study         Petrochemistry and Polymer Science  
Thesis Advisor        Assistant Professor Voravee P. Hoven, Ph. D.  
Thesis Co-advisor   Associate Professor Tirayut Vilaivan, D. Phil

---

Accepted by the Faculty of Science, Chulalongkorn University in Partial  
Fulfillment of the Requirements for the Master's Degree

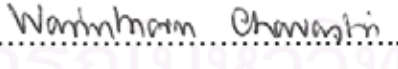
  
..... Dean of the Faculty of Science  
(Professor Piamsak Menasveta, Ph. D.)

Thesis Committee

  
..... Chairman  
(Associate Professor Supawan Tantayanon, Ph. D.)

  
..... Thesis Advisor  
(Assistant Professor Voravee P. Hoven, Ph. D.)

  
..... Thesis Co-advisor  
(Associate Professor Tirayut Vilaivan, D. Phil)

  
..... Member  
(Assistant Professor Warinthorn Chavasiri, Ph. D.)

  
..... Member  
(Assistant Professor Toemsak Srihirin, Ph. D.)

จรรยา อนันต์ธนวัฒน์ : การสังเคราะห์และการตรึงพอลิเอไมด์นิวคลีอิกแอซิดบนผิวทอง.  
(SYNTHESIS AND ATTACHMENT OF POLYAMIDE NUCLEIC ACID  
ON GOLD SURFACE) อ. ที่ปรึกษา : ผศ. ดร. วรวิทย์ โสเวน อ. ที่ปรึกษาร่วม : รศ. ดร.  
ธีรยุทธ วิไลวัลย์ 93 หน้า. ISBN 974-14-2077-3.

ในงานวิจัยนี้ได้ทำการสังเคราะห์พอลิเอไมด์นิวคลีอิกแอซิด (พีเอ็นเอ) ชนิดใหม่ที่มีการดัดแปลงให้มีหมู่ฟังก์ชันที่ปลายเป็นไทออลด้วยวิธีการสังเคราะห์เพปไทด์บนวัฏภาคของแข็งและทำการตรึงพีเอ็นเอที่สังเคราะห์ได้บนผิวควอตซ์คริสตัลที่เคลือบด้วยทองโดยอาศัยการสร้างโมเลกุลชั้นเดียวที่เกิดการเรียงตัวได้เองของสารประกอบไทออลผ่านซัลเฟอร์อะตอมสำหรับใช้ในการตรวจวัดการจับยึดกับดีเอ็นเอ ปริมาณของพีเอ็นเอที่ตรึงอยู่บนผิวทองและปริมาณการจับยึดของดีเอ็นเอกับพีเอ็นเอที่ผิวทองถูกวิเคราะห์ด้วยเทคนิคควอตซ์คริสตัล ไมโครบาลานซ์ (ควิซีเอ็ม) ซึ่งว่องไวต่อการเปลี่ยนแปลงมวลสารบนผิวทอง จากผลการทดลองแสดงให้เห็นว่าปริมาณของพีเอ็นเอที่ตรึงอยู่บนผิวทองจะเพิ่มขึ้นตามความเข้มข้นของสารละลายพีเอ็นเอที่ใช้ ขั้นตอนการบล็อกด้วยสเปซบล็อกกิงโมเลกุลมีความสำคัญอย่างมากต่อการเตรียมพื้นผิวที่จะสามารถนำไปตรวจวัดการจับยึดกับดีเอ็นเอได้ สภาวะที่เหมาะสมในการตรึงพีเอ็นเอ คือ การใช้สารละลายพีเอ็นเอเข้มข้น  $1.0 \mu\text{M}$  และเวลาที่ใช้ในการตรึงคือ 24 ชั่วโมง และสภาวะที่เหมาะสมที่ใช้ในการตรวจวัดการจับยึดกับดีเอ็นเอ คือ การใช้ดีเอ็นเอที่มีความเข้มข้น  $50 \mu\text{M}$  ในสารละลายโซเดียมฟอสเฟตบัฟเฟอร์ pH 7 เข้มข้น  $0.5 \text{ mM}$  และเวลาที่ใช้ในการจับยึด คือ 1 ชั่วโมง นอกจากนี้ได้ทำการศึกษาอิทธิพลของ pH และปริมาณเกลือที่มีต่อการจับยึดดังกล่าวอีกด้วย จากนั้นได้นำผิวทองที่ผ่านการตรึงพีเอ็นเอไปตรวจวัดการจับยึดกับดีเอ็นเอที่มีลำดับเบสที่เป็นเบสคู่สม โดยสมบูรณ์และดีเอ็นเอที่มีลำดับเบสผิดไปที่ไม่ใช่เบสคู่สมเพื่อศึกษาความจำเพาะเจาะจงในการจับยึด จากผลของควิซีเอ็ม แสดงให้เห็นว่าความสามารถในการจับยึดของพีเอ็นเอที่ถูกตรึงอยู่บนผิวทองกับดีเอ็นเอเป้าหมายจะขึ้นอยู่กับชนิดของนิวคลีโอเบสของพีเอ็นเอและดีเอ็นเอเป็นสำคัญ และการนำพีเอ็นเอมาประยุกต์ใช้งานร่วมกับเทคนิคควิซีเอ็มสามารถบอกความแตกต่างของการจับยึดกับดีเอ็นเอที่มีลำดับเบสผิดไปเพียงตำแหน่งเดียวได้

สาขาวิชา ปิโตรเคมีและวิทยาศาสตร์พอลิเมอร์ ลายมือชื่อนิสิต.....จรรยา อนันต์ธนวัฒน์.....  
ปีการศึกษา.....2548..... ลายมือชื่ออาจารย์ที่ปรึกษา.....  
ลายมือชื่ออาจารย์ที่ปรึกษาร่วม.....

## 4772246723 : MAJOR PETROCHEMISTRY AND POLYMER SCIENCE

KEY WORD: POLYAMIDE NUCLEIC ACID / PNA / QCM / SELF ASSEMBLY MONOLAYER / DNA

CHEERAPORN ANANTHANAWAT : SYNTHESIS AND ATTACHMENT OF POLYAMIDE NUCLEIC ACID ON GOLD SURFACE. THESIS ADVISOR : ASSIST. PROF. VORAVEE P. HOVEN, Ph.D. THESIS CO-ADVISOR : ASSOC. PROF. TIRAYUT VILAIVAN, D. Phil 93 pp. ISBN 974-14-2077-3

Two novel thiol-modified polyamide nucleic acids (PNA) were synthesized by solid phase peptide synthesis and directly attached on gold coated quartz crystals by self assembly monolayer (SAM) formation via S atom for detection of DNA hybridization. The amount of immobilized PNA and the extent of DNA hybridization were detected by quartz crystal microbalance (QCM) which is an extremely sensitive mass sensor. From the result, it can be demonstrated that the amount of immobilized PNA on the gold electrode increased with the PNA concentration. The blocking step is critical to the success of subsequent DNA hybridization. The optimal immobilization condition is PNA concentration: 1.0  $\mu\text{M}$  and immobilization time: 24 h and the optimal hybridization condition is DNA concentration: 50  $\mu\text{M}$ , sodium phosphate buffer pH 7 concentration: 0.5 mM and hybridization time: 1 h. Moreover, the effect of pH and ionic strength were also investigated. Hybridization of immobilized PNA with perfect matched and mismatched DNA sequences were observed to determine the specificity of hybridization. The QCM results indicated that the binding affinity of PNA immobilized on the gold surface with target DNA is extremely dependent on the nucleobases of PNA and DNA. Finally, single mismatch discrimination has been achieved by a combination of PNA with QCM technique.

Field of study Petrochemistry and Polymer Science Student's signature.....*Cher Ant.*.....  
 Academic year .....2005..... Advisor's signature.....*Vp. Hoven.*.....  
 Co-advisor's signature.....*Tirayut Main*.....

## ACKNOWLEDGEMENTS

I wish to thank and express my deepest gratitude to my advisor, Assistant Professor Voravee P. Hoven and my co-advisor, Associate Professor Dr. Tirayut Vilaivan, for kindness, guidance, suggestions, financial support and assistance throughout the course of this research.

I am sincerely grateful to the members of the thesis committee: Associate Professor Supawan Tantayanon, Assistant Professor Warinthorn Chavasiri and Assistant Professor Toemsak Srikhirin for their comments, suggestions and time to read thesis.

I would like to thank Mr. Chaturong Suparpprom, Mrs. Choladda Srisuwannaket and Miss Patcharee Ngamviriyavong for some synthesis intermediate compounds and starting materials.

The Research Fund from Organic Synthesis Research Unit (Faculty of Science, Chulalongkorn University), National Research Council of Thailand and National Nanotechnology Center are gratefully acknowledged. Gold sputtering facility and contact angle goniometer provided by the National Material and Metal Technology Center (MTEC) are greatly appreciated.

Many thanks go to all OSRU members for their assistance and suggestions concerning experimental techniques during my thesis work.

Finally, I would like to thank my parents who had encouraged me with sincere, my family for their moral support throughout the research and my best friends for their love, understanding, encouragement and social support.

สถาบันวิทยบริการ  
จุฬาลงกรณ์มหาวิทยาลัย

## CONTENT

	page
Abstract in Thai.....	iv
Abstract in English.....	v
Acknowledgements.....	vi
List of Tables.....	x
List of Figures.....	xi
List of Schemes.....	xvii
List of Abbreviations.....	xviii
CHAPTER I INTRODUCTION.....	1
1.1 Polyamide nucleic acid (PNA).....	1
1.2 Immobilization of nucleic acids on gold surface.....	3
1.3 Piezoelectric Biosensor.....	6
1.4 Objectives of this research.....	8
CHAPTER II EXPERIMENTAL SECTION.....	9
2.1 General Procedure.....	9
2.1.1 Materials.....	9
2.1.2 Methods.....	9
2.2 Experimental procedure.....	10
2.2.1 Synthesis of intermediate.....	10
2.2.2 Synthesis of activated PNA monomers.....	11
(a) Thymine (T) monomer.....	11
(b) Guanine (G) monomer.....	13
(c) Adenine (A) monomer.....	15
(d) Cytosine (C) monomer.....	16
2.2.3 Synthesis of Spacer.....	18
2.2.4 Synthesis of S-protected thiols.....	20
2.2.5 Synthesis of thiol-modified PNA oligomer.....	21

(a) Preparation of the reaction pipette and apparatus for solid phase peptide synthesis.....	21
(b) Solid phase peptide synthesis .....	22
2.2.6 Biophysical studies of thiol-modified PNA nonamer in solution.....	26
(a) $T_m$ experiments.....	26
2.2.7 Immobilization and hybridization with target DNA of thiol-modified PNA nonamer on gold surface.....	26
(a) QCM measurement.....	27
(b) AFM analysis.....	28
(c) RAIRS analysis.....	28
(d) Water contact angle analysis.....	28
CHAPTER III RESULTS AND DISCUSSION.....	30
3.1 Synthesis of activated PNA monomers.....	30
3.2 Synthesis of spacer.....	34
3.3 Synthesis of S-protected thiols.....	35
3.4 Synthesis of thiol-modified PNA nonamer by solid phase peptide synthesis.....	36
3.5 Biophysical studies of thiol-modified PNA nonamer in solution.....	48
3.5.1 $T_m$ experiments.....	48
3.6 Immobilization of thiol-modified PNA nonamer on gold surface...	54
3.6.1 QCM analysis.....	54
3.6.2 AFM analysis.....	55
3.6.3 RAIRS analysis.....	56
3.6.4 Water contact angle analysis.....	58
3.7 Hybridization of thiol-modified PNA nonamer on gold surface with target DNA.....	58
3.7.1 QCM experiments.....	58
(a) Immobilization procedures.....	58
(b) Optimal hybridization condition.....	60
(c) Optimal immobilization condition.....	63
(d) Effect of pH.....	65
(e) Effect of ionic strength.....	66



(f) Specificity of DNA hybridization reaction.....	67
CHAPTER IV CONCLUSION.....	72
REFERENCES.....	74
APPENDIX A.....	80
APPENDIX B.....	85
VITAE.....	93



สถาบันวิทยบริการ  
จุฬาลงกรณ์มหาวิทยาลัย

## LIST OF TABLES

	page
Table 3.1 Deprotection of Dpm and Boc protecting groups.....	30
Table 3.2 Protection of Fmoc.....	31
Table 3.3 Activation of PNA monomers by Pfp ester.....	32
Table 3.4 Percent coupling efficiency, $t_R$ and mass spectral data of the two thiol-modified PNA nonamers ( <b>33</b> and <b>35</b> ).....	48
Table 3.5 $T_m$ values of hybrids between thiol-modified PNA nonamer and oligonucleotides.....	54
Table A1 Data from UV analysis of HS(CH <sub>2</sub> ) <sub>2</sub> CO-T <sub>9</sub> -LysNH <sub>2</sub> ( <b>33</b> ) & dA <sub>9</sub> at 20.0-90.0 °C.....	81


  
 สถาบันวิทยบริการ  
 จุฬาลงกรณ์มหาวิทยาลัย

## LIST OF FIGURES

	page
Figure 1.1 Structures of PNA and DNA.....	1
Figure 1.2 Chemical structures of a PNA molecule and a DNA molecule.....	2
Figure 1.3 Structure of (a) (1 <i>S</i> , 2 <i>S</i> )-ACPC PNA or Vilaivan's PNA and (b) Nielsen's PNA.....	3
Figure 1.4 Strategy for indirect immobilization of nucleic acid on gold surface.....	4
Figure 1.5 Strategy for direct immobilization of nucleic acid on gold surface.....	4
Figure 2.1 Schematic representation of the manual technique for solid phase peptide synthesis; (a) coupling, deprotecting and cleaving process; (b) washing process.....	22
Figure 3.1 Reaction mechanism for the protection of N-atom with Fmoc group .....	32
Figure 3.2 Reaction mechanism for the protection of the Fmoc free acid with Pfp .....	33
Figure 3.3 Structure of Fmoc Pfp ester derivative monomers ( <b>12</b> , <b>15</b> , <b>18</b> and <b>21</b> ) for solid phase peptide synthesis.....	34
Figure 3.4 Synthesis of Fmoc-ACPC-Pfp spacer ( <b>28</b> ).....	35
Figure 3.5 Reaction mechanism for the protection of the S atom with Dpm....	36
Figure 3.6 The protocol for solid phase peptide synthesis of thiol-modified PNA nonamer.....	38
Figure 3.7 TentaGel S RAM Fmoc resin.....	38
Figure 3.8 Mechanism for deprotection of Fmoc protecting group from resin bound peptide.....	39
Figure 3.9 The mechanism for coupling of anchoring via HOAt activation....	40
Figure 3.10 The mechanism for capping of the unreacted amino group residue with 10% lauroyl chloride/DIEA in DMF.....	41
Figure 3.11 The mechanism for coupling of S-protected thiol via HATU activation .....	42

Figure 3.12 The mechanism for cleavage the thiol-modified PNA nonamer from the resin and deprotection at S-atom by treatment with 10% anisole in trifluoroacetic acid.....	44
Figure 3.13 Chromatogram of HS(CH <sub>2</sub> ) <sub>2</sub> CO-T <sub>9</sub> -LysNH <sub>2</sub> ( <b>33</b> ): (a) before and (b) after purification by reverse phase HPLC.....	45
Figure 3.14 Chromatogram of HS(CH <sub>2</sub> ) <sub>2</sub> CO-TTCTATGTT-LysNH <sub>2</sub> ( <b>35</b> ): (a) before and (b) after purification by reverse phase HPLC.....	46
Figure 3.15 MALDI-TOF mass spectra of (a) HS(CH <sub>2</sub> ) <sub>2</sub> CO-T <sub>9</sub> -LysNH <sub>2</sub> ( <b>33</b> ) and (b) HS(CH <sub>2</sub> ) <sub>2</sub> CO-TTCTATGTT-LysNH <sub>2</sub> ( <b>35</b> ) after purification by reverse phase HPLC.....	47
Figure 3.16 The UV absorbance of single stranded DNA and double helical DNA.....	49
Figure 3.17 The UV absorbance of <i>T<sub>m</sub></i> experiment.....	50
Figure 3.18 Melting curves of HS(CH <sub>2</sub> ) <sub>2</sub> CO-T <sub>9</sub> -LysNH <sub>2</sub> ( <b>33</b> ) with d(5'-AAA AAAAAA-3') or dA <sub>9</sub> (perfect match), d(5'-AAAAXAAAA-3') (single mismatch, X = T, C and G) and d(5'-AAAXAXAAA-3') (double mismatch, X = T, C and G). The <i>T<sub>m</sub></i> was measured at molar ratio of PNA : DNA = 1:1; concentration of PNA strand = 1 μM; 0.5 mM sodium phosphate buffer pH 7; heating rate 1 °C/min.....	51
Figure 3.19 Melting curves of HS(CH <sub>2</sub> ) <sub>2</sub> CO-T <sub>9</sub> -LysNH <sub>2</sub> ( <b>33</b> ) with dA <sub>9</sub> (perfect match). The <i>T<sub>m</sub></i> was measured at a ratio of PNA : DNA = 1:1; concentration of PNA strand = 1 μM; 0.5 mM sodium phosphate buffer pH 6, 7 and 8; heating rate 1 °C/min.....	52
Figure 3.20 Melting curves of HS(CH <sub>2</sub> ) <sub>2</sub> CO-T <sub>9</sub> -LysNH <sub>2</sub> ( <b>33</b> ) with dA <sub>9</sub> (perfect match). The <i>T<sub>m</sub></i> was measured at a ratio of PNA : DNA = 1:1; concentration of PNA strand = 1 μM; 0.5 mM sodium phosphate buffer pH 7 + 0, 1 and 10 mM NaCl; heating rate 1 °C/min.....	52

Figure 3.21 Melting curves of HS(CH <sub>2</sub> ) <sub>2</sub> CO-TTCTATGTT-LysNH <sub>2</sub> ( <b>35</b> ) with d(5'-AACATAGAA-3') (perfect match), d(5'-AACAXA GAA-3') (single mismatch, X = G, A and C) and dA <sub>9</sub> (triple mismatch). The <i>T<sub>m</sub></i> was measured at a ratio of PNA : DNA = 1:1; concentration of PNA strand = 1 μM; 0.5 mM sodium phosphate buffer pH 7; heating rate 1 °C/min.....	53
Figure 3.22 ΔF <sub>i</sub> obtained upon increasing the PNA HS(CH <sub>2</sub> ) <sub>2</sub> CO-T <sub>9</sub> -Lys NH <sub>2</sub> ( <b>33</b> ) concentration. ....	55
Figure 3.23 AFM images of (a) bare gold surface (b) HS(CH <sub>2</sub> ) <sub>2</sub> CO-T <sub>9</sub> -Lys NH <sub>2</sub> ( <b>33</b> ) PNA immobilized on gold surface for 24 h using PNA concentration of 5.0 μM .....	56
Figure 3.24 IR (KBr method) spectrum of HS(CH <sub>2</sub> ) <sub>2</sub> CO-T <sub>9</sub> -LysNH <sub>2</sub> ( <b>33</b> ) PNA.....	57
Figure 3.25 RAIRS spectra of HS(CH <sub>2</sub> ) <sub>2</sub> CO-T <sub>9</sub> -LysNH <sub>2</sub> ( <b>33</b> ) PNA on gold surface obtained by increasing PNA concentration: (a) 1.0 μM and (b) 5.0 μM at immobilization time of 24 h.....	57
Figure 3.26 ΔF <sub>h</sub> obtained from hybridization reaction between surface-immobilized HS(CH <sub>2</sub> ) <sub>2</sub> CO-T <sub>9</sub> -LysNH <sub>2</sub> ( <b>33</b> ) PNA prepared by procedure I, II and III with complementary DNA (dA <sub>9</sub> ).....	59
Figure 3.27 AFM images of HS(CH <sub>2</sub> ) <sub>2</sub> CO-T <sub>9</sub> -LysNH <sub>2</sub> ( <b>33</b> ) PNA immobilized on gold surface for 24 h using PNA concentration of 5.0 μM. (a) before blocking step and (b) after blocking step with 1.0 mM mercaptoethanol.....	60
Figure 3.28 ΔF <sub>h</sub> obtained from hybridization reaction between surface-immobilized HS(CH <sub>2</sub> ) <sub>2</sub> CO-T <sub>9</sub> -LysNH <sub>2</sub> ( <b>33</b> ) PNA with complementary DNA (dA <sub>9</sub> ) under different sodium phosphate buffer concentrations.....	61
Figure 3.29 ΔF <sub>h</sub> obtained from hybridization reaction between surface-immobilized HS(CH <sub>2</sub> ) <sub>2</sub> CO-T <sub>9</sub> -LysNH <sub>2</sub> ( <b>33</b> ) PNA with complementary DNA (dA <sub>9</sub> ) under different DNA concentrations.....	62

Figure 3.30 $\Delta F_h$ obtained from hybridization reaction between surface-immobilized $\text{HS}(\text{CH}_2)_2\text{CO-T}_9\text{-LysNH}_2$ ( <b>33</b> ) PNA with complementary DNA ( $\text{dA}_9$ ) under different hybridization times.....	63
Figure 3.31 $\Delta F_h$ obtained from hybridization reaction between surface-immobilized $\text{HS}(\text{CH}_2)_2\text{CO-T}_9\text{-LysNH}_2$ ( <b>33</b> ) PNA with complementary DNA ( $\text{dA}_9$ ) under different PNA concentration.....	64
Figure 3.32 $\Delta F_h$ obtained from hybridization reaction between surface-immobilized $\text{HS}(\text{CH}_2)_2\text{CO-T}_9\text{-LysNH}_2$ ( <b>33</b> ) PNA with complementary DNA ( $\text{dA}_9$ ) under different immobilization times.....	65
Figure 3.33 $\Delta F_h$ obtained from hybridization reaction between surface-immobilized $\text{HS}(\text{CH}_2)_2\text{CO-T}_9\text{-LysNH}_2$ ( <b>33</b> ) PNA with complementary DNA ( $\text{dA}_9$ ) under different pH.....	66
Figure 3.34 $\Delta F_h$ obtained from hybridization reaction between surface-immobilized $\text{HS}(\text{CH}_2)_2\text{CO-T}_9\text{-LysNH}_2$ ( <b>33</b> ) PNA with complementary DNA ( $\text{dA}_9$ ) under different NaCl concentration.....	67
Figure 3.35 $\Delta F_h$ obtained from hybridization reaction between surface-immobilized $\text{HS}(\text{CH}_2)_2\text{CO-T}_9\text{-LysNH}_2$ ( <b>33</b> ) PNA with $\text{dA}_9$ (perfect match), $\text{d}(5'\text{-AAAAT} \underline{\text{T}}$ $\text{AAAA-3'})$ (single mismatch), $\text{d}(5'\text{-AAAT} \underline{\text{TAT}}$ $\text{AAA-3'})$ (double mismatch), $\text{d}(5'\text{-AAT} \underline{\text{ATA}}$ $\underline{\text{TAA-3'})}$ and $\text{d}(5'\text{-AACAT} \underline{\text{AGAA-3'})}$ (triple mismatch).....	68
Figure 3.36 $\Delta F_h$ obtained from hybridization reaction between surface-immobilized $\text{HS}(\text{CH}_2)_2\text{CO-T}_9\text{-LysNH}_2$ ( <b>33</b> ) PNA with $\text{dA}_9$ (perfect match), $\text{d}(5'\text{-AAAAX} \underline{\text{X}}$ $\text{AAAA-3'})$ (single mismatch, X = T, C and G) and $\text{d}(5'\text{-AAAX} \underline{\text{AX}}$ $\underline{\text{AAA-3'})}$ (double mismatch, X = T, C and G).....	69

Figure 3.37 $\Delta F_h$ obtained from hybridization reaction between surface-immobilized HS(CH <sub>2</sub> ) <sub>2</sub> CO-TTCTATGTT-LysNH <sub>2</sub> ( <b>35</b> ) PNA with d(5'-AACATAGAA-3') (perfect match), d(5'-AACAXA GAA-3') (single mismatch, X = A, C and G) and dA <sub>9</sub> (triple mismatch).....	70
Figure 3.38 $\Delta F_h$ obtained from hybridization reaction between surface-immobilized HS(CH <sub>2</sub> ) <sub>2</sub> CO-T <sub>9</sub> -LysNH <sub>2</sub> ( <b>33</b> ) PNA and HS(CH <sub>2</sub> ) <sub>2</sub> CO-TTCTATGTT-LysNH <sub>2</sub> ( <b>35</b> ) PNA with dA <sub>9</sub> and d(5'-AACATAGAA-3').....	71
Figure A1 (a) Melting curve and (b) UV- $T_m$ first derivative curve of HS(CH <sub>2</sub> ) <sub>2</sub> CO-T <sub>9</sub> -LysNH <sub>2</sub> ( <b>33</b> ) with dA <sub>9</sub> . Condition: 0.5 mM sodium phosphate buffer pH 7 and molar ratio of PNA : DNA = 1:1.....	84
Figure B1 <sup>1</sup> H NMR spectrum (400 MHz, DMSO- <i>d</i> <sub>6</sub> ) of <i>N</i> -fluoren-9-ylmethoxycarbonylamino- <i>cis</i> -4-(thymine-1-yl)-D-proline ( <b>11</b> ).....	86
Figure B2 <sup>1</sup> H NMR spectrum (400 MHz, DMSO- <i>d</i> <sub>6</sub> ) of <i>N</i> -fluoren-9-ylmethoxycarbonylamino- <i>cis</i> -4-(thymine-1-yl)-D-proline pentafluorophenyl ester ( <b>12</b> ).....	86
Figure B3 <sup>1</sup> H NMR spectrum (400 MHz, DMSO- <i>d</i> <sub>6</sub> + 1 drop TFA) of <i>N</i> -fluoren-9-ylmethoxycarbonylamino- <i>cis</i> -4-( <i>N</i> <sup>2</sup> -isobutyryl guanine-9-yl)-D-proline ( <b>14</b> ).....	87
Figure B4 <sup>1</sup> H NMR spectrum (400 MHz, DMSO- <i>d</i> <sub>6</sub> ) of <i>N</i> -fluoren-9-ylmethoxycarbonylamino- <i>cis</i> -4-( <i>N</i> <sup>4</sup> -benzoyladenine-9-yl)-D-proline ( <b>17</b> ).....	87
Figure B5 <sup>1</sup> H NMR spectrum (400 MHz, CDCl <sub>3</sub> ) of <i>N</i> -fluoren-9- <i>cis</i> -4-( <i>N</i> <sup>4</sup> -benzoyladenine-9-yl)-D-proline pentafluorophenyl ester ( <b>18</b> ).....	88
Figure B6 <sup>1</sup> H NMR spectrum (400 MHz, DMSO- <i>d</i> <sub>6</sub> ) of <i>N</i> -fluoren-9-ylmethoxycarbonylamino- <i>cis</i> -4-( <i>N</i> <sup>4</sup> -benzocytosine-1-yl)-D-proline ( <b>20</b> ).....	88
Figure B7 <sup>1</sup> H NMR spectrum (400 MHz, CDCl <sub>3</sub> ) of ethyl (1 <i>S</i> , 2 <i>S</i> )-2-[(1' <i>S</i> )-phenylethyl]-aminocyclopentanecarboxylate ( <b>24</b> ).....	89

Figure B8 $^1\text{H}$ NMR spectrum (400 MHz, $\text{DMSO-}d_6$ ) of <i>N</i> -fluoren-9-ylmethoxycarbonyl-2-amino-cyclopentane carboxylic acid ( <b>27</b> ).....	89
Figure B9 $^1\text{H}$ NMR spectrum (400 MHz, $\text{CDCl}_3$ ) of <i>N</i> -fluoren-9-ylmethoxycarbonyl-2-aminocyclopentane carboxylic acid pentafluorophenyl ester ( <b>28</b> ).....	90
Figure B10 $^1\text{H}$ NMR spectrum (400 MHz, $\text{CDCl}_3$ ) of 3-benzhydrylthio-propionic acid ( <b>30</b> ).....	90
Figure B11 $^{13}\text{C}$ NMR spectrum (100 MHz, $\text{CDCl}_3$ ) of 3-benzhydrylthio-propionic acid ( <b>30</b> ).....	91
Figure B12 $^1\text{H}$ NMR spectrum (400 MHz, $\text{CDCl}_3$ ) of 11-benzhydrylthio-undecanoic acid ( <b>32</b> ).....	91
Figure B13 $^{13}\text{C}$ NMR spectrum (100 MHz, $\text{CDCl}_3$ ) of 11-benzhydrylthio-undecanoic acid ( <b>32</b> ).....	92



**LIST OF SCHEMES**

	page
Scheme 1 Synthesis of proline derivatives modified with nucleobases.....	11



สถาบันวิทยบริการ  
จุฬาลงกรณ์มหาวิทยาลัย

## LIST OF ABBREVIATIONS

A	adenine
A <sup>Bz</sup>	N <sup>4</sup> -benzoyladenine
Abs	absorbance
ACPC	D-prolyl-2-aminocyclopentane-carboxylic acid
AFM	atomic force microscopy
B	nucleobase
Boc	<i>tert</i> -butoxycarbonyl
br	broad
Bz	benzoyl
c	concentration
C	cytosine
°C	degree celcius
calcd	calculated
C <sup>Bz</sup>	N <sup>4</sup> -benzoylcytosine
CCA	$\alpha$ -cyano-4-hydroxy cinnamic acid
CDCl <sub>3</sub>	deuterated chloroform
CH <sub>3</sub> CN	acetonitrile
d	doublet
DIAD	diisopropylazodicarboxylate
DIEA	<i>N, N'</i> -dimethylaminopyridine
DMF	<i>N, N'</i> -dimethylformamide
DMSO- <i>d</i> <sub>6</sub>	deuterated dimethylsulfoxide
DNA	deoxyribonucleic acid
Dpm	diphenylmethyl
EDC	1-ethyl-3-(3-dimethylaminopropyl)-carbodiimide hydrochloride
EtOAc	ethyl acetate
f	frequency
Fmoc	9-fluorenylmethoxycarbonyl
FmocOSu	9-fluorenylmethyl <i>N</i> -succimidyl carbonate
FT-IR	fourier transform infrared spectroscopy
g	gram

G	guanine
G <sup>Ibu</sup>	<i>N</i> <sup>2</sup> -isobutyrylgaunine
h	hour
H	proton
HATU	O-(7-azabenzotriazol-1-yl)- <i>N, N, N', N'</i> -tetramethyluronium hexafluorophosphate
HOAt	1-hydroxy-7-azabenzotriazole
HPLC	high performance liquid chromatography
Hz	hertz
Ibu	isobutyryl
IR	infrared spectroscopy
<i>J</i>	coupling constant
KBr	potassium bromide
KHz	kilohertz
Lys	lysine
m	multiplet
MALDI-TOF	matrix-assisted laser desorption/ionization-time of flight
mg	milligram
MHz	megahertz
min	minute
mL	milliliter
mmol	millimole
mm	millimeter
mp.	melting point
NHS	<i>N</i> -hydroxysuccinimide
nm	nanometer
NMR	nuclear magnetic resonance
Pfp	pentafluorophenyl
PfpOTfa	pentafluorophenyl trifluoroacetic acid
Ph	phenyl
PNA	polyamide nucleic acid or peptide nucleic acid
ppm	part per million
QCM	quartz crystal microbalance
RAIRS	reflection absorption infrared spectroscopy

s	singlet
SAM	self assembly monolayer
SPPS	solid phase peptide synthesis
STM	scanning tunneling microscopy
t	triplet
T	thymine
T <sup>Bz</sup>	N <sup>3</sup> -benzoylthymine
TFA	trifluoroacetic acid
THF	tetrahydrofuran
TLC	thin layer chromatography
T <sub>m</sub>	melting temperature
t <sub>R</sub>	retention time
v	volume
UV	ultraviolet
XPS	X-ray photoelectron spectroscopy
μL	microliter
μm	micrometer
μmol	micromole
δ	chemical shift



สถาบันวิทยบริการ  
จุฬาลงกรณ์มหาวิทยาลัย

## CHAPTER I

### INTRODUCTION

#### 1.1 Polyamide nucleic acid (PNA)

Polyamide nucleic acid or peptide nucleic acid (PNA) is a DNA analogue originally introduced by Nielson et al. in 1991.[1] PNAs consist of repeating *N*-(2-aminoethyl)-glycine units linked together by amide bonds. The purine (Adenine: A, Guanine: G) and pyrimidine (Cytosine: C, Thymine: T) bases are attached to the backbone by methylene carbonyl linkages (**Figure 1.1**). Unlike DNA or RNA analogs, PNAs do not contain any (pentose) sugar moieties or phosphate groups. Besides the obvious structural difference, PNA is set apart from DNA in that the backbone of PNA is acyclic, achiral, and electrically neutral.

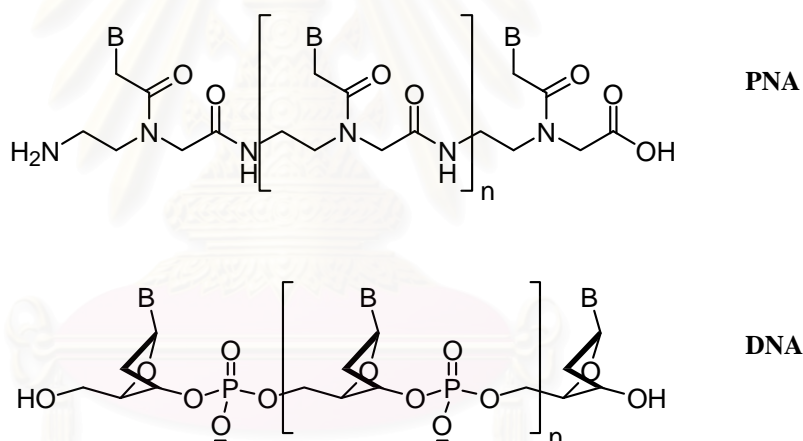


**Figure 1.1** Structures of PNA and DNA; B = nucleobase

The neutral character of the PNA backbone resulted in a stronger binding between complementary PNA·DNA strands than between complementary DNA·DNA strands at low to medium ionic strength. This is attributed to the lack of charge repulsion between the PNA strand and the DNA strand. Interestingly, not only is the affinity higher for PNA·DNA duplexes, but the specificity was also found to be higher. The Watson-Crick base pairing rules are strictly followed in the hybridization between PNA and nucleic acids (**Figure 1.2**). Furthermore, a mismatch in a

PNA·DNA duplex is generally more destabilizing than a mismatch in a DNA·DNA duplex.[2]

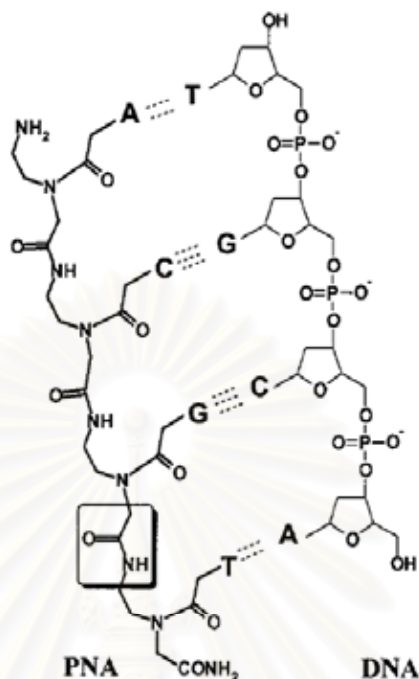


**Figure 1.2** Chemical structures of a PNA molecule and a DNA molecule. The amide (peptide) bond characteristic of PNA is boxed in.

These favorable properties of PNA have attracted wide attention in medicinal chemistry for development of gene therapeutic (antisense and antigene) drugs[3] and in biotechnology for development of diagnostic tools,[4] especially nucleic acid biosensor. The success of PNA have attracted much attention from many research groups to search for alternative structures which may behave similar to PNA or even have extra features currently not present or remained to be developed in Nielsen's PNA such as solubility, ability to penetrate cell membranes, and specific direction of binding.

In 2005, Vilaivan and his colleagues have reported synthesis of a novel conformationally rigid pyrrolidiny PNA based on D-prolyl-2-aminocyclopentane-carboxylic acid (ACPC) backbones. They reported that the stereochemistry of the backbone is very important in determining the binding properties. Only the PNA containing (1*S*, 2*S*)-ACPC (**Figure 1.3a**) can form a very stable 1:1 complex with the complementary DNA in a sequence-specific manner. In addition, thymine decamer (1*S*, 2*S*)-ACPC PNA can bind to the complementary DNA with a higher affinity than Nielsen's PNA (**Figure 1.3b**).[5]

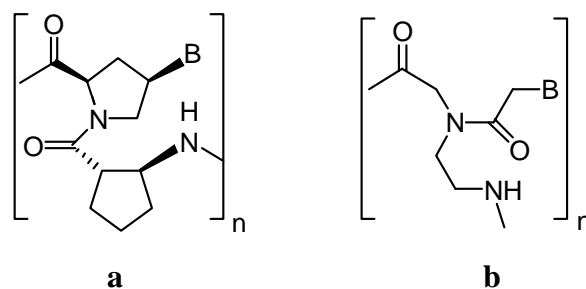


**Figure 1.3** Structures of (a) (1*S*, 2*S*)-ACPC PNA or Vilaiwan's PNA and (b) Nielsen's PNA

## 1.2 Immobilization of nucleic acids on gold surface

Highly stable molecular layers prepared by the self-assembling method have been applied for the development of various detection systems such as electrochemical detection, optical detection, and so on. Self-assembled monolayers (SAMs) are crystalline chemisorbed organic single layers formed on a solid substrate by spontaneous organization of molecules. Thiol compounds and gold is one of the well-established combination.[6]

Self-assembling process of thiol compounds on gold is initiated by the strong chemical interactions between the sulfur and the gold surface. This interaction is considered as a result of chemisorption that forces a thiolate molecule to adsorb commensurate with a gold lattice. Then, the tail-to-tail interaction of the molecules created by lateral interchain, nonbonded interactions, such as by van der Waals, steric, repulsive, and electrostatic forces, are strong enough to align the molecules parallel on the gold surface and create a crystalline film.[6,7] In this technique, the solid substrate is simply dipped into a solution containing the adsorbing molecules. Therefore, the packing and ordering of molecules is controlled by a chemisorption mechanism. The adsorption to the surface has been shown to proceed by two mechanisms, (1) ionic dissociation and more favourably by (2) radical formation.[8]



In most cases, organic disulfides, thiols and sulfides have been utilized for the preparation of stable SAMs on the gold surfaces.

The mechanism of the self assembling process of various alkylthiols and the orientation of the molecular layer on a gold surface have been investigated thoroughly by using Fourier transform infrared spectroscopy (FT-IR),[9] scanning tunneling microscopy (STM),[6] atomic force microscopy (AFM),[10] X-ray photoelectron spectroscopy (XPS),[11,12] electro-chemistry,[13] Raman spectroscopy,[14] ellipsometry,[15,16] and quartz crystal microbalance (QCM).[17,18]

For the development of nucleic acid SAMs for biosensor applications, thiols have proven to be the functional group of choice in the formation of SAMs. One method uses an indirect approach to immobilize nucleic acid on a gold surface, where a thiol containing a functional end-group like a carboxylic acid group is used to build a SAM. The nucleic acid is then attached to this SAM via an amide bond by using coupling reagents like 1-ethyl-3-(3-dimethylaminopropyl)-carbodiimide hydrochloride (EDC) and *N*-hydroxysuccinimide (NHS) (**Figure 1.4**).[19]

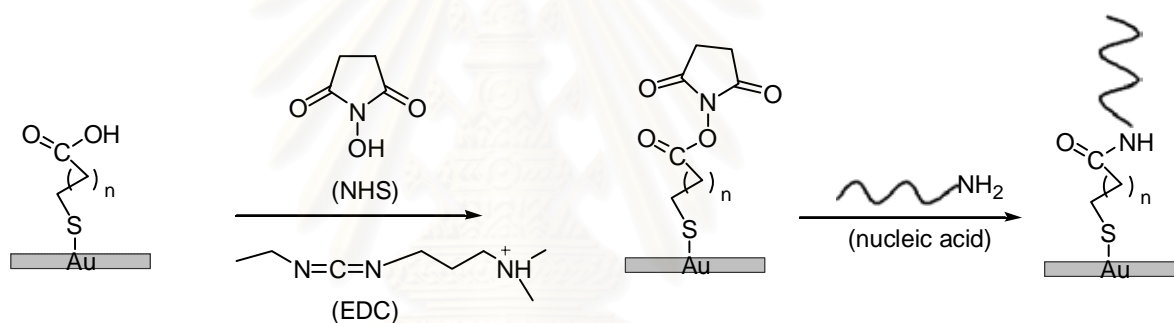


**Figure 1.4** Strategy for indirect immobilization of nucleic acid on gold surface

Another approach, later referred to as a direct immobilization, uses thiol-modified nucleic acid (**Figure 1.5**).[20-23] In this case, the nucleic acid molecule can be directly immobilized onto a gold surface by SAM formation via S atom. In a second step, the remaining surface of the biosensor is covered with a layer of another thiol molecule in order to prevent the nucleic acid from associating and non-specifically binding to the gold surface.

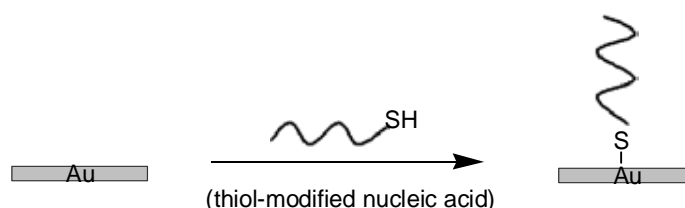


**Figure 1.5** Strategy for direct immobilization of nucleic acid on gold surface



The ability to attach nucleic acid directly in a single step not only makes the process more convenient and reduces time required but also offers enormous flexibility of tailoring the density of nucleic acid.

In 2003, Feldner and co-workers[24] have studied two different processes for immobilizing Nielsen's PNA via thiols on gold surface. The process of immobilizing PNA on gold surfaces was carried out in two different ways distinguished by the terms one-step-immobilization and two-step-immobilization. For the one-step-immobilization process, PNA with the sequence N-TTTTCCCTCTCTC-C containing free amino groups and 3,3'-dithio-bis(propionic acid *N*-hydroxysuccinimide ester) (DTSP) were used in the reaction mixture to modify the PNA prior to immobilization. In the two-step-immobilization, the gold surface was first modified by the thiol using the ability of DTSP to form an SAM and then attaching PNA to it via an amide bond. Deprotonated (M-H)<sup>-</sup> signals of the different PNA bases as well as characteristic peaks of DTSP fragments were used in time-of-flight secondary ion mass spectrometry (TOF-SIMS) measurements to study and optimize the different immobilization processes. The data show that the best result could be achieved at a concentration of 10 mM and immobilization time of 24 h. The binding of PNA to the DTSP layer takes significantly longer than attaching DTSP to the surface. From the obtained data it was concluded that the two-step-immobilization method described above is preferable to the first one.

In 2004, Arlinghaus and co-workers[25] have used TOF-SIMS to examine different immobilization processes of PNA and their influence on the hybridization efficiency of unlabeled DNA fragments to complementary PNA. Two different approaches have been used to immobilize PNA onto gold surfaces. One method was to immobilize thiol-modified PNA in a single step reaction to the gold surface via an Au-S bond. The other method was to crosslink the *N*-terminal end of the PNA to a preformed functionalized SAM similar to the work by Feldner[24] above. DNA could readily be identified by detecting PO<sub>2</sub><sup>-</sup> and PO<sub>3</sub><sup>-</sup> or other phosphate-containing molecules from the DNA backbone. The influence of length and type of spacer molecules, which increase the distance between the biosensor surface and the PNA sequence, on the hybridization efficiency was also investigated. It was found that a greater spacer length leads to increased hybridization efficiency.

In 2005, Mateo-Marti and co-workers[26] have characterized SAMs of thiol-modified PNA adsorbed on gold surfaces by using reflection absorption infrared spectroscopy (RAIRS) and X-ray photoemission spectroscopy (XPS) techniques. They have used PNA molecules with the sequence Cys-O-O-AATCCCCCGCAT when the “O” spacer unit is a molecule of 8-amino-3,6-dioxaoctanoic acid used to separate the hybridization portion of the molecule from the surface. The change in the molecular orientation has been studied by infrared spectroscopy and atomic force microscopy (AFM). They have found that the molecular orientation of PNAs strongly depends on surface coverage. At low coverage, PNA chains lie flat on the surface, while at high coverage, PNA molecules realign their molecular axes with the surface normal and form SAMs without the need of co-immobilization of spacers or other adjuvant molecules. PNA immobilization has been followed by analyzing the N(1s) XPS core-level peak. A combination of the above-mentioned techniques allows them to confirm that the structure of the SAMs is stabilized by intermolecular interactions through noncomplementary adjacent nucleic bases.

### **1.3 Piezoelectric Biosensor**

A biosensor is an analytical tool consisting of biologically active material used in close conjunction with a device that will convert a biochemical signal into a quantifiable electrical signal. A biosensor has two components: a receptor and a detector. The receptor is responsible for the selectivity of the sensor. Examples include enzymes, antibodies, lipid layers, and nucleic acid. The detector, which plays the role of the transducer, translates the physical or chemical change by recognizing the analyte and relaying it through an electrical signal.[27]

Currently, there is increasing interest in the detection of specific nucleic acid (DNA or PNA) sequences using biosensor methods, which do not require the use of labels such as radioisotopes, enzymes, and fluorophores.[28] The non-labeling biosensor systems based on nucleic acids not only eliminate the need for such labels but also offer the potential advantage of rapid, real-time solution monitoring of nucleic acid hybridization, as well as high sensitivity and specificity. The basis of operation for a nucleic acid biosensor is the complementary coupling between the specific nucleic acid sequences within target analytes and the specific nucleic acid sequences immobilized onto the solid support (i.e. transducer).

Methods used for the direct detection of nucleic acid binding through base pairing (without using specific labels) have been reported based on electrochemical,[29] optical,[30-31] and piezoelectric[32-35] techniques. Piezoelectric transducer offers the advantages of a solid-state construction, chemical inertness, durability, and ultimately the possibility of low cost mass production.

The theory of piezoelectricity was first postulated by the Curie brothers[36] in 1880 who discovered that the application of stress to a quartz crystal induced an electrical potential across the crystal surface. Its potential as a sensor was first realized by Sauerbrey[37] who developed the relationship between the resonant frequency change of an oscillating piezoelectric crystal and the mass deposited on crystal surface

$$\Delta F = -2.3 \times 10^6 \times F^2 \Delta M/A \quad (3)$$

where,  $\Delta F$  = frequency change in oscillating crystal in Hz,  $F$  = frequency of piezoelectric quartz crystal in MHz,  $\Delta M$  = mass of deposited in g, and  $A$  = area of electrode surface in  $\text{cm}^2$ .

The AT-Cut quartz crystals as piezoelectric materials can function in a 'microbalance' mode and is known as quartz crystal microbalance (QCM). The QCM is an extremely sensitive mass sensor, capable of measuring sub-nanogram levels of mass changes. The potential for the detection of DNA hybridization based on QCM devices has recently been demonstrated.[32-35] The QCM sensors were used to kinetically measure DNA hybridization in solution,[38] quantitatively study sequence-specific binding of peptides to a duplex DNA,[39] and directly monitor DNA polymerase chain reaction.[40]

Many research groups have characterized the immobilization of DNA oligomers on gold surface and subsequent hybridization with target DNA using QCM. [19,23,33,35,41-43] But there is currently only a few research groups studying the hybridization of PNA with target DNA using QCM.

Wang and co-workers[44] studied the hybridization of 15 mer thiol-PNA probe synthesized in Nielsen's laboratory [Sequence: Cys-linker-GGCAGTGCC TCACAA-NH<sub>2</sub>; linker: (CO)(NHCH<sub>2</sub>)(CH<sub>2</sub>OCH<sub>2</sub>)<sub>2</sub>(CO)] with DNA oligomer using QCM. They demonstrated that QCM transducers can be used to follow in real time the kinetics of hybridization of PNA with DNA. They have also shown that a

remarkable mismatch discrimination can be achieved by coupling PNA probes with QCM transducers. This hybridization experiment with a perfect matched DNA yielded an average frequency change in the range of 15.8-21.0 Hz. In contrast, no frequency change is observed upon adding the mismatched DNA. Such ability of PNA/QCM biosensors to distinguish between perfect matches and mismatches is of great importance in genetic screening and therapy.

Stafshede and co-workers[45] studied the hybridization of PNA which is the same sequence in Wang's work with target DNA. They demonstrated that at 60 °C, an addition of a perfect matched 15 mer DNA to the immobilized PNA on the gold surface gives a net frequency decrease (6-7 Hz) corresponding to the hybridization between DNA and the PNA-covered surface, whereas an addition of the singly mismatched 15 mer DNA causes no net frequency shift under the same conditions. As a result, QCM is a simple and rapid technique which can sensitively distinguish between fully matched and singly mismatched DNA sequences by an appropriate choice of temperature.

To the best of our knowledge, the DNA hybridization on gold surface previously investigated is based on Nielsen's PNA, none has been reported on PNA systems developed by Vilaivan and co-workers[5] in particular (1*S*, 2*S*) ACPC-PNA. Taking advantages of the high binding affinity of Vilaivan's PNA to complementary DNA and powerful discrimination for DNA over DNA and Nielsen's PNA, this research aims to develop QCM-based biosensor based on Vilaivan's ACPC PNA. It is expected that this newly-developed biosensor would show superior DNA hybridization in terms of efficiency and specificity to DNA or Nielsen's PNA biosensors.

#### **1.4 Objectives of this research**

The objective of this research is to synthesize a novel thiol-modified Vilaivan's PNA and to seek for a suitable procedure for immobilization of the synthesized thiol-modified PNA on gold-coated piezoelectric quartz crystals that can best result in highly sensitive detection of DNA hybridization. Moreover, effect of pH and ionic strength, and specificity of DNA hybridization with immobilized PNA on gold surface are investigated using QCM.

## CHAPTER II

### EXPERIMENTAL SECTION

#### 2.1 General Procedure

##### 2.1.1 Materials

All chemicals were purchased from Fluka (Switzerland), Merck (Germany) or Aldrich Chemical Co., Ltd. (USA), and were purified as appropriate. Commercial grade solvents for column chromatography were distilled before use. Solvents for reactions were reagent grade and used without purification. Nitrogen was obtained from TIG with 99.5 % purity. Acetonitrile for HPLC experiment was HPLC grade, obtained from BDH and was filtered through a membrane filter (13 mm  $\phi$ , 0.45  $\mu\text{m}$  Nylon Lida) before use. Anhydrous *N, N'*-dimethylformamide (< 0.01%  $\text{H}_2\text{O}$ ) for solid phase peptide synthesis was obtained from Fluka and was used without further purification. The solid support for peptide synthesis (TentaGel S RAM Fmoc resin) and trifluoroacetic acid were obtained from Fluka. The protected amino acids (Fmoc-L-Lys(Boc)-OPfp) was obtained from Calbiochem Novabiochem Co., Ltd. (USA). Oligonucleotides were purchased from Bioservice Unit, National Science and Technology Development Agency (Thailand). MilliQ water was obtained from ultrapure water systems with Millipak<sup>®</sup> 40 filter unit 0.22  $\mu\text{m}$ , Millipore (USA).

##### 2.1.2 Methods

The weight of all substances was determined on a Metler Toledo electrical balance. Melting points were recorded on an Electrothermal 9100 capillary melting point apparatus. Rotary evaporator was of Büchi Rotavapor R-200 with a water aspirator model B-490. UV cabinet for UV-visualization of TLC was made in-house by Mr. Chanchai Khongdeesameor. The magnetic stirrers were of Corning (USA). The high vacuum was delivered by a Refco pump from Refco Manufacturing Ltd. (Switzerland). Thin layer chromatography was performed on Merck D.C. silica gel 60 F<sub>254</sub> 0.2 mm. precoated aluminium plates cat. no. 1.05554. Column chromatography was performed on silica gel 70-230 mesh (for normal chromatography) or 230 mesh (for flash column chromatography). Reverse phase HPLC experiments were performed on Water 600<sup>TM</sup> system equipped with gradient pump and Water 996<sup>TM</sup>

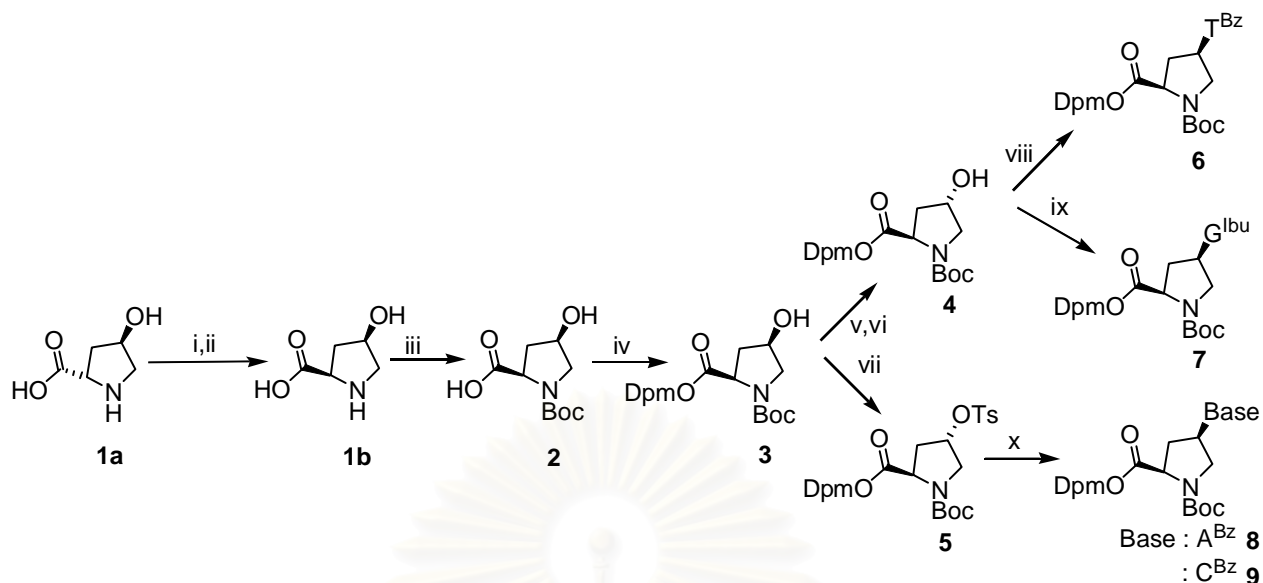
photodiode array detector; optionally alternate to Rheodyne 7725 manual sample loop (100  $\mu$ l sample size for analytical scale). A MetaChem<sup>TM</sup> C<sub>18</sub> HPLC column 3  $\mu$ m particle size 4.6 x 50 mm (Technologies Inc., USA) was used for analytical purposes. Peak monitoring and data processing were available for integrated operating with the Empower software. Fractions from HPLC were collected manually and were assisted by real-time HPLC chromatogram monitoring. The combined fractions were speed vaporization under reduced pressure using Heto Vacuum Centrifuge and MAXI dry-plus (Denmark).  $T_m$  experiment was measured on a CARY 100 Bio UV-Visible spectrophotometer (Varian Inc., USA). <sup>1</sup>H and <sup>13</sup>C spectra were recorded on Varian Mercury-400 plus operating at 400 and 100 MHz, respectively (Varian Inc., USA). MALDI-TOF mass spectra of thiol-modified PNA were analyzed on Microflex MALDI-TOF mass spectrometry (Bruker Daltonics, Germany) using doubly recrystallized  $\alpha$ -cyano-4-hydroxy cinnamic acid (CCA) as a matrix. Trifluoroacetic acid (0.1%) in acetonitrile:water (1:2) was used as a diluent for the preparation of MALDI-TOF samples. IR spectra were recorded on a Nicolet Impact 410 (USA) by the potassium bromide (KBr) method.

## 2.2 Experimental procedure

### 2.2.1 Synthesis of intermediate: proline derivatives modified with nucleobases

The intermediate proline derivatives of thymine (**6**), guanine (**7**), adenine (**8**), and cytosine (**9**) were synthesized as described previously (**Scheme 1**) [46-48] by Mr. Chaturong Suparpprom, Miss Patcharee Ngamviriyavong and Mrs. Choladda Srisuwannaket.

สถาบันวิทยบริการ  
จุฬาลงกรณ์มหาวิทยาลัย

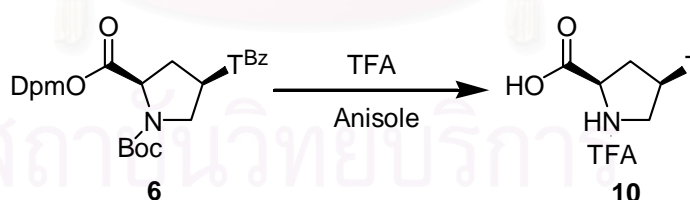


**Scheme 1** i.  $\text{Ac}_2\text{O}$ , heat  $90^\circ\text{C}$  16 h; ii. 2 M HCl, reflux 5 h; iii.  $\text{Boc}_2\text{O}$ ,  $t\text{BuOH}$ , NaOH (aq), overnight; iv.  $\text{Ph}_2\text{CN}_2$ , EtOAc, overnight; v.  $\text{HCO}_2\text{H}$ ,  $\text{Ph}_3\text{P}$ , DIAD, THF, overnight; vi.  $\text{NH}_3$ , MeOH, 2 h; vii. TsCl,  $\text{Ph}_3\text{P}$ , DIAD, THF, overnight; viii.  $N^3\text{-T}^{\text{Bz}}$ ,  $\text{Ph}_3\text{P}$ , DIAD, THF, overnight; ix.  $N^2\text{-IbuG(ONpe)}$ ,  $\text{Ph}_3\text{P}$ , DIAD, dioxane, overnight; x.  $N^6\text{-A}^{\text{Bz}}$  or  $N^4\text{-C}^{\text{Bz}}$ ,  $\text{K}_2\text{CO}_3$ , DMF, heat  $90^\circ\text{C}$ , 5 h

## 2.2.2 Synthesis of activated PNA monomers

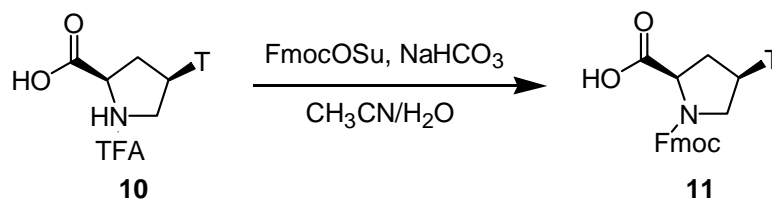
### (a) Thymine (T) monomer

#### *cis*-4-(Thymin-1-yl)-D-proline (10)



*N*-Boc-*cis*-4-( $N^3$ -benzoylthymine-1-yl)-D-proline diphenylmethyl ester (**6**) (1.20 g, 2.17 mmol) was mixed with anisole (1 mL) and trifluoroacetic (2 mL) at ambient temperature and allowed to stand overnight. The volatiles were removed by a stream of  $\text{N}_2$  gas. Then diethyl ether (20 mL) was added to the residue to precipitate the required compound. The solid was collected by filtration and dried in vacuum to afford the completely deprotected T monomer (**10**) as white solid (0.7210 g, 94%).

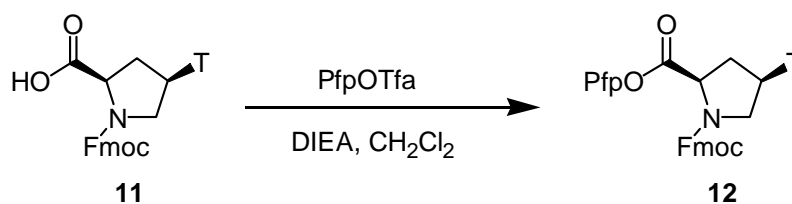
***N*-Fluoren-9-ylmethoxycarbonylamino-*cis*-4-(thymine-1-yl)-*D*-proline (**11**)**



*cis*-4-(Thymine-1-yl)-*D*-proline (**10**) (0.7210 g, 2.04 mmol) and NaHCO<sub>3</sub> (0.5141 g, 6.12 mmol) were dissolved in 1:1 CH<sub>3</sub>CN : H<sub>2</sub>O (6 mL). Then FmocOSu (0.8748 g, 2.45 mmol) was slowly added with stirring at room temperature and the pH of the reaction mixture was controlled at 8 by periodical addition of NaHCO<sub>3</sub>. After 4 h, the solvent was removed by rotary evaporation under reduced pressure. The residue was diluted with 20 mL of water and extracted with diethyl ether (3x20 mL). Then the pH of aqueous phase was adjusted to 2 with 10% HCl solution. The white crystalline precipitate formed was collected by filtration, washed with water, diethyl ether, and air-dried to give titled compound (**11**) (0.3993 g, 42%).

$\delta_{\text{H}}$  (400 MHz, DMSO-*d*<sub>6</sub>) 1.79 (3H, s, thymine CH<sub>3</sub>), 2.18-2.26 [1H, m, 1 × CH<sub>2</sub>(3')], 2.58-2.76 [1H, m, 1 × CH<sub>2</sub>(3')], 3.46-3.54 [1H, m, 1 × CH<sub>2</sub>(5')], 3.85-3.92 [1H, m, 1 × CH<sub>2</sub>(5')], 4.18-4.49 [4H, m, Fmoc aliphatic CH, Fmoc aliphatic CH<sub>2</sub> and CH(2')], 4.93-4.99 [1H, m, CH(4')], 7.36 (2H, t, *J* = 7.2 Hz, Fmoc aromatic CH), 7.44 (2H, t, *J* = 7.2 Hz, Fmoc aromatic CH), 7.61 (1H, s, thymine CH), 7.69 (2H, d, *J* = 7.2 Hz, Fmoc aromatic CH), 7.91 (2H, d, *J* = 8.0 Hz, Fmoc aromatic CH) and 11.36 (1H, s, thymine NH)

***N*-Fluoren-9-ylmethoxycarbonylamino-*cis*-4-(thymine-1-yl)-*D*-proline pentafluorophenyl ester (**12**)**



In a screwed cap test tube, to a suspension of *N*-fluorenylmethoxycarbonyl amino-*cis*-4-(thymine-1-yl)-*D*-proline (**11**) (0.3993 g, 0.86 mmol) and PfpOTfa (445  $\mu$ L, 2.58 mmol) in dichloromethane (3 mL) was added DIEA (588  $\mu$ L, 3.44 mmol).

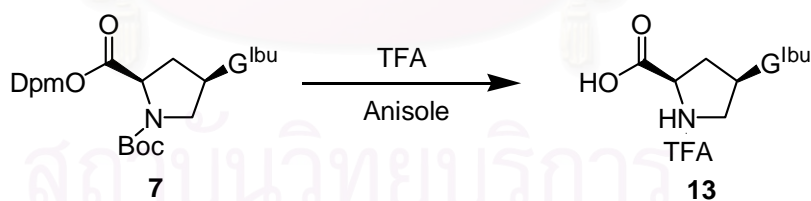


The resulting mixture was stirred further for another one hour. After the reaction was complete as indicated by TLC analysis, the mixture was diluted with dichloromethane and extracted with 10% HCl solution. Then the organic layer was washed with aq. NaHCO<sub>3</sub>. The combined organic phase was dried over magnesium sulfate and evaporated under reduced pressure. The residue was purified by flash column chromatography eluting with 100% ethyl acetate on silica gel to give clear viscous oil (0.4213 g, 78 %). This was re-precipitated from EtOAc by placing in a closed chamber containing hexane vapor to afford the desired product (**12**) as a white solid. The solid was then dried under vacuum to remove the residual solvent.

$\delta_{\text{H}}$  (400 MHz, CDCl<sub>3</sub>) 1.97 (3H, s, thymine CH<sub>3</sub>), 2.34-2.47 [1H, m, 1  $\times$  CH<sub>2</sub>(3')], 2.95-3.06 [1H, m, 1  $\times$  CH<sub>2</sub>(3')], 3.60-4.10 [2H, m, 2  $\times$  CH<sub>2</sub>(5')], 4.29 (1H, m, Fmoc aliphatic CH), 4.55-4.60 (2H, m, Fmoc aliphatic CH<sub>2</sub>), 4.68-4.83 [1H, m, CH(2')], 5.21-5.34 [1H, m, CH(4')], 7.14 (1H, s, thymine CH), 7.33-7.37 (2H, t,  $J = 7.2$  Hz, Fmoc aromatic CH), 7.42-7.46 (2H, t,  $J = 7.2$  Hz, Fmoc aromatic CH), 7.59-7.61 (2H, d,  $J = 7.2$  Hz, Fmoc aromatic CH), 7.80-7.82 (2H, d,  $J = 7.6$  Hz, Fmoc aromatic CH) and 8.45 (1H, s, thymine NH)

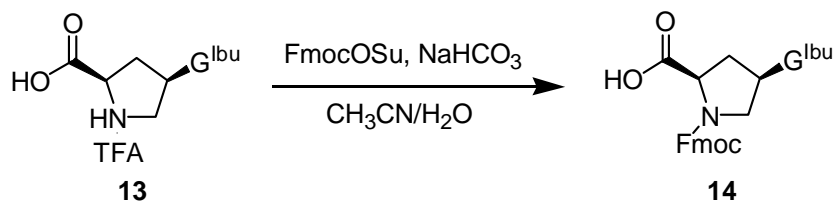
#### (b) Guanine (G) monomer

##### *cis*-4-(*N*<sup>2</sup>-Isobutyrylguanin-9-yl)-D-proline (**13**)



Synthesis of the titled compound (**13**) was accomplished using the same procedure as described for compound (**10**). Starting from *N*-Boc-*cis*-4-(*N*<sup>2</sup>-isobutyrylguanin-9-yl)-D-proline diphenylmethyl ester (**7**) (0.6008 g, 1 mmol), anisole (1 mL) and trifluoroacetic acid (2 mL) afforded compound (**13**) (0.4405 g, 98%) as a white solid.

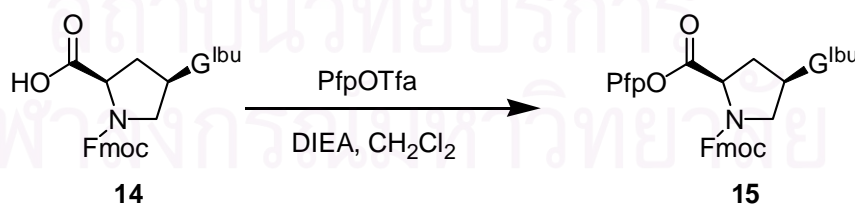
***N*-Fluoren-9-ylmethoxycarbonylamino-*cis*-4-(*N*<sup>2</sup>-isobutyrylguanin-9-yl)-*D*-proline (14)**



Synthesis of the titled compound (**14**) was accomplished using the same procedure as described for compound (**11**). Starting from *cis*-4-(*N*<sup>2</sup>-isobutyrylguanin-9-yl)-*D*-proline (**13**) (0.4403 g, 0.98 mmol), FmocOSu (0.4215 g, 1.18 mmol) and NaHCO<sub>3</sub> (0.2470 g, 2.94 mmol) in 1:1 CH<sub>3</sub>CN : H<sub>2</sub>O (3 mL) afforded compound (**14**) (0.2596 g, 48%) as a white solid.

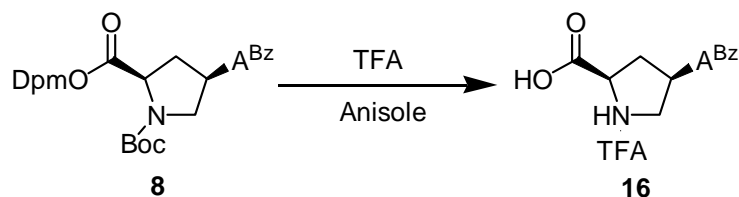
$\delta_{\text{H}}$  (400 MHz, DMSO-*d*<sub>6</sub>) 1.13 [6H, d,  $J = 6.0$  Hz, CH(CH<sub>3</sub>)<sub>2</sub>], 2.50-2.68 [1H, m, 1 × CH<sub>2</sub>(3')], 2.81-2.84 [1H, hep,  $J = 6.8$  Hz, CH(CH<sub>3</sub>)<sub>2</sub>], 2.91-3.08 [1H, m, 1 × CH<sub>2</sub>(3')], 3.09-4.05 [1H, 2 × m, 1 × CH<sub>2</sub>(5')], 4.14-4.56 [5H, m, 1 × CH<sub>2</sub>(5'), CH<sub>2</sub>(2'), Fmoc aliphatic CH and Fmoc aliphatic CH<sub>2</sub>], 5.02-5.11 [1H, s, CH<sub>2</sub>(4')], 7.31-7.34 (2H, t,  $J = 6.8, 7.2$  Hz, Fmoc aromatic CH), 7.39-7.43 (2H, t,  $J = 7.2$  Hz, Fmoc aromatic CH), 7.69 (2H, d,  $J = 6.4$  Hz, Fmoc aromatic CH), 7.87 (2H, d,  $J = 7.6$  Hz, Fmoc aromatic CH), 8.98 (1H, d,  $J = 16$  Hz, guanine CH) and 11.95 (1H, s, guanine NH)

***N*-Fluoren-9-ylmethoxycarbonylamino-*cis*-4-(*N*<sup>2</sup>-isobutyrylguanin-9-yl)-*D*-proline pentafluorophenyl ester (15)**

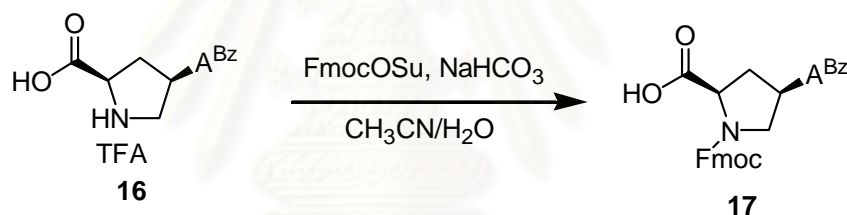


Synthesis of the titled compound (**15**) was accomplished by Mrs. Choladda Srisuwannaket using the same procedure as described for compound (**12**).

## (c) Adenine (A) monomer

*cis*-4-(*N*<sup>4</sup>-Benzoyladenin-9-yl)-D-proline (16)

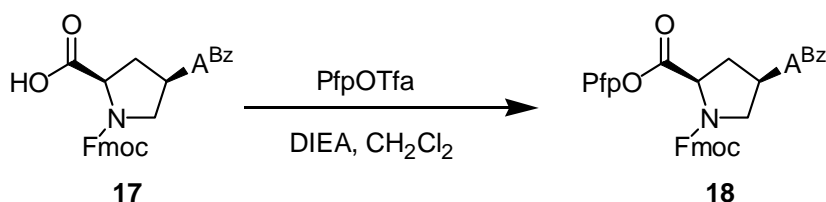
Synthesis of the titled compound (**16**) was accomplished using the same procedure as described for compound (**10**). Starting from *N*-Boc-*cis*-4-(*N*<sup>4</sup>-benzoyladenin-9-yl)-D-proline diphenylmethyl ester (**8**) (0.5458 g, 0.88 mmol), anisole (1 mL) and trifluoroacetic acid (2 mL) afforded *cis*-4-(*N*<sup>4</sup>-benzoyladenin-9-yl)-D-proline (**16**) (0.3828 g, 93%) as a white solid.

*N*-Fluoren-9-ylmethoxycarbonylamino-*cis*-4-(*N*<sup>4</sup>-benzoyladenin-9-yl)-D-proline (17)

Synthesis of the titled compound (**17**) was accomplished using the same procedure as described for compound (**11**). Starting from *cis*-4-(*N*<sup>4</sup>-benzoyladenin-9-yl)-D-proline (**16**) (0.3828 g, 0.82 mmol), FmocOSu (0.3516 g, 0.98 mmol) and NaHCO<sub>3</sub> (0.2067 g, 2.46 mmol) in 1:1 CH<sub>3</sub>CN : H<sub>2</sub>O (6 mL) afforded compound (**17**) (0.4106 g, 81%) as a white solid.

$\delta_{\text{H}}$  (400 MHz, DMSO-*d*<sub>6</sub>) 2.65-2.72 [1H, m, 1 × CH<sub>2</sub>(3')], 2.91-3.06 [1H, m, 1 × CH<sub>2</sub>(3')], 3.96-4.01 [1H, m, 1 × CH<sub>2</sub>(5')], 4.23-4.35 [5H, m, 1 × CH<sub>2</sub>(5'), CH<sub>2</sub>(2'), Fmoc aliphatic CH<sub>2</sub> and Fmoc aliphatic CH], 5.28-5.30 [1H, m, CH<sub>2</sub>(4')], 7.35-7.46 (4H, m, Fmoc aromatic CH), 7.59 (2H, t, *J* = 7.4 Hz, benzoyl CH), 7.66-7.75 (3H, m, benzoyl CH), 7.93 (2H, d, *J* = 7.6 Hz, Fmoc aromatic CH), 8.08 (2H, d, *J* = 8.0 Hz, Fmoc aromatic CH), 8.61 [1H, s, adenine CH(2)] 8.79 and 8.81 [1H, 2 × s, adenine CH(8)]

***N*-Fluoren-9-ylmethoxycarbonylamino-*cis*-4-(*N*<sup>4</sup>-benzoyladenin-9-yl)-*D*-proline pentafluorophenyl ester (**18**)**

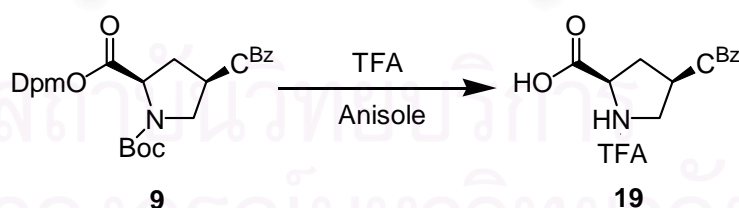


Synthesis of the titled compound (**18**) was accomplished using the same procedure as described for compound (**12**). Starting from *N*-fluoren-9-ylmethoxy carbonyl-amino-*cis*-4-(*N*<sup>4</sup>-benzoyladenin-9-yl)-*D*-proline (**17**) (0.1349 g, 0.23 mmol), PfpOTfa (122  $\mu$ L, 0.70 mmol) and DIEA (161  $\mu$ L, 0.94 mmol) in dichloromethane (1.5 mL) afforded compound (**18**) (0.1604 g, 92 %) as a white solid.

$\delta_{\text{H}}$  (400 MHz,  $\text{CDCl}_3$ ) 2.83-2.92 [1H, m, 1  $\times$   $\text{CH}_2$ (3')], 3.12-3.16 [1H, m, 1  $\times$   $\text{CH}_2$ (3')], 4.03-4.05 [1H, m, 1  $\times$   $\text{CH}_2$ (5')], 4.15-4.23 [2H, m, 1  $\times$   $\text{CH}_2$ (5') and  $\text{CH}_2$ (2')], 4.50-4.59 (2H, m, Fmoc aliphatic  $\text{CH}_2$ ), 4.77-4.85 (1H, m, Fmoc aliphatic  $\text{CH}$ ), 5.29 [1H, m,  $\text{CH}_2$ (4')], 7.26-7.37 (4H, m, Fmoc aromatic  $\text{CH}$ ), 7.46-7.57 (5H, m, benzoyl  $\text{CH}$ ), 7.73 (2H, d,  $J = 7.2$  Hz, Fmoc aromatic  $\text{CH}$ ), 8.01 (2H, d *br*, Fmoc aromatic  $\text{CH}$ ), 8.23 [1H, s, adenine  $\text{CH}$ (2)] and 8.75 [1H, s, adenine  $\text{CH}$ (8)]

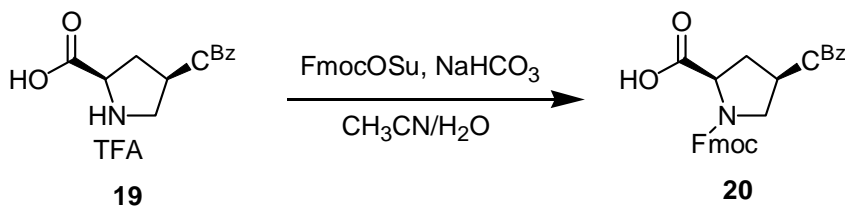
**(d) Cytosine (C) monomer**

***cis*-4-(*N*<sup>4</sup>-Benzolcytosin-1-yl)-*D*-proline (**19**)**



Synthesis of the titled compound (**19**) was accomplished using the same procedure as described for compound (**10**). Starting from *N*-Boc-*cis*-4-(*N*<sup>4</sup>-benzolcytosin-1-yl)-*D*-proline diphenylmethyl ester (**9**) (0.5062 g, 0.85 mmol), anisole (1 mL) and trifluoroacetic acid (2 mL) afforded compound (**19**) (0.3710 g, 98%) as a white solid.

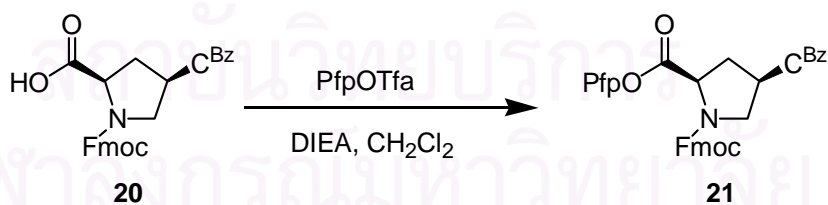
***N*-Fluoren-9-ylmethoxycarbonylamino-*cis*-4-(*N*<sup>4</sup>-benzoylcytosin-1-yl)-*D*-proline (20)**



Synthesis of the titled compound (**20**) was accomplished using the same procedure as described for compound (**11**). Starting from *cis*-4-(*N*<sup>4</sup>-benzoylcytosin-1-yl)-*D*-proline (**19**) (0.3710 g, 0.84 mmol), FmocOSu (0.3602 g, 1.0 mmol) and NaHCO<sub>3</sub> (0.2117 g, 2.52 mmol) in 1:1 CH<sub>3</sub>CN : H<sub>2</sub>O (3 mL) afforded compound (**20**) (0.4425 g, 97%) as a white solid.

$\delta_{\text{H}}$  (400 MHz, DMSO-*d*<sub>6</sub>) 2.54-2.80 [1H, m, 1 × CH<sub>2</sub>(3')], 2.93-3.09 [1H, m, 1 × CH<sub>2</sub>(3')], 3.94-4.01 [1H, m, 1 × CH<sub>2</sub>(5')], 4.21-4.41 [5H, m, 1 × CH<sub>2</sub>(5'), CH(2'), Fmoc aliphatic CH and Fmoc aliphatic CH<sub>2</sub>], 5.26 [1H, m, CH(4')], 7.35-7.38 (2H, m, Fmoc aromatic CH), 7.44-7.48 (2H, m, Fmoc aromatic CH), 7.55-7.72 (5H, m, benzoyl CH), 7.92 (2H, d, *J* = 8.0 Hz, Fmoc aromatic CH), 8.06 (2H, d, *J* = 8.0 Hz, Fmoc aromatic CH), 8.58 [1H, s, cytosine CH(3)], 8.79 [1H, d, *J* = 8.8 Hz, cytosine CH(6)] and 11.24 (1H, s, cytosine NH)

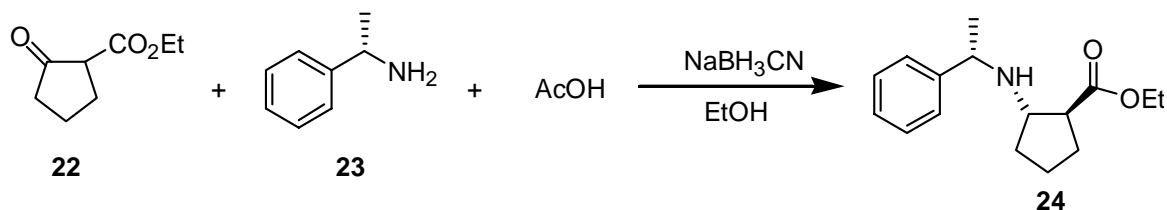
***N*-Fluoren-9-ylmethoxycarbonylamino-*cis*-4-(*N*<sup>4</sup>-benzoylcytosin-1-yl)-*D*-proline pentafluorophenyl ester (**21**)**



Synthesis of the titled compound (**21**) was accomplished by Mrs. Choladda Srisuwannaket using the same procedure as described for compound (**12**).

### 2.2.3 Synthesis of Spacer

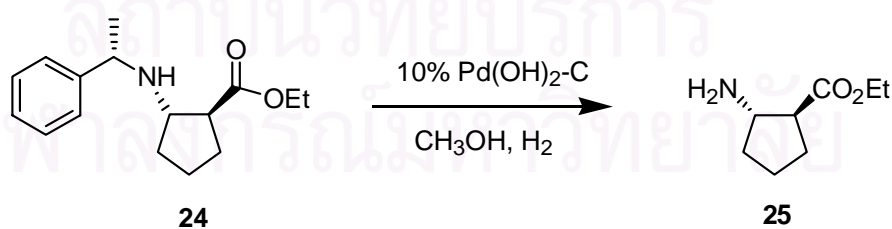
#### Ethyl (1*S*, 2*S*)-2-[(1'*S*)-phenylethyl]-aminocyclopentanecarboxylate (**24**)



The titled compound (**24**) was synthesized according to the published procedure.[49] Starting from  $\beta$ -ketoester (**22**) (3.10 mL, 21 mmol), (*S*)-(-)- $\alpha$ -methyl benzylamine (**23**) (2.50 g, 21 mmol), glacial acetic acid (1.20 g, 19 mmol) and sodium cyanoborohydride (2.0 g, 32 mmol) in ethanol (10 mL) afforded the mixture of ethyl-2-(1-phenylethyl)-aminocyclopentanecarboxylate. After a separation of this mixture by column chromatography, compound (**24**) was obtained as clear viscous oil (1.5462 g, 29%).

$\delta_{\text{H}}$  (400 MHz, CDCl<sub>3</sub>) 1.26 (3H, t,  $J = 7.0$  Hz, CO<sub>2</sub>CH<sub>2</sub>CH<sub>3</sub>), 1.37 (3H, d,  $J = 6.0$  Hz, NHCHCH<sub>3</sub>), 1.59-1.72 (2H, m, CH<sub>2</sub>CH<sub>2</sub>CH<sub>2</sub>), 1.78-1.88 (2H, m, NHCHCH<sub>2</sub>), 2.01-2.03 (2H, m, CH<sub>2</sub>CHCO), 2.61 (1H, q,  $J = 7.0$  Hz, CHCO<sub>2</sub>Et), 3.24 (1H, q,  $J = 7.2$  Hz, NHCHCH<sub>2</sub>), 3.87 (1H, q,  $J = 6.4$  Hz, NHCHCH<sub>3</sub>), 4.14 (2H, m, CO<sub>2</sub>CH<sub>2</sub>CH<sub>3</sub>) and 7.23-7.36 (5H, m, phenyl)

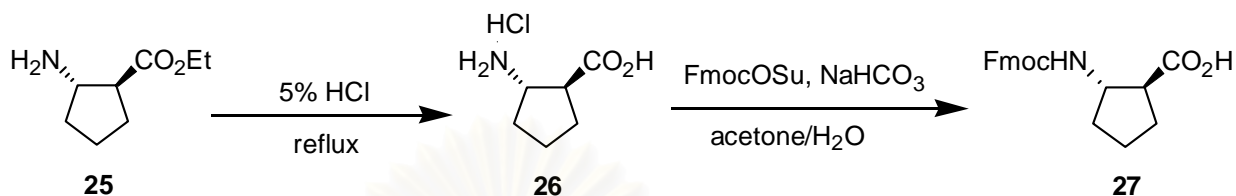
#### 2-Amino-cyclopentanecarboxylic acid ethyl ester (**25**)



Synthesis of the titled compound (**25**) was accomplished by a reaction between ethyl (1*S*, 2*S*)-2-[(1'*S*)-phenylethyl]-amino-cyclopentanecarboxylate (**24**) (1.3167 g, 5 mmol) and 10% Pd(OH)<sub>2</sub> on charcoal (0.12 g) in methanol (10 mL). The mixture was stirred at ambient temperature overnight under a hydrogen balloon, after which TLC monitoring indicated a complete reaction. Then the Pd precipitate was

removed by filtration. The solvent in the filtrate was removed by rotary evaporation under reduced pressure to give the compound (**25**) (0.6529 g, 82%) as colorless oil.

***N*-Fluoren-9-ylmethoxycarbonyl-2-amino-cyclopentanecarboxylic acid (**27**)**

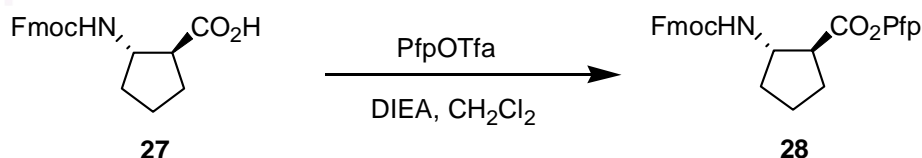


A solution of 2-amino-cyclopentanecarboxylic acid ethyl ester (**25**) (0.6529 g, 4.16 mmol) in 5% aqueous HCl (10 mL) was heated at reflux until the starting material was completely consumed (2-3 h) according to TLC. The reaction mixture was cooled to room temperature and the solvent was removed by rotary evaporation to give the compound (**26**) as a white solid.

Synthesis of the compound (**27**) was accomplished using the same procedure as described for compound (**11**). Starting from compound (**26**) obtained above, FmocOSu (1.48 g, 4.16 mmol) and NaHCO<sub>3</sub> (1.05 g, 12.48 mmol) in 1:1 acetone : H<sub>2</sub>O (10 mL) afforded compound (**27**) (0.8925 g, 61% from **25**) as a white solid.

$\delta_{\text{H}}$  (400 MHz, DMSO-*d*<sub>6</sub>) 1.41-1.72 (4H, 2×m, CH<sub>2</sub>CH<sub>2</sub>CH<sub>2</sub> and NHCHCH<sub>2</sub>), 1.87-1.93 (2H, m, CH<sub>2</sub>CHCO), 2.58 (1H, m, CHCO), 4.04 (1H, t, *J* = 7.4 Hz, NHCH), 4.22-4.27 (2H, m, Fmoc aliphatic CH and Fmoc aliphatic CH<sub>2</sub>) and 7.33-7.89 (8H, m, Fmoc aromatic CH),  $[\alpha]_{\text{D}}^{25} = +36.4$ , *c* = 1.0 in MeOH

***N*-Fluoren-9-ylmethoxycarbonyl-2-amino-cyclopentanecarboxylic acid pentafluorophenyl ester (**28**)**



Synthesis of the titled compound (**28**) was accomplished using the same procedure as described for compound (**12**). Starting from *N*-fluoren-9-ylmethoxycarbonyl-2-amino-cyclopentanecarboxylic acid (**27**) (0.3514 g, 1.0 mmol), PfpOTfa

(517  $\mu\text{L}$ , 3.0 mmol) and DIEA (684  $\mu\text{L}$ , 4.0 mmol) in dichloromethane (3 mL) afforded compound (**28**) (0.1825 g, 35%) as a white solid.

$\delta_{\text{H}}$  (400 MHz,  $\text{CDCl}_3$ ) 1.87 (2H, m,  $\text{CH}_2\text{CH}_2\text{CH}_2$ ), 2.10 (2H, m,  $\text{NHCHCH}_2$ ), 2.22 (2H, m,  $\text{CH}_2\text{CHCO}$ ), 3.11 (1H, m,  $\text{CHCO}$ ), 4.25 (1H, t,  $J = 6.2$  Hz,  $\text{NHCH}$ ), 4.39 (1H, t,  $J = 7.2$  Hz, Fmoc aliphatic  $\text{CH}$ ), 4.48 (2H, d,  $J = 6.4$  Hz, Fmoc aliphatic  $\text{CH}_2$ ), 4.94 (1H, s *br*,  $\text{NH}$ ) and 7.32-7.81 (8H, m, Fmoc aromatic  $\text{CH}$ )

## 2.2.4 Synthesis of S-protected thiols

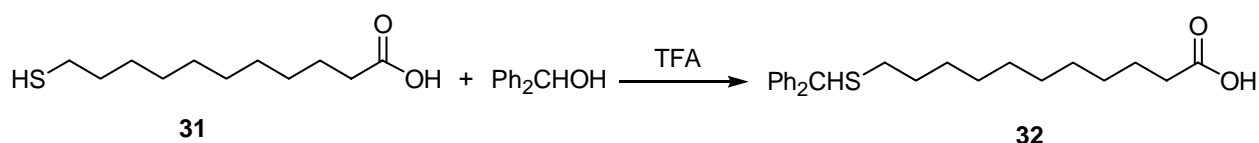
### 3-Benzhydrylthio-propionic acid (**30**)



To a mixture of 3-mercaptopropionic acid (**29**) (0.0870  $\mu\text{L}$ , 1 mmol) and  $\text{Ph}_2\text{CHOH}$  (0.1840 g, 1 mmol) was slowly added TFA (2 mL) until the reaction was homogeneous. When TLC analysis revealed that reaction was completed (0.5-1 h), the volatile was removed by a stream of  $\text{N}_2$  gas. The residue was diluted with 5 mL of diethyl ether and extracted with water (3x5 mL). The organic phase was evaporated by rotary evaporation under reduced pressure to give compound (**30**) (0.2493 g, 92%) as a white solid.

mp. = 87.5-89.0  $^\circ\text{C}$ ,  $\delta_{\text{H}}$  (400 MHz,  $\text{CDCl}_3$ ) 2.57 (2H, t,  $\text{CH}_2\text{CO}_2\text{H}$ ), 2.66 (2H, t,  $\text{CH}_2\text{CH}_2\text{CO}_2\text{H}$ ), 5.20 (1H, s,  $\text{CHPh}_2$ ) and 7.23-7.43 (10H, m, aromatic  $\text{CH}$ )  $\delta_{\text{C}}$  (100 MHz,  $\text{CDCl}_3$ ) 26.8 ( $\text{CH}_2\text{CH}_2\text{CO}_2\text{H}$ ), 34.0 ( $\text{CH}_2\text{CO}_2\text{H}$ ), 54.3 ( $\text{CHPh}_2$ ), 127.3, 128.3, 128.6 and 140.9 (aromatic  $\text{C}$ ) and 177.4 ( $\text{CO}_2\text{H}$ )

### 11-Benzhydrylthio-undecanoic acid (**32**)





Synthesis of the compound (**32**) was accomplished using the same procedure as described for compound (**30**). Starting from 11-mercaptopundecanoic acid (**31**) (0.1092 g, 0.50 mmol), Ph<sub>2</sub>CHOH (0.1840 g, 0.50 mmol) and TFA (1 mL) afforded compound (**32**) (0.0809 g, 42%) as a white solid.

mp. = 53.5-55.0 °C,  $\delta_{\text{H}}$  (400 MHz, CDCl<sub>3</sub>) 1.26 and 1.32 (12H, 2×s br, CH<sub>2</sub>), 1.53-1.62 (2H, m, CH<sub>2</sub>CH<sub>2</sub>CO<sub>2</sub>H), 1.62-1.69 (2H, m, SCH<sub>2</sub>CH<sub>2</sub>), 2.36-2.43 (4H, m, SCH<sub>2</sub> and CH<sub>2</sub>CO<sub>2</sub>H), 5.17 (1H, s, CHPh<sub>2</sub>) and 7.23-7.46 (10H, m, aromatic CH)  $\delta_{\text{C}}$  (100 MHz, CDCl<sub>3</sub>) 24.7 (CH<sub>2</sub>CH<sub>2</sub>CO<sub>2</sub>H), 28.8, 29.0, 29.1, 29.2, 29.3 and 29.4 (CH<sub>2</sub>), 32.3 (SCH<sub>2</sub> and SCH<sub>2</sub>CH<sub>2</sub>), 34.1 (CH<sub>2</sub>CO<sub>2</sub>H), 54.2 (CHPh<sub>2</sub>), 127.1, 128.3, 128.5 and 141.6 (aromatic C)

### 2.2.5 Synthesis of thiol-modified PNA oligomer

#### (a) Preparation of the reaction pipette and apparatus for solid phase peptide synthesis

All peptide syntheses were carried out using a home-made peptide synthesis column equipped with a fritted glass tip as described below. A new glass Pasteur pipette was plugged with a small amount of glass powder and sintered on a small flame. The length of the sintered glass should be about 3-5 mm. The resin was weighed accurately into the pipette and the pipette was equipped with a rubber teat. The resin in the pipette should be swollen in the required solvent at least 2 h before use. For each reactions, the reagent was directly sucked in, ejected out or hold on by manual control for the specified period of time. Occasional agitation may be performed using this device under manual control. All washing could be done by filling the solvent via the top of the pipette. The excess solvent was ejected out by squeezing the rubber teat as shown in **Figure 2.1**.

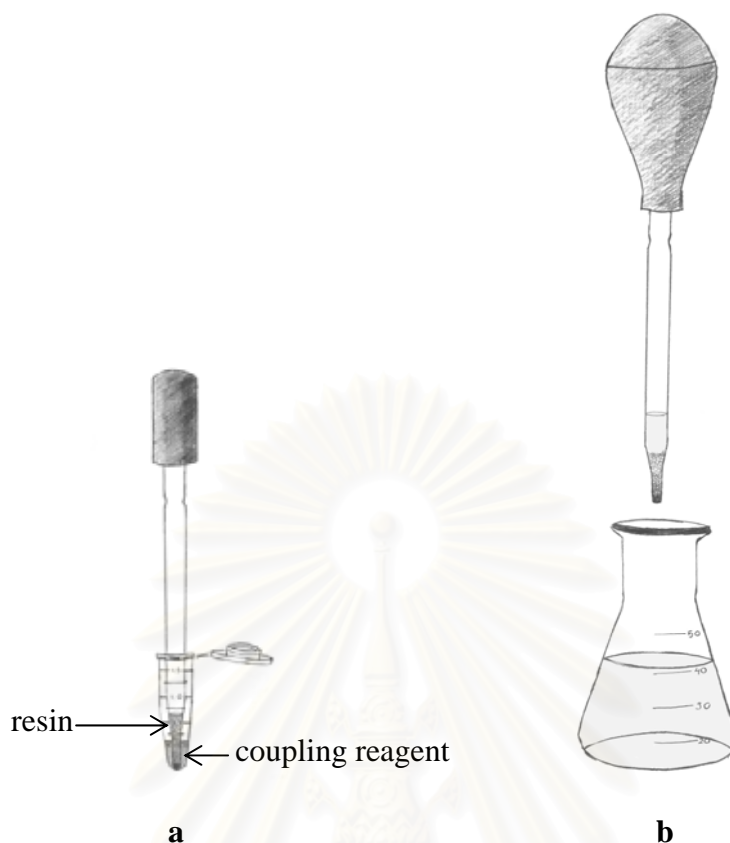


**Figure 2.1** Schematic representation of the manual technique for solid phase peptide synthesis; (a) coupling, deprotecting, and cleaving process; (b) washing process.

### (b) Solid phase peptide synthesis

Synthesis of each thiol-modified PNA carried out on 1.0  $\mu\text{mol}$  scale. The synthesis consists of 8 steps as follows.

#### i) Removing Fmoc protecting group from the resin

The reaction pipette containing TentaGel S RAM Fmoc resin (4.2 mg, 1.0  $\mu\text{mol}$ ) was prepared as described above. The resin was treated with 20% piperidine in DMF (piperidine 50  $\mu\text{L}$  and DMF 200  $\mu\text{L}$ ) in a 1.5 mL eppendorf tube for 15 min at room temperature with occasional agitation. After the specified period of time, the reagent was squeezed off and the reaction column was washed exhaustively with DMF.

### **ii) Anchoring the first amino acid (Lys) residue**

Fmoc-L-Lysine was first attached to the free amino group on the RAM resin employing Fmoc-L-Lys(Boc)-OPfp. Fmoc-L-Lys(Boc)-OPfp (6.30 mg, 10.0  $\mu\text{mol}$ ) and HOAt (1.36 mg, 10.0  $\mu\text{mol}$ ) were dissolved in anhydrous DMF (30  $\mu\text{L}$ ) in a 1.5 mL eppendorf tube. Then DIEA (3.5  $\mu\text{L}$ , 20.0  $\mu\text{mol}$ ) was added to the reaction mixture by a micropipette. The prepared resin was soaked in this solution with occasional agitation for 1 h at room temperature. After the specified period of time, the reagent was squeezed off and the reaction column was washed exhaustively with DMF.

### **iii) Deprotecting Fmoc group at N-terminus**

After the reaction was completed, the resin was treated with 20% piperidine in DMF (piperidine 50  $\mu\text{L}$  and DMF 200  $\mu\text{L}$ ) in a 1.5 mL eppendorf tube for 15 min at room temperature with occasional agitation. After the specified period of time, the reagent was squeezed off and the reaction column was washed exhaustively with DMF. The used deprotecting reagent can be used to determine the coupling efficiency by diluting with an appropriate volume of methanol and then the UV-absorbance of dibenzofulvene-piperidine adduct at 254 nm was measured. The first UV-absorbance of the adduct, released from preloaded Fmoc-L-Lys(Boc)-resin, was assumed to be 100%. The coupling efficiency generally reflects the extent of the solid phase reaction. The efficiency should be at least >90% for each step in order to give an acceptable yield of the PNA oligomer from the synthesis. If the overall efficiency drops below 50%, the coupling must be terminated to save the valuable monomers.

### **iv) Coupling with PNA monomer**

The free amino group, generated from the deprotection step iii, was further coupled with a designated PNA monomer. PNA monomer (4.0  $\mu\text{mol}$ ) and HOAt (0.54 mg, 4.0  $\mu\text{mol}$ ) were dissolved in 30  $\mu\text{L}$  anhydrous DMF. Then DIEA (1.4  $\mu\text{L}$ , 8.0  $\mu\text{mol}$ ) was added to the reaction mixture by a micropipette. The reaction pipette was treated with this solution for 1 h at room temperature with occasional agitation. After the specified period of time, the reagent was squeezed off and the reaction column was washed exhaustively with DMF.

**v) End capping**

After the coupling step, the free amino residue was capped with 10% lauroyl chloride/DIEA in anhydrous DMF (lauroyl chloride 5  $\mu\text{L}$ , DIEA 5  $\mu\text{L}$  and DMF 40  $\mu\text{L}$ ) in a 1.5 mL eppendorf tube to prevent deletion of sequences and facilitate purification.[50] The reaction pipette was occasionally agitated in the solution for 15 min at room temperature. After the specified period of time, the reagent was squeezed off and the reaction column was washed exhaustively with DMF.

**vi) Modifying the N-terminus of PNA oligomer with thiol**

After the final cleavage of Fmoc, the PNA oligomer was doubly treated with a solution of an activated S-protected thiol. S-protected thiol (4.0  $\mu\text{mol}$ ) and HATU (1.32 mg, 3.5  $\mu\text{mol}$ ) was dissolved in 30  $\mu\text{L}$  anhydrous DMF. Then DIEA (1.4  $\mu\text{L}$ , 8.0  $\mu\text{mol}$ ) was added to the reaction mixture by a micropipette. The reaction pipette was treated with the solution for 1 h at room temperature with occasional agitation. After the specified period of time, the reagent was squeezed off and the reaction column was washed exhaustively with DMF.

After coupling with S-protected thiol, the free residue was capped with 10% lauroyl chloride/DIEA in anhydrous DMF (lauroyl chloride 5  $\mu\text{L}$ , DIEA 5  $\mu\text{L}$  and DMF 40  $\mu\text{L}$ ) in a 1.5 mL eppendorf tube. The reaction pipette was occasionally agitated in the solution for 15 min at room temperature. After the specified period of time, the reagent was squeezed off and the reaction column was washed exhaustively with DMF.

**vii) Cleaving the thiol-modified PNA oligomer from the resin and deprotection at S-atom**

The cleavage of PNA oligomer from the resin was done in concurrent with the removal of the protecting group (diphenylmethyl) at S-atom by treatment with 10% anisole in trifluoroacetic acid (anisole 10  $\mu\text{L}$  and TFA 90  $\mu\text{L}$ ) at room temperature for 2 h with occasional agitation. During the treatment, the resin becomes red. After the specified period of time, TFA was removed by a nitrogen stream in the fume hood. The method was repeated to ensure a complete cleavage of the peptide from the resin. The sticky residue was treated with diethyl ether to precipitate the crude PNA. The suspension was centrifuged and decanted. The crude peptide was centrifugally

washed with diethyl ether 4-5 times. Finally, the crude peptide was air-dried at room temperature and stored dried at  $-20\text{ }^{\circ}\text{C}$  until use.

#### viii) Purification and identification

The crude peptide was prepared for HPLC analysis by dissolving a mixture in  $200\text{ }\mu\text{L}$  deionized water. The solution was filtered through a nylon membrane filter ( $0.45\text{ }\mu\text{m}$ ). Analysis and purification was performed by reverse phase HPLC, monitoring by UV-absorbance at  $260\text{ nm}$  and eluting with a gradient system of  $0.01\%$  TFA in acetonitrile/water. The HPLC gradient system used two solvent systems which are solvent A ( $0.01\%$  trifluoroacetic acid in acetonitrile) and solvent B ( $0.01\%$  trifluoroacetic acid in milliQ water). The elution began with A:B ( $10:90$ ) for  $5\text{ min}$  followed by a linear gradient up to A:B ( $90:10$ ) over a period of  $30\text{ min}$ , then hold for  $5\text{ min}$  before reverted back to A:B ( $10:90$ ). After freeze drying, the identity of the PNA oligomer was verified by MALDI-TOF mass spectrometry.

Synthesis of  $\text{HS}(\text{CH}_2)_2\text{CO-T}_9\text{-LysNH}_2$  (**33**) began with step i and ii. A cycle of PNA monomer attachment (deprotection (step iii), coupling with the desired PNA monomer (step iv), and end capping (step v)) was then performed alternately with a cycle of spacer attachment (deprotection (step iii), coupling with spacer (step iv), and end capping (step v)). After 9 PNA monomers were coupled, step vi, vii, and viii were consecutively followed. The PNA monomer, spacer and S-protected thiol used for the synthesis were Fmoc-T-Pfp (**12**) ( $2.5\text{ mg}$ ,  $4.0\text{ }\mu\text{mol}$ ), Fmoc-ACPC-Pfp (**28**) ( $2.07\text{ mg}$ ,  $4.0\text{ }\mu\text{mol}$ ) and DpmS( $\text{CH}_2$ ) $_2$ CO $_2$ H (**30**) ( $1.09\text{ mg}$ ,  $4.0\text{ }\mu\text{mol}$ ), respectively. After purification, the HPLC peak of  $\text{HS}(\text{CH}_2)_2\text{CO-T}_9\text{-LysNH}_2$  (**33**) appeared at  $t_R = 22.56\text{ min}$ .

Synthesis of  $\text{HS}(\text{CH}_2)_{10}\text{CO-T}_9\text{-LysNH}_2$  (**34**) was performed using a similar procedure as described for  $\text{HS}(\text{CH}_2)_2\text{CO-T}_9\text{-LysNH}_2$  (**33**) in the previous paragraph. The PNA monomer, spacer and S-protected thiol used for the synthesis were Fmoc-T-Pfp (**12**) ( $2.5\text{ mg}$ ,  $4.0\text{ }\mu\text{mol}$ ), Fmoc-ACPC-Pfp (**28**) ( $2.07\text{ mg}$ ,  $4.0\text{ }\mu\text{mol}$ ) and DpmS( $\text{CH}_2$ ) $_{10}$ CO $_2$ H (**32**) ( $1.54\text{ mg}$ ,  $4.0\text{ }\mu\text{mol}$ ), respectively. HPLC purification of this compound was unsuccessful.

Synthesis of HS(CH<sub>2</sub>)<sub>2</sub>CO-TTCTATGTT-LysNH<sub>2</sub> (**35**) was performed using a similar procedure as described for HS(CH<sub>2</sub>)<sub>2</sub>CO-T<sub>9</sub>-LysNH<sub>2</sub> (**33**) except that the resin in the reaction pipette was treated with aqueous ammonia/dioxane 1:1 at 60 °C for 6 h prior to step vii in order to remove nucleobase protecting groups (Bz, Ibu). PNA monomers used for the synthesis were Fmoc-T-Pfp (**12**) (2.5 mg, 4.0 μmol), Fmoc-G-Pfp (**15**) (2.9 mg, 4.0 μmol), Fmoc-A-Pfp (**18**) (3.0 mg, 4.0 μmol) and Fmoc-C-Pfp (**21**) (2.8 mg, 4.0 μmol). Spacer and S-protected thiol used for the synthesis were Fmoc-ACPC-Pfp (**28**) (2.07 mg, 4.0 μmol) and DpmS(CH<sub>2</sub>)<sub>2</sub>CO<sub>2</sub>H (**30**) (1.09 mg, 4.0 μmol), respectively. After purification, the HPLC peak of HS(CH<sub>2</sub>)<sub>2</sub>CO-TTCTATGTT-LysNH<sub>2</sub> (**35**) appeared at  $t_R = 22.44$  min.

## 2.2.6 Biophysical studies of thiol-modified PNA nonamer in solution

### (a) $T_m$ experiments [51]

$T_m$  experiments were performed on a CARY 100 Bio UV-Visible spectrophotometer (Varian Ltd.) equipped with a thermal melt system. The sample for  $T_m$  measurement was prepared by mixing calculated amounts of stock DNA and PNA solutions to give a final concentration of 2 μM nucleotides at a ratio of PNA : DNA = 1:1 and 0.5 mM sodium phosphate buffer (pH 7.0) and the final volumes were adjusted to 3.0 mL by an addition of deionized water. The samples were transferred to a 10 mm quartz cell with a Teflon stopper and equilibrated at the starting temperature for at least 30 min. The OD<sub>260</sub> was recorded in steps from 20-90 °C (block temperature) with a temperature increment of 1 °C/min. The results were normalized by dividing the absorbance at each temperature by the initial absorbance. Analysis of the data was performed on a PC compatible computer using Microsoft Excel XP (Microsoft Corp.) (See Appendix A for detail of data analysis)

### 2.2.7 Immobilization and hybridization with target DNA of thiol-modified PNA nonamer on gold surface

Immobilization and hybridization with target DNA of thiol-modified PNA nonamer on gold surface was mainly monitored by Quartz crystal microbalance (QCM). Surface functionality, topography, and wettability of gold surfaces before and after immobilization were characterized by atomic force microscopy (AFM),

reflection absorption infrared spectroscopy (RAIRS), and water contact angle analysis, respectively.

### **(a) QCM measurement**

The QCM crystals used were 5-MHz AT Cut crystals PM-700 series plating monitor (Maxtex, Inc.) The QCM cell was designed so that only one gold-coated side of the quartz disk was in contact with the solution.

Before immobilization, the bare gold electrode on a quartz crystal was cleaned with piranha solution (3:1 H<sub>2</sub>SO<sub>4</sub> : 30% H<sub>2</sub>O<sub>2</sub>) (Note: This is a dangerous cleaning solution and care must be taken in solution handling). After the gold electrode was thoroughly rinsed with milliQ water, dried with light stream of N<sub>2</sub> (g) and mounted on the QCM cell. The frequency change was monitored until a stable baseline (F<sub>1</sub>) was obtained.

#### **(i) Immobilization**

Three different procedures were employed for immobilization of thiol-modified PNA based on the direct chemisorption of thiol on gold surface:

##### *I. Thiol-modified PNA procedure*

In this procedure, the cleaned gold electrode was immersed in a solution of thiol-modified PNA (5.0 μM, 1.5 mL) and incubated at room temperature for 24 h.

##### *II. Thiol-modified PNA and blocking thiol procedure*

Following procedure I, the electrode was treated with a blocking thiol solution (mercaptoethanol 1 mM, 1.5 mL) at room temperature for 1 h.

##### *III. Mixed thiol- modified PNA and blocking thiol procedure*

The cleaned gold electrode was immersed in mixed solutions (v/v) of 50 % 5.0 μM thiol-modified PNA and 50 % 1 mM blocking thiol solution for 24 h at room temperature.

After rinsing with milliQ water and drying with light stream of N<sub>2</sub> (g), the gold electrode was again mounted on the QCM cell and the frequency was recorded until it reached the equilibrium value (F<sub>2</sub>). The frequency shift as a result of PNA immobilization is assigned as ΔF<sub>i</sub> (a difference between F<sub>1</sub> and F<sub>2</sub>). To determine the optimal condition for immobilization, effects of thiol-modified PNA concentration (0.5, 1, 2 and 5 μM) and immobilization time (2, 3, 6, 24 and 48 h) were investigated.

### **(ii) Hybridization**

After the immobilization step, the thiol-modified PNA SAMs on gold electrode were treated with the target DNA in sodium phosphate buffer pH 7 (200  $\mu\text{L}$ ) at selected concentration and hybridization time. Then the gold electrode was rinsed with milliQ water, dried with light stream of  $\text{N}_2(\text{g})$  and mounted on the QCM cell. The equilibrium frequency value obtained at this step is designated as  $F_3$ . The frequency shift caused by hybridization is assigned as  $\Delta F_h$  which is a difference between  $F_2$  and  $F_3$ . Effects of the sodium phosphate buffer pH 7 concentration (0, 0.05, 0.50, 5.0 and 50 mM), DNA concentration (20, 50 and 100  $\mu\text{M}$ ), hybridization time (0.5, 1 and 3 h), pH (6, 7 and 8) and ionic strength (0, 1 and 10 mM NaCl) on hybridization efficiency were investigated.

### **(b) AFM analysis**

AFM images on the gold electrode of the quartz crystals were recorded using a commercial Seiko Instrument SPA 400 (Japan). To avoid tip and sample damages, topographic images were taken in a non-contact dynamic mode. Cantilevers with a tip, resonance frequency of 124 KHz and force constant of 14 N/m were used.

### **(c) RAIRS analysis**

All spectra of gold-coated glass slides containing a chromium passivation layer (50 nm) before and after SAM formation of thiol-modified PNA nonamer were collected by a Nicolet Magna 750 FT-IR spectrometer equipped with a liquid-nitrogen-cooled mercury-cadmium-telluride (MCT) detector. Spectra in the infrared region (4000-650  $\text{cm}^{-1}$ ) were collected with 256 co-addition scans at a spectral resolution of 4  $\text{cm}^{-1}$ . A commercial accessory (The Seagull<sup>TM</sup>, Harrick Scientific, USA) was employed for all spectral acquisition. A polarized radiation with a 80° angle of incidence was employed.

### **(d) Water contact angle analysis**

Contact angle meter, model 100-00 Contact Angle Goniometer, Ramé-Hart, Inc., USA was used for the determination of water contact angles of gold-coated glass slides containing a chromium passivation layer (50 nm) before and after SAM formation of thiol-modified PNA nonamer. A droplet of testing MilliQ water is placed



on the tested surface by bringing the surface into contact with a droplet suspended from a needle of the syringe. The measurements were carried out in air at the room temperature. Advancing angle was recorded while water was added to the drop. The reported angle is an average of 3 measurements on different area of each sample.



สถาบันวิทยบริการ  
จุฬาลงกรณ์มหาวิทยาลัย

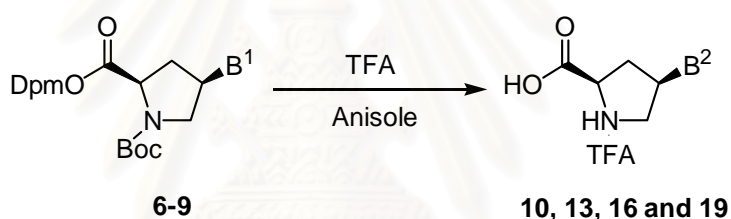
## CHAPTER III

### RESULTS AND DISCUSSION

#### 3.1 Synthesis of activated PNA monomers

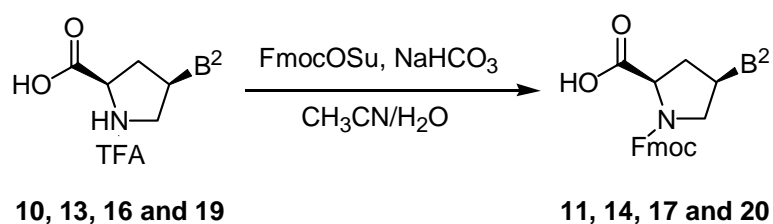
To deprotect the Dpm and Boc protecting groups of the intermediate proline derivatives **6-9**,<sup>[46-48]</sup> the compounds were reacted with trifluoroacetic acid and anisole. The free amino acids carrying nucleobases were easily separated from other by-products by washing with diethyl ether to give the TFA salts (**10, 13, 16 and 19**) as white solids (**Table 3.1**). In case of thymine, the benzoyl group was also cleaved to obtain *cis*-4-(thymine-1-yl)-D-proline (**10**).

**Table 3.1** Deprotection of Dpm and Boc protecting groups



starting material	B <sup>1</sup>	product	B <sup>2</sup>	% yield
<b>6</b>	T <sup>Bz</sup>	<b>10</b>	T	94
<b>7</b>	G <sup>Ibu</sup>	<b>13</b>	G <sup>Ibu</sup>	98
<b>8</b>	A <sup>Bz</sup>	<b>16</b>	A <sup>Bz</sup>	93
<b>9</b>	C <sup>Bz</sup>	<b>19</b>	C <sup>Bz</sup>	98

The free acid compounds (**10, 13, 16 and 19**) were reacted with FmocOSu and NaHCO<sub>3</sub> in 1:1 CH<sub>3</sub>CN : H<sub>2</sub>O to protect the N-atoms with Fmoc group. After the reaction was completed, the solvent was removed. The residue was diluted with water and extracted with diethyl ether. The white crystalline products (**11, 14, 17 and 20**) were obtained when the pH of aqueous phase was adjusted to 2 (**Table 3.2**).

**Table 3.2** Protection of Fmoc

starting material	product	B <sup>2</sup>	% yield
10	11	T	42
13	14	G <sup>Ibu</sup>	48
16	17	A <sup>Bz</sup>	81
19	20	C <sup>Bz</sup>	97

From <sup>1</sup>H NMR spectra of compound (**11, 14, 17 and 20**) the peaks of Fmoc group were observed in all cases indicating successful protection of the Fmoc group. For example, NMR spectrum of *N*-fluoren-9-ylmethoxycarbonylamino-*cis*-4-(thymine-1-yl)-D-proline (**11**) showed a characteristic peak of Fmoc at 4.18-4.49 (Fmoc aliphatic CH<sub>2</sub> and Fmoc aliphatic CH), 7.36, 7.44, 7.69 and 7.91 (Fmoc aromatic CH) ppm. The mechanism for this step is demonstrated in **Figure 3.1**.

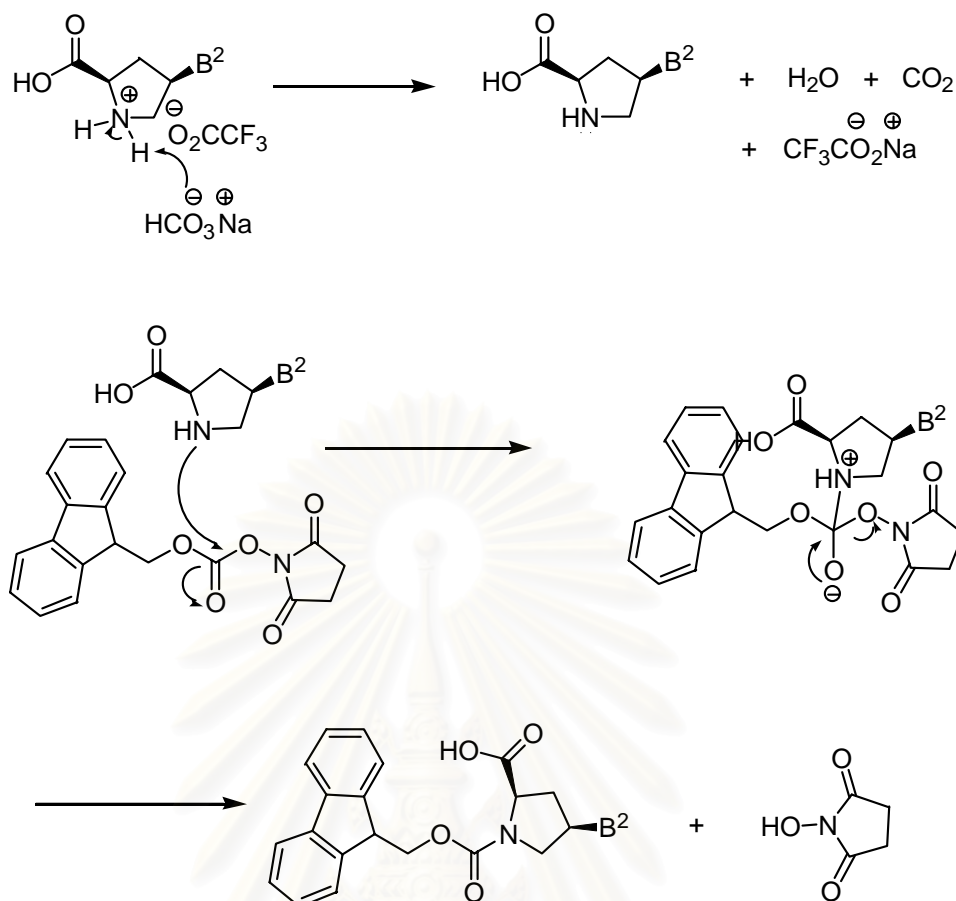
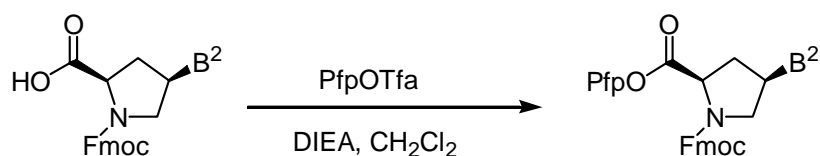


**Figure 3.1** Reaction mechanism for the protection of N-atom with Fmoc group.

After the protection of N-atom with Fmoc group, the Fmoc free acid compounds (**11**, **14**, **17** and **20**) were reacted with PfpOTfa and DIEA. This reaction was completed within 1 h according to TLC analysis. The product was purified by acid-base extraction followed by chromatographic purification. The chromatography must be performed quickly to avoid decomposition of the product on the column. The products were obtained as white solids (**Table 3.3**).

**Table 3.3** Activation of PNA monomers by Pfp ester



starting material	product	B <sup>2</sup>	% yield
11	12	T	78
14	15	G <sup>Ibu</sup>	- *
17	18	A <sup>Bz</sup>	92
20	21	C <sup>Bz</sup>	- *

\* Compound 15 and 21 were synthesized by Mrs. Choladda Srisuwannaket.

<sup>1</sup>H NMR spectra of the Fmoc free acid derivative and the Fmoc Pfp ester derivative were quite similar since the Pfp moiety is <sup>1</sup>H NMR silent. The major difference between polarity of both compounds was readily observed by TLC. Fmoc Pfp ester derivative of (18) has R<sub>f</sub> = 0.20 (100% ethyl acetate), while Fmoc free acid derivative (17) has R<sub>f</sub> = 0 (100% ethyl acetate). The mechanism for this step is demonstrated in **Figure 3.2**.

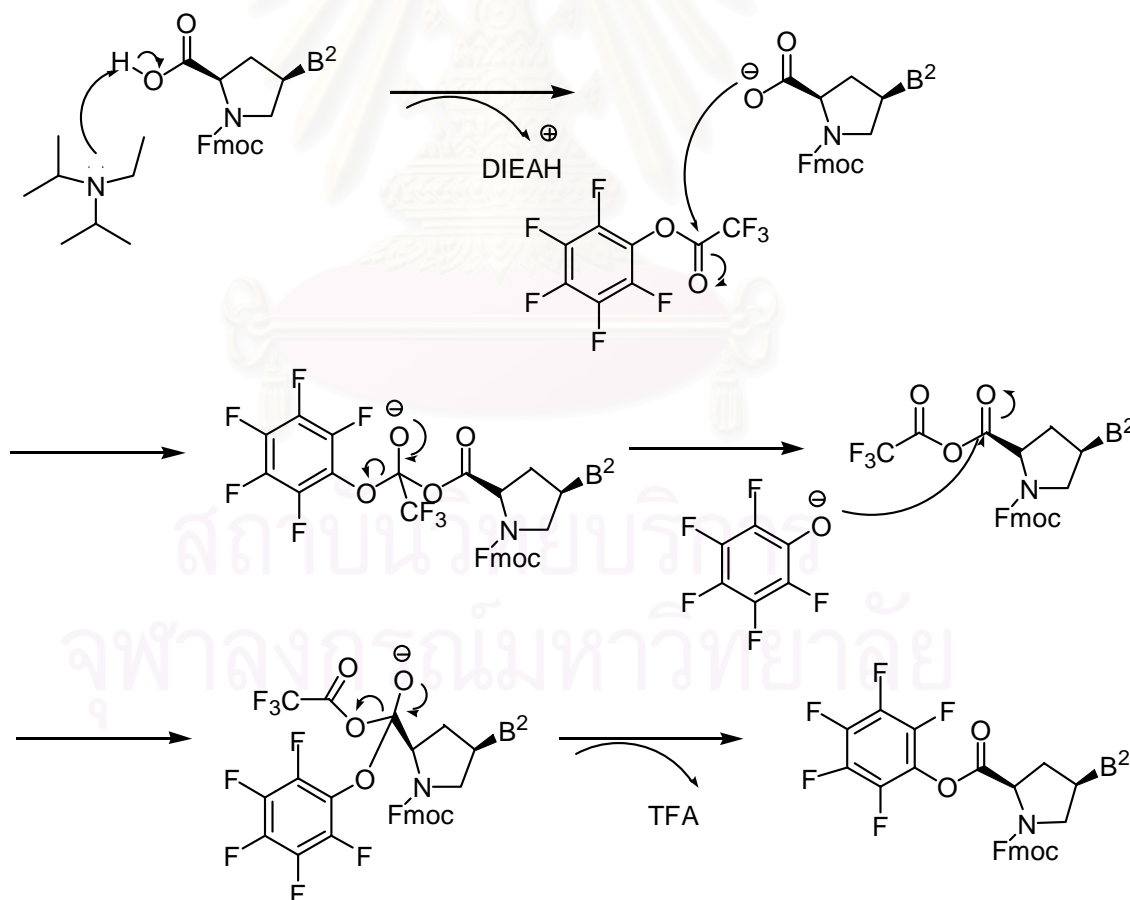


**Figure 3.2** Reaction mechanism for the protection of the Fmoc free acid with Pfp.

The Fmoc Pfp ester derivatives (**12**, **15**, **18** and **21**) were used as monomer in solid phase peptide synthesis which will be described in the next section.

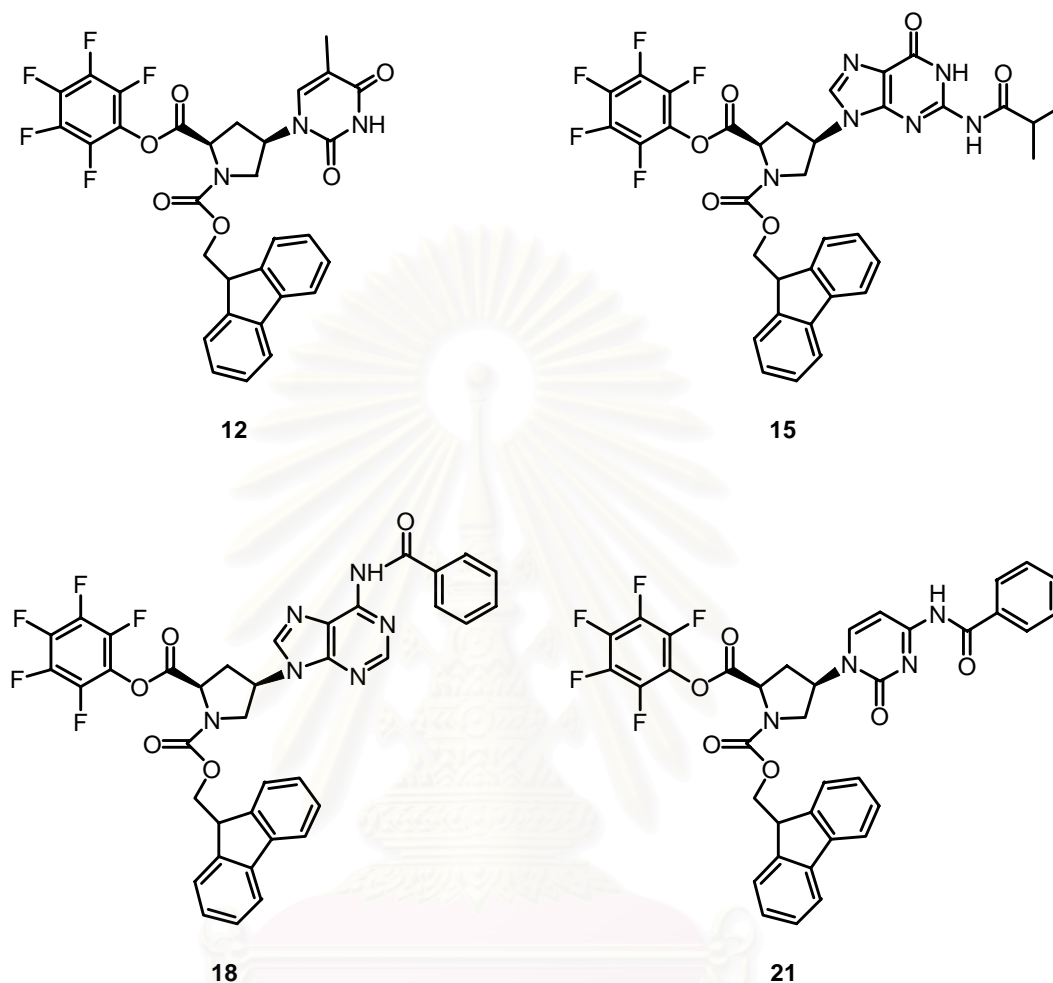


**Figure 3.3** Structure of Fmoc Pfp ester derivative monomers (**12**, **15**, **18** and **21**) for solid phase peptide synthesis.

### 3.2 Synthesis of spacer

Synthesis of Fmoc (1*S*, 2*S*)-2-amino-cyclopentanecarboxylic acid pentafluorophenyl ester (**28**) was accomplished starting from ethyl (1*S*, 2*S*)-2-[(1'*S*)-phenylethyl]-aminocyclopentanecarboxylate (**24**) (**Figure 3.4**).<sup>[49]</sup> After hydrogenation and hydrolysis, the free acid (**26**) was obtained as a white solid. This compound (**26**) was reacted with FmocOSu and NaHCO<sub>3</sub> in the same way as described for the protection of Fmoc of activated PNA monomer to give the Fmoc free acid (**27**) as a white solid in 61 % yield (from **25**). The product (**27**) showed a characteristic peak of Fmoc in <sup>1</sup>H NMR spectrum at 4.19, 4.42, 7.30, 7.39, 7.56 and 7.74 ppm. Moreover, the structure

was further confirmed by comparison of the specific rotation value ( $[\alpha]_D^{25} = +36.4$ ,  $c = 1.0$  in MeOH) with the value reported in the literature ( $[\alpha]_D^{25} = +36.3$ ,  $c = 1.2$  in MeOH).

After the protection of Fmoc, the Fmoc free acid (**27**) was reacted with PfpOTfa and DIEA in the same way as described for Pfp activation of the PNA monomers to afford the Fmoc-ACPC-Pfp spacer (**28**) as a white solid in 35 % yield.

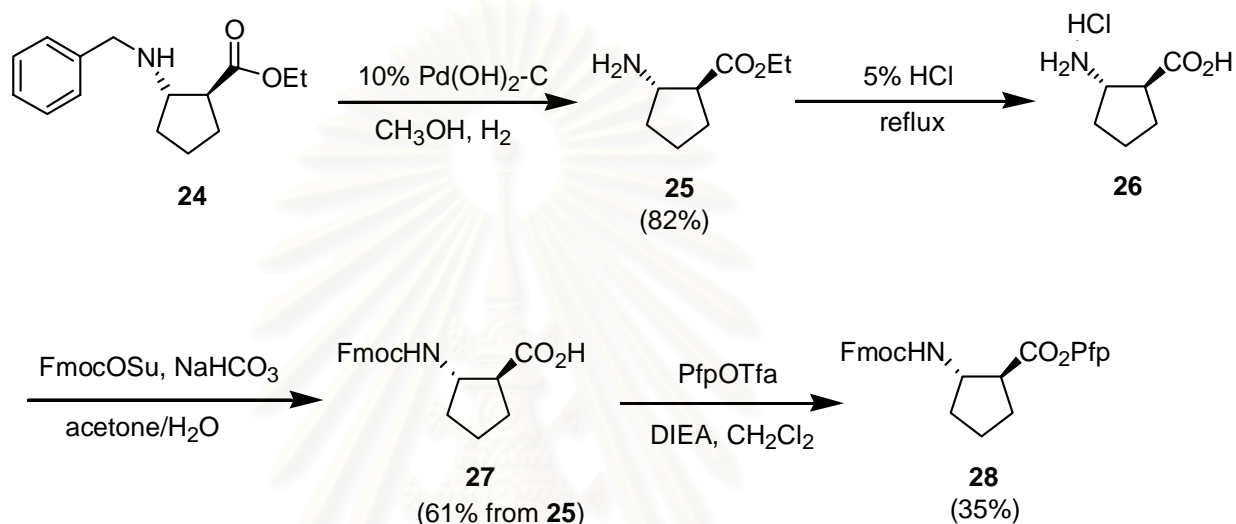
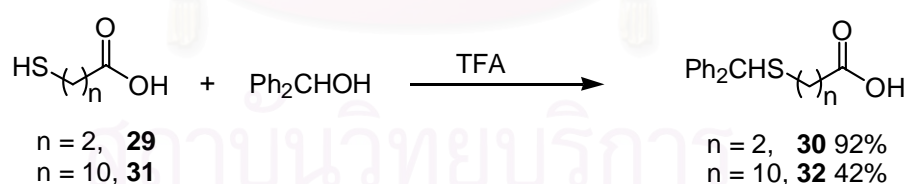


**Figure 3.4** Synthesis of Fmoc-ACPC-Pfp spacer (**28**).

### 3.3 Synthesis of S-protected thiols



For direct attachment of PNA on gold surface, the PNAs were first modified with a thiol group so that they can build a self-assembly monolayer (SAM) on gold surface. The S atom of thiol compounds (**29** and **31**) must be protected with temporary protecting group before being used in solid phase peptide synthesis in order to prevent intramolecular cyclization initiated by the free S at the N-terminus. Diphenylmethyl (Dpm) was considered for this purpose because it can protect during the peptide synthesis. Deprotection of the Dpm protecting group occurred under the same condition used for cleaving the PNA oligomer from the resin.

To protect S atom with Dpm protecting group, a mixture of thiol compound (**29** or **31**) and Ph<sub>2</sub>CHOH was slowly added TFA until the reaction mixture was homogeneous. TLC analysis revealed that the reaction had completed, the volatile was removed by a stream of N<sub>2</sub> gas. The residue was diluted with diethyl ether and extracted with water. The organic phase was evaporated to give compounds **30** and **32** as white solids in 92 % and 42 % yield, respectively. The mechanism for this step is shown in **Figure 3.5**.

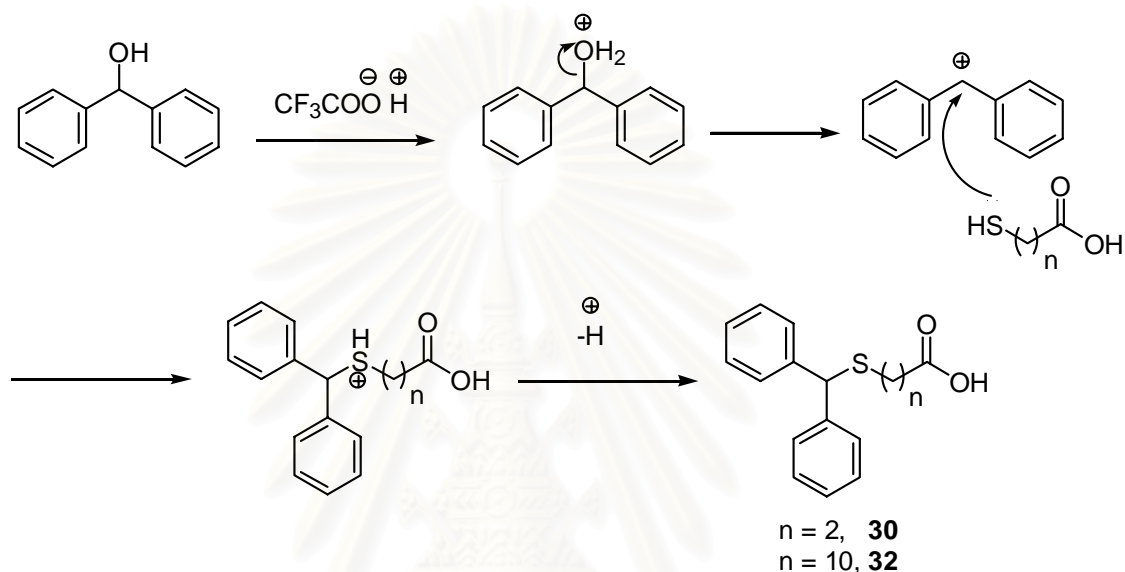


**Figure 3.5** Reaction mechanism for the protection of the S atom with Dpm.

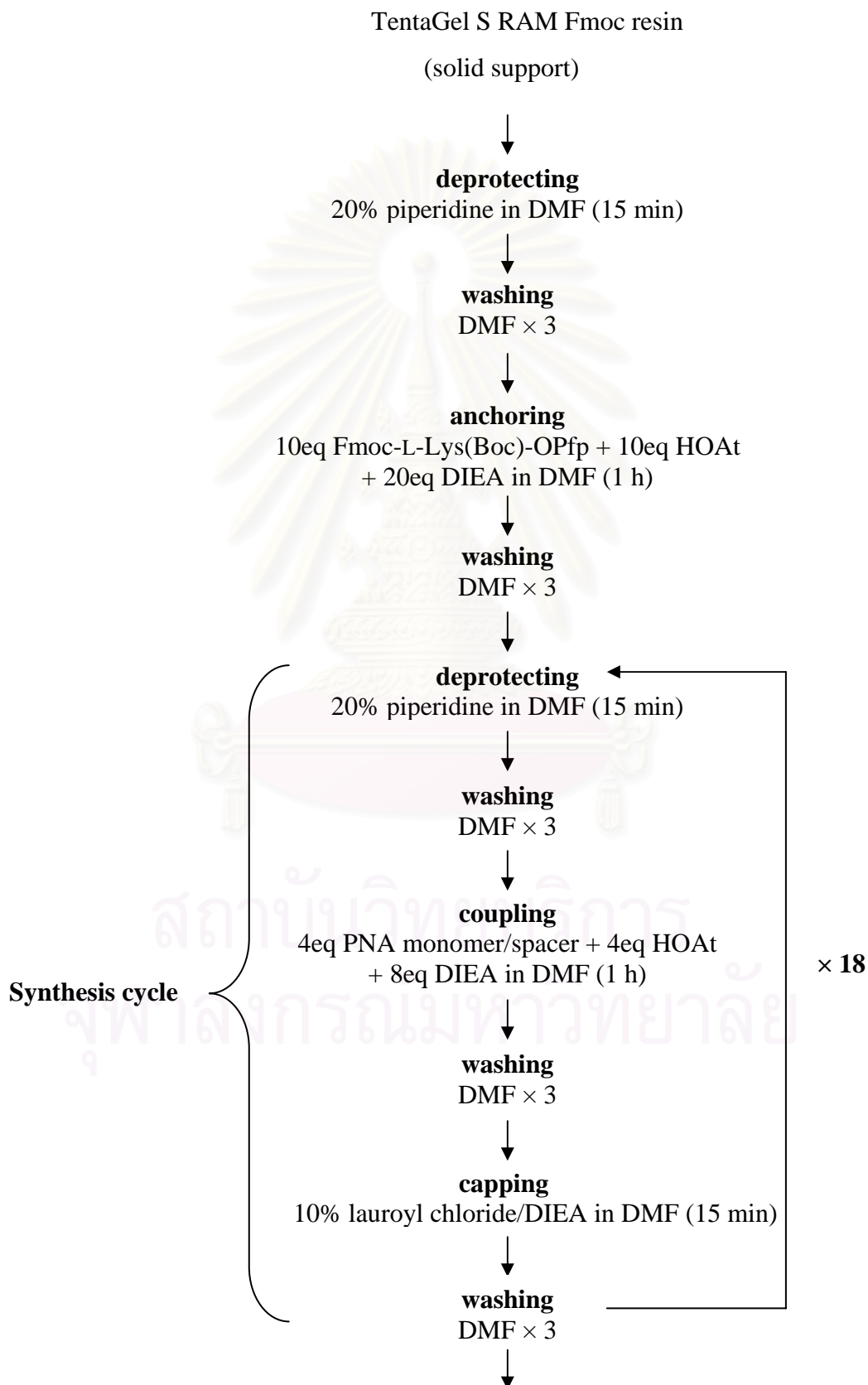
### 3.4 Synthesis of thiol-modified PNA nonamer by solid phase peptide synthesis

Solid Phase Peptide Synthesis (SPPS) was introduced by Merrifield in 1963. [52] The technique involves growing of a peptide chain from amino acid building blocks on a heterogeneously solid support such as polystyrene resin. The reaction involves simple washing and filtration steps therefore minimizing product losses, producing higher-yield (milligram levels of material) and higher-purity peptides. The entire process occurs in the same reaction vessel.

Synthetic peptides are usually produced in a stepwise fashion starting from C (carboxyl) terminus to N (amino) terminus in a series of coupling cycles. In this work, three thiol-modified PNA nonamers were synthesized by solid phase peptide synthesis methodology. The results will be presented and discussed in each part as follows.



In practice, the micromole-scale syntheses of the three thiol-modified PNA nonamer were carried out manually in glass columns made from Pasteur pipette as described in section 2.2.5 using a methodology as shown in **Figure 3.6**.



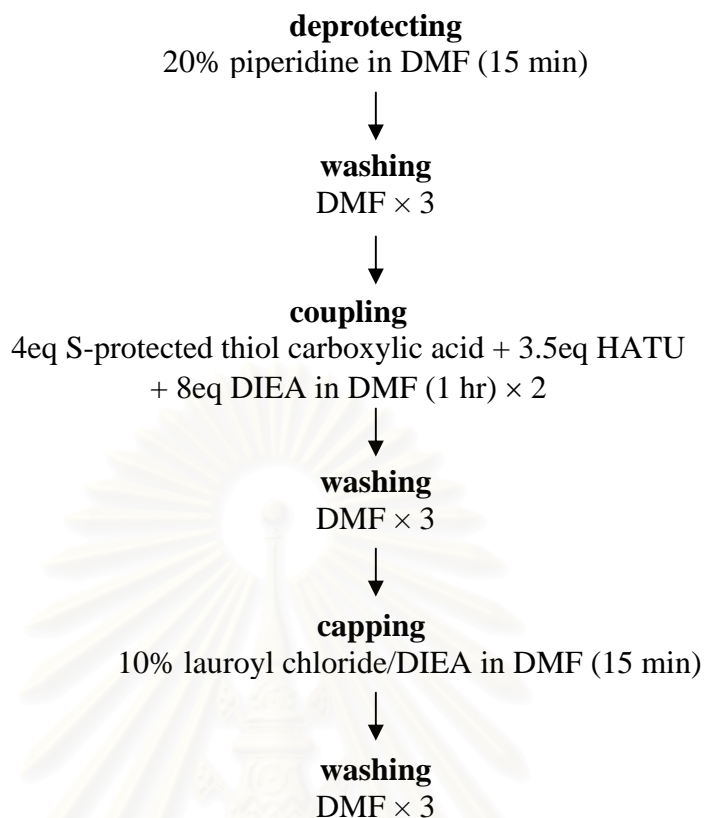


**Figure 3.6** The protocol for solid phase peptide synthesis of thiol-modified PNA nonamer.

The TentaGel S RAM resin (**Figure 3.7**) contains an acid labile Rink amide linker. The peptide-linker bonds are easily cleaved with 60-95 % TFA to provide peptide amides. In addition, RAM resin is also stable to piperidine, it is therefore compatible to Fmoc chemistry for solid phase. Moreover, the amino linker of RAM resin allow easy coupling with active esters to form amide bonds therefore giving higher loading efficiency as compared to resins containing hydroxyl linker such as Wang resin.

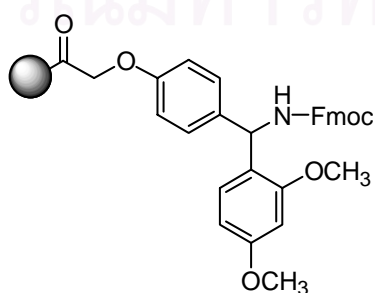


**Figure 3.7** TentaGel S RAM Fmoc resin.

The TentaGel S RAM Fmoc resin contains poly(ethylene glycol) modifier which is swellable in many solvents, making it an ideal support for peptide synthesis. In the first step, the resin was swollen in anhydrous DMF. In the next step, the deprotection was carried out by treatment of the resin with 20% piperidine in DMF for 15 min in order to remove the terminal Fmoc protecting group, which was released from the resin-bound peptide by an  $E_1CB$ -type mechanism (**Figure 3.8**) via the stabilized dibenzocyclopentadienyl anion. This was eventually trapped by piperidine to form a dibenzofulvene-piperidine adduct.

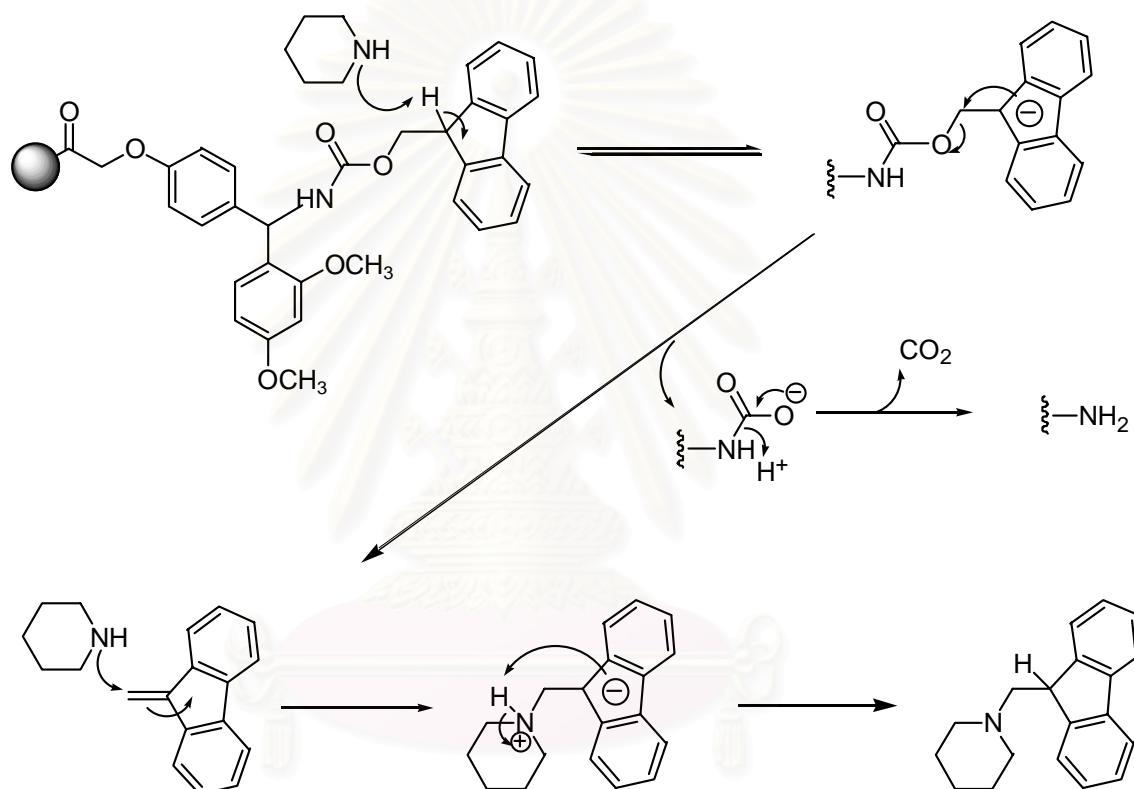


**Figure 3.8** Mechanism for deprotection of Fmoc protecting group from resin bound peptide.

Lysine was introduced at the C-terminus of peptide chain to prevent the self aggregation of the peptide chain and to increase the solubility of the peptide in aqueous medium due to the repulsion of the positively charged side chain.[1, 53-55] After deprotection, the resin was anchored with Fmoc-L-Lys(Boc)-OPfp as the first amino acid residue. This required the presence of HOAt as an auxiliary nucleophile or “activator” and DIEA as a base according to the mechanism in **Figure 3.9**. Due to the heterogeneous nature of SPPS which does not allow efficient mixing, the reaction at 1:1 stoichiometric proportion of reactants would require an impractically long

reaction time. Bearing this in mind, excess and high concentration (4 equivalents, > 0.1 M) of coupling reagents were generally used in order to enhance the coupling efficiency within a reasonable time scale.

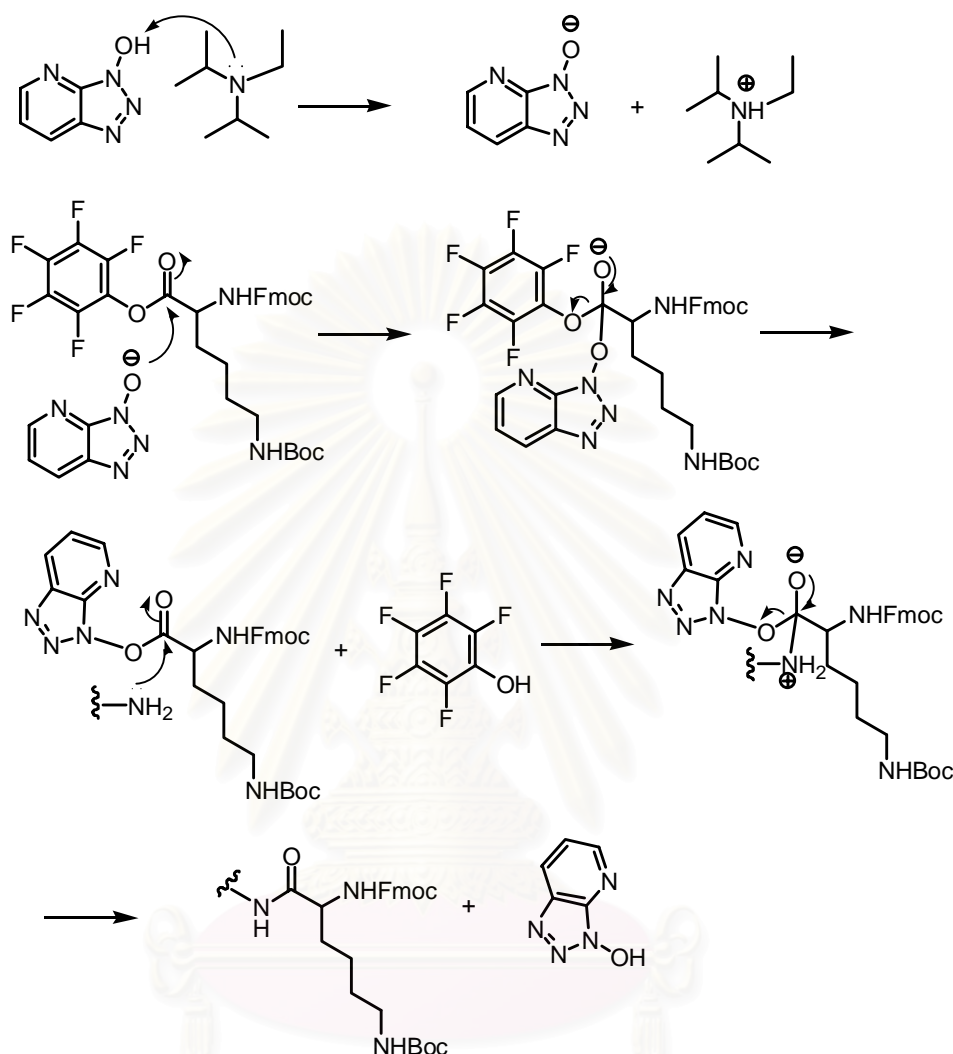


**Figure 3.9** The mechanism for coupling of anchoring via HOAt activation.

The next step of the synthesis cycle consisted of i) deprotection of the Fmoc group, ii) alternated coupling with PNA monomer and spacer and iii) capping with lauroyl chloride. Extensive washing with DMF was performed after each step.

The mechanisms for deprotection of the Fmoc group and coupling with PNA monomer or spacer in the synthesis cycle were similar to the mechanisms shown in **Figure 3.8** and **3.9**, respectively.

Estimation of the coupling efficiency could be performed by diluting the resulting deprotecting solution with an appropriate volume of methanol and then measuring the UV-absorption of the dibenzofulvene-piperidine adduct at 264 nm. The

absorption value is related to the total amounts of Fmoc group remained on the resin-bound peptide before deprotection step and indirectly indicated the efficiency of the previous coupling cycle.[56] For the sake of convenience, it was proposed that the first absorption value obtained after deprotection of Fmoc-Lys-peptide-resin corresponded to 100 % coupling efficiency. Therefore, comparison of the net absorption with this initial value could be used to calculate the percent of coupling efficiency after each coupling step and the overall efficiency of the synthesis could be evaluated.

In practice, even after coupling with excess reagent, the coupling efficiency was not always approaching 100%. Some of the residual free amino groups on the resin remained uncoupled and was still reactive enough to react with the monomer in the next coupling cycles. This situation was therefore resulted in skipping of one coupling cycle which brought about missing of a repeating unit in peptide chain. In fact, this might happen more than once and might occur anywhere in peptide chain. The resulting “incomplete peptide” is generally called “deletion sequences” and would contaminate the peptide product. However, it was possible to solve this problem by “capping” the unreacted amino group residue at N-terminus on resin with 10% lauroyl chloride/DIEA in DMF in order to diminish the nucleophilicity of the nitrogen atom at the N-terminus so that it will stop growing in the next coupling cycles. The use of a hydrophobic capping reagent such as lauroyl chloride also changed the polarity of incomplete peptide chain which would be easy to purify by reverse phase HPLC, hence it is the capping reagent of choice.[50] The mechanism of the capping step is demonstrated in **Figure 3.10**.

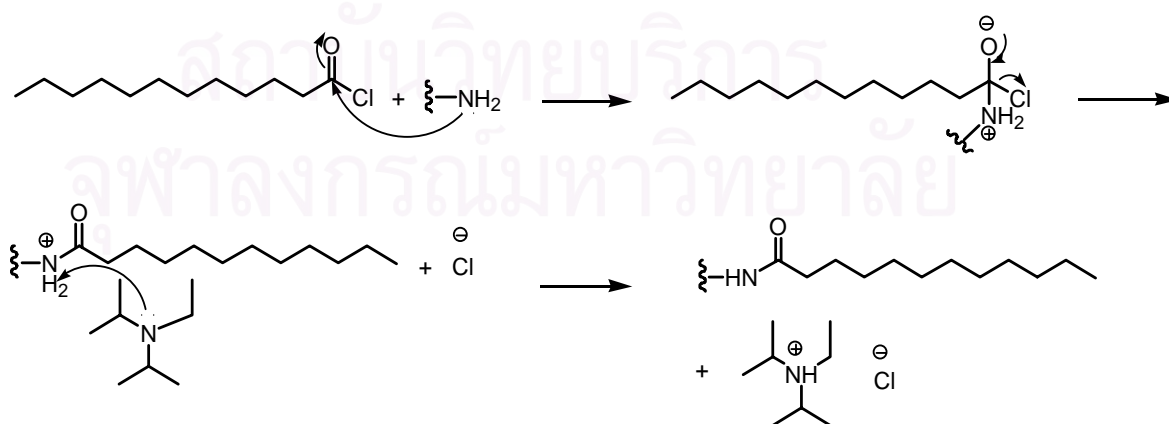


**Figure 3.10** The mechanism for capping of the unreacted amino group residue with 10% lauroyl chloride/DIEA in DMF.

The synthesis cycle was repeated until the growing peptide chain was extended up to nonamer. After final cleavage of Fmoc, the N-terminus was coupled with the S-protected thiol modifier. This was carried out in the presence of HATU and DIEA according to the mechanism in **Figure 3.11** to give the thiol-modified PNA nonamer in S-protected form.

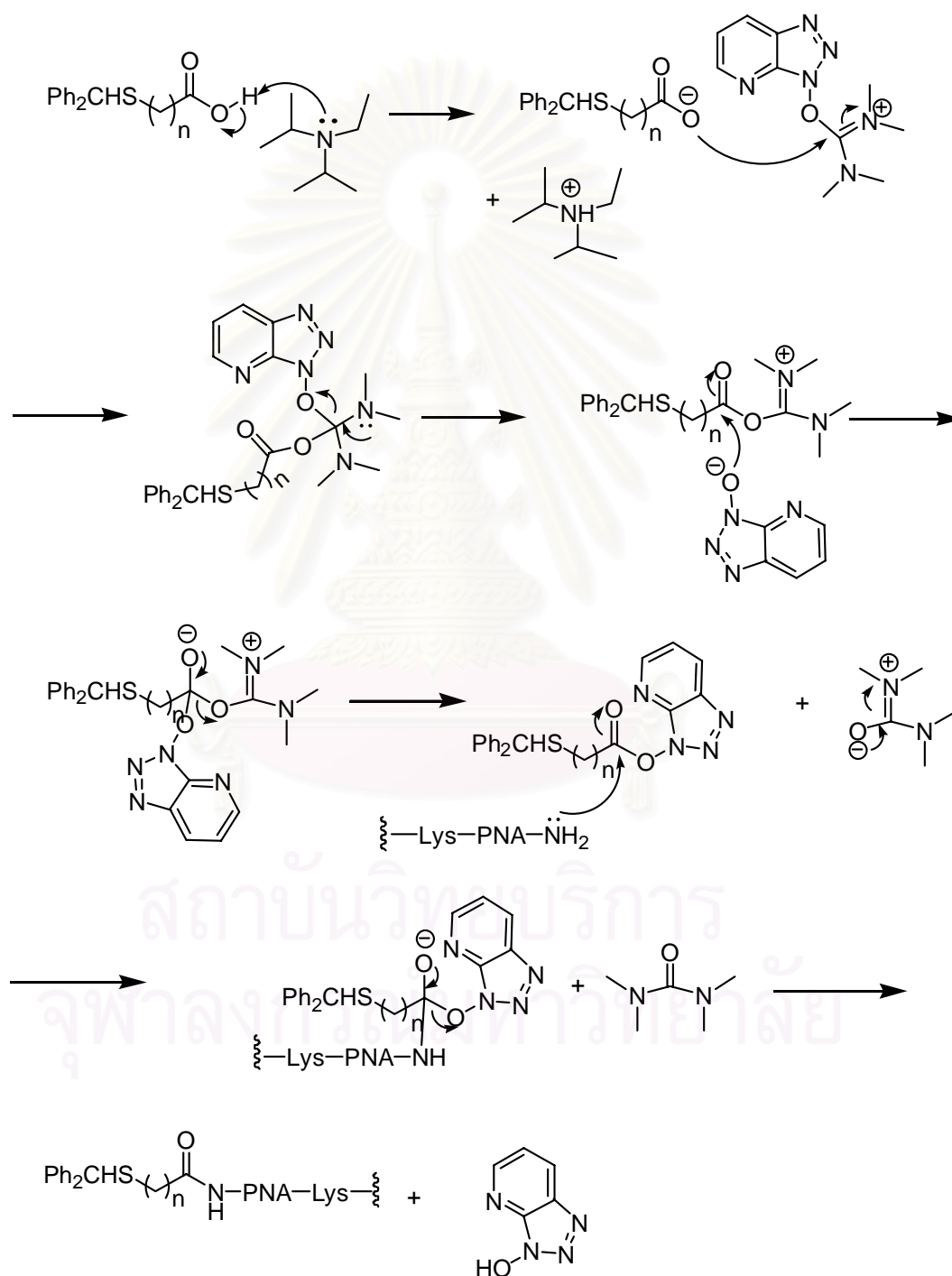


**Figure 3.11** The mechanism for coupling of S-protected thiol via HATU activation.

In the case of nonamer  $\text{HS}(\text{CH}_2)_2\text{CO-TTCTATGTT-LysNH}_2$  (**35**), the nucleobase protecting groups (Bz, Ibu) remained on the peptide chain. This must be first deprotected after completion of the synthesis by treatment of the resin with aqueous ammonia/dioxane 1:1 at 60 °C for 6 h. Finally, the nonamer resin bound peptide was released from the resin and the protecting group (diphenylmethyl) on the S-atom was removed by treatment with 10% anisole in trifluoroacetic acid for 2 h according to the mechanism in **Figure 3.12**. During the time, the resin became red due to the formation of a resin-bound diphenylmethyl cation. The volatile trifluoroacetic acid was removed by a nitrogen stream in the fume hood which gave a gummy residue. A white precipitate obtained from washing this gummy residue with ether and air-drying can directly be used for self-assembly monolayer (SAMs) formation on gold-coated piezoelectric quartz crystals.



สถาบันวิทยบริการ  
จุฬาลงกรณ์มหาวิทยาลัย

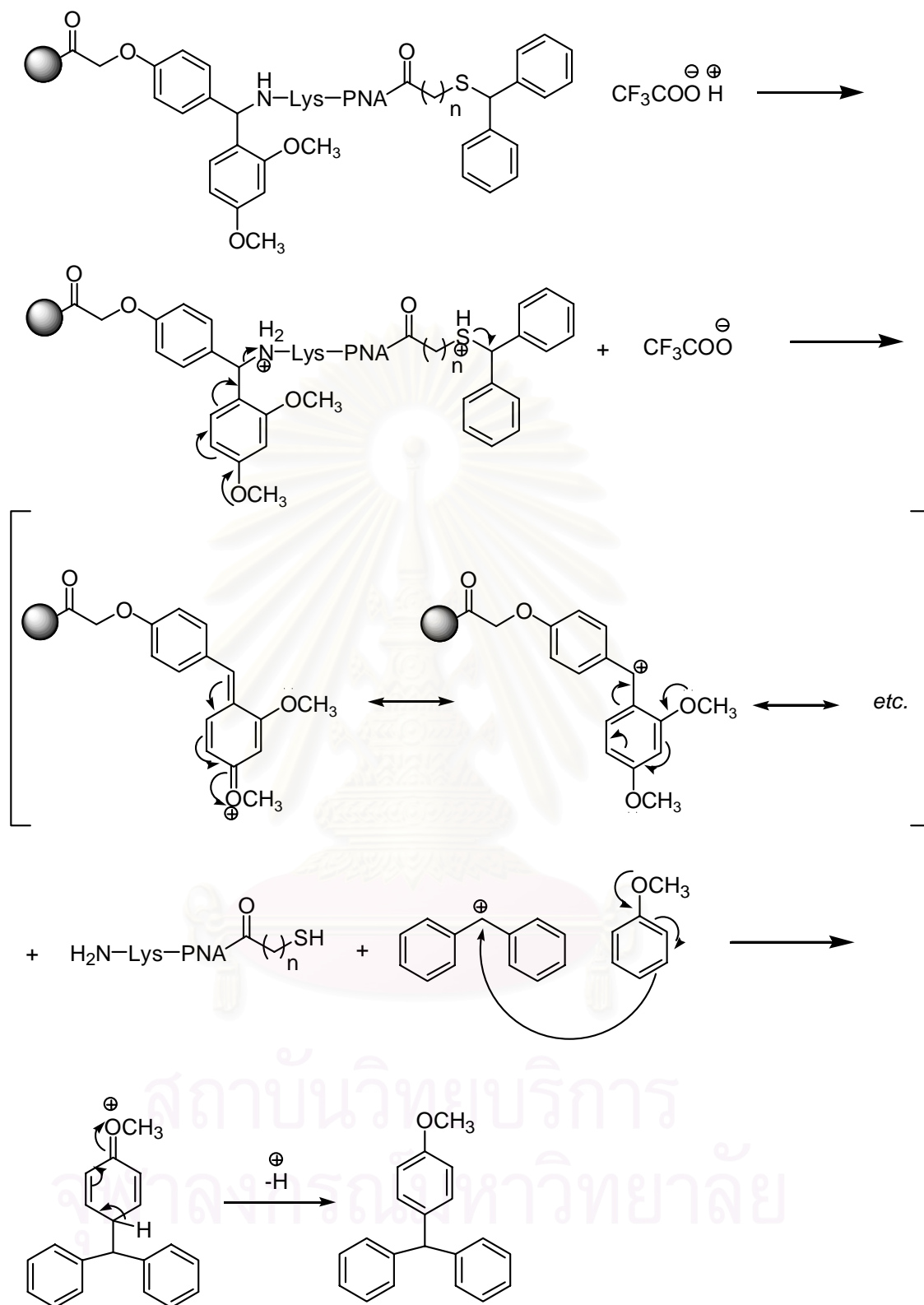
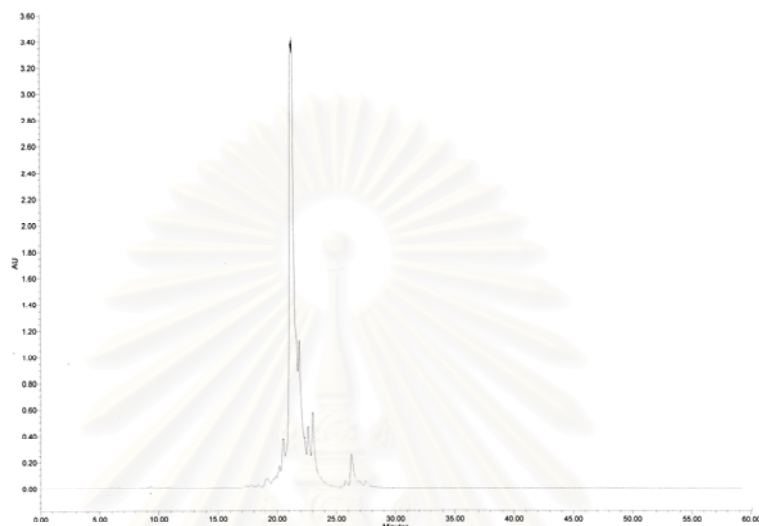


**Figure 3.12** The mechanism for cleavage the thiol-modified PNA nonamer from the resin and deprotection at S-atom by treatment with 10% anisole in trifluoroacetic acid.



The crude PNAs were purified by reverse phase HPLC using the gradient system as described in section 2.2.5 (b)(viii). The HPLC chromatogram of HS(CH<sub>2</sub>)<sub>2</sub>CO-T<sub>9</sub>-LysNH<sub>2</sub> (**33**) and HS(CH<sub>2</sub>)<sub>2</sub>CO-TTCTATGTT-LysNH<sub>2</sub> (**35**) are shown in **Figure 3.13** and **3.14**, respectively.



(a)



(b)

**Figure 3.13** Chromatogram of HS(CH<sub>2</sub>)<sub>2</sub>CO-T<sub>9</sub>-LysNH<sub>2</sub> (**33**): (a) before and (b) after purification by reverse phase HPLC.

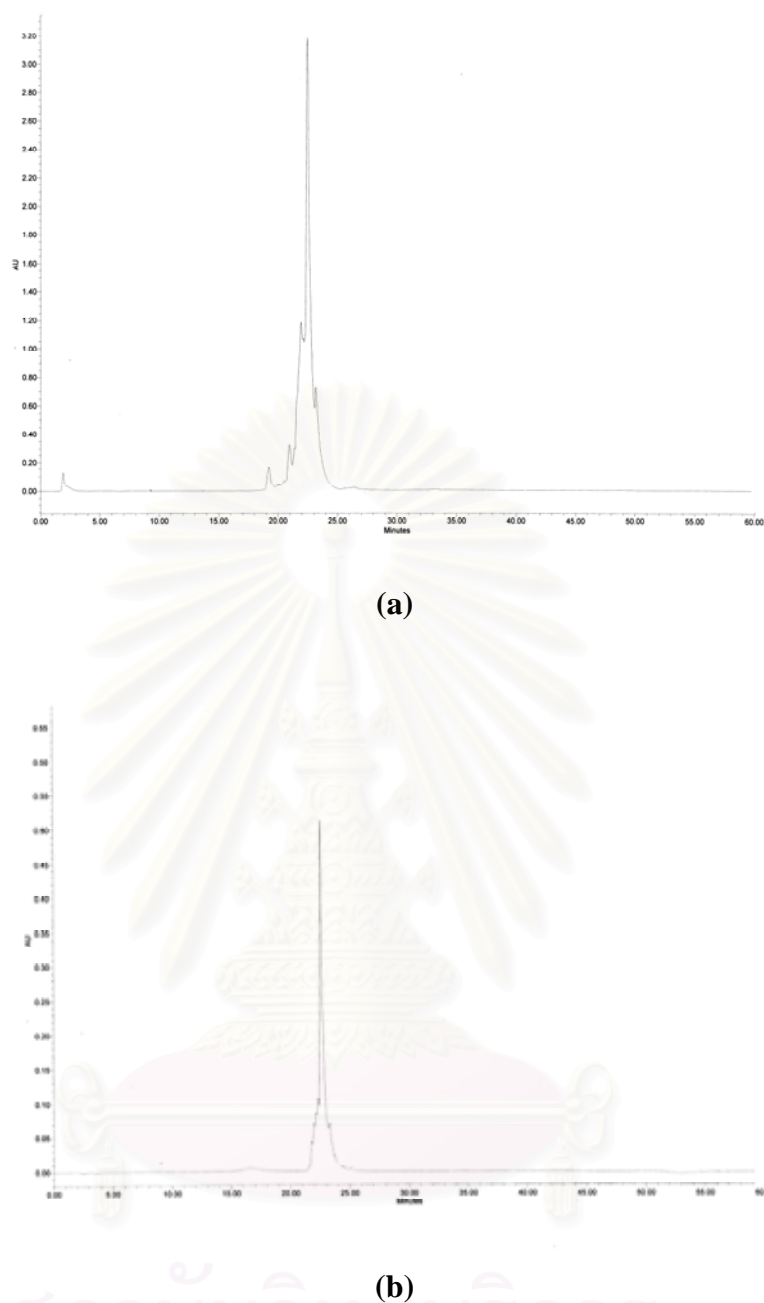
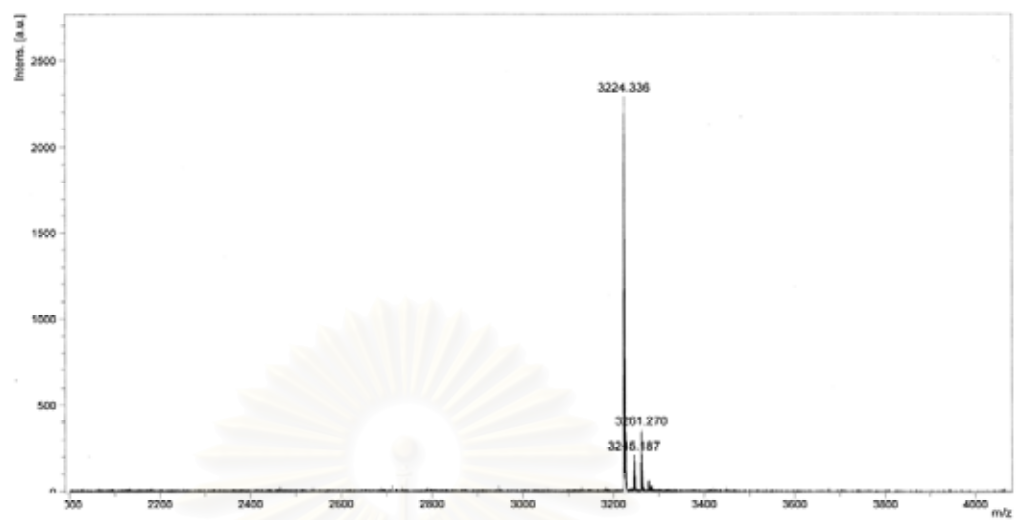
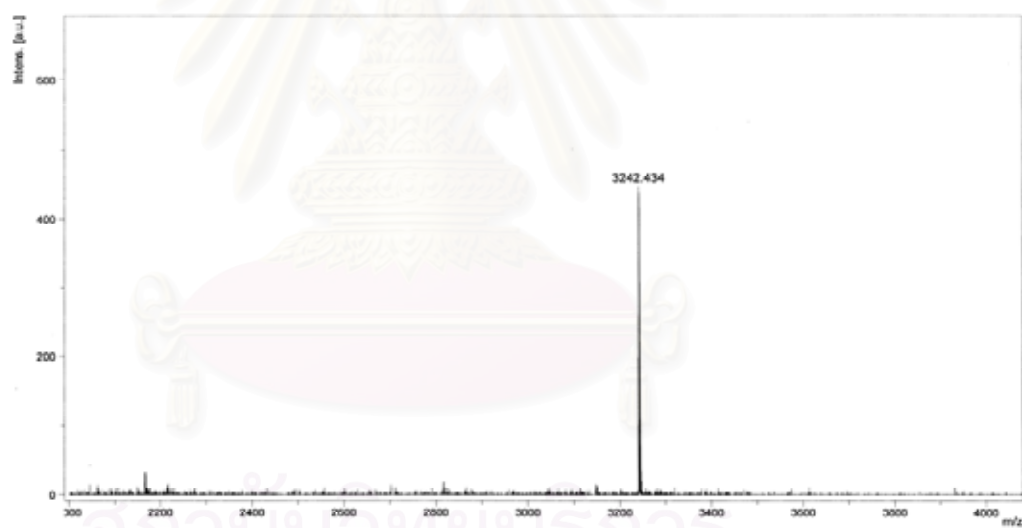


**Figure 3.14** Chromatogram of HS(CH<sub>2</sub>)<sub>2</sub>CO-TTCTATGTT-LysNH<sub>2</sub> (35): (a) before and (b) after purification by reverse phase HPLC.

The thiol-modified PNA nonamers were obtained after reverse phase HPLC separation as a single sharp peak (**Figure 3.13(b)** and **3.14(b)**) and were characterized by MALDI-TOF mass spectrometry (**Figure 3.15**).



(a)



(b)

**Figure 3.15** MALDI-TOF mass spectra of (a)  $\text{HS}(\text{CH}_2)_2\text{CO-T}_9\text{-LysNH}_2$  (**33**) and (b)  $\text{HS}(\text{CH}_2)_2\text{CO-TTCTATGTT-LysNH}_2$  (**35**) after purification by reverse phase HPLC.

The coupling efficiency calculated from UV-absorption, retention time ( $t_R$ ) obtained from HPLC and mass detected from MALDI-TOF in each nonamer were illustrated in **Table 3.4**. In all cases, the quasi-molecular ions were clearly observed with MW within  $\pm 1.0$  Da to the calculated values, thus confirming the identities of all PNA synthesized.

**Table 3.4** Percent coupling efficiency,  $t_R$  and mass spectral data of the two thiol-modified PNA nonamers (**33** and **35**)

thiol-modified PNA nanomer	scale ( $\mu\text{mol}$ )	% efficiency* (overall)	$t_R$ (min)	mass	
				$\text{M}\cdot\text{H}^+$ (calcd)	$\text{M}\cdot\text{H}^+$ (found)
HS(CH <sub>2</sub> ) <sub>2</sub> CO-T <sub>9</sub> - LysNH <sub>2</sub> ( <b>33</b> )	1.0	77	20.6	3223.45	3224.34
HS(CH <sub>2</sub> ) <sub>2</sub> CO- TTCTATGTT- LysNH <sub>2</sub> ( <b>35</b> )	1.0	60	22.4	3242.48	3242.43

\* calculated from the initial absorbance of dibenzofulvene-piperidine adduct from deprotection of Fmoc lysine with the absorbance obtained from Fmoc deprotection of the last cycle.

In the case of HS(CH<sub>2</sub>)<sub>10</sub>CO-T<sub>9</sub>-LysNH<sub>2</sub> (**34**), there was a problem in the purification step by reverse phase HPLC due to its extreme hydrophobicity. HS(CH<sub>2</sub>)<sub>10</sub>CO-T<sub>9</sub>-LysNH<sub>2</sub> (**34**) which has a hydrophobic part (CH<sub>2</sub>)<sub>10</sub> prefers to partition on the stationary phase of reverse column (C<sub>18</sub>). Therefore, HS(CH<sub>2</sub>)<sub>10</sub>CO-T<sub>9</sub>-LysNH<sub>2</sub> (**34**) was not selected for further study and no characterization data was available.

### 3.5 Biophysical studies of thiol-modified PNA nonamer in solution

#### 3.5.1 $T_m$ experiments

DNA denaturation refers to the melting of double stranded DNA to generate two single strands. This involves the breaking of hydrogen bonds between the bases in the duplex. The purine and pyrimidine bases in DNA absorb UV light maximally at a wavelength of approximately 260 nm (**Figure 3.16**).<sup>[57]</sup> In double-stranded DNA, however, the magnitude of this absorption is decreased as a consequence of base-

stacking interactions.[57] When DNA is denatured, these interactions are disrupted and an increase in absorbance is seen. This absorbance change is called the hyperchromic effect. The extent of the effect can be monitored as a function of temperature. The denaturation of double stranded DNA is therefore easily followed spectrophotometrically.

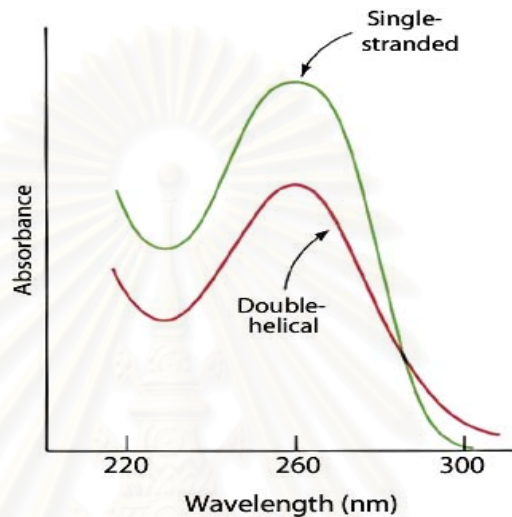


**Figure 3.16** The UV absorbance of single stranded DNA and double helical DNA.

Measurement of the absorbance of a DNA complex at 260 nm while slowly increasing the temperature provides a convenient mean to observe denaturation. In a typical thermal denaturation experiment, the polynucleotide absorbance typically changes very slowly at first, then rapidly rises to a maximum value (**Figure 3.17**). The temperature at which the DNA molecules are 50% denatured is the melting temperature ( $T_m$ ), which indicates the stability of the double-stranded DNA.

จุฬาลงกรณ์มหาวิทยาลัย

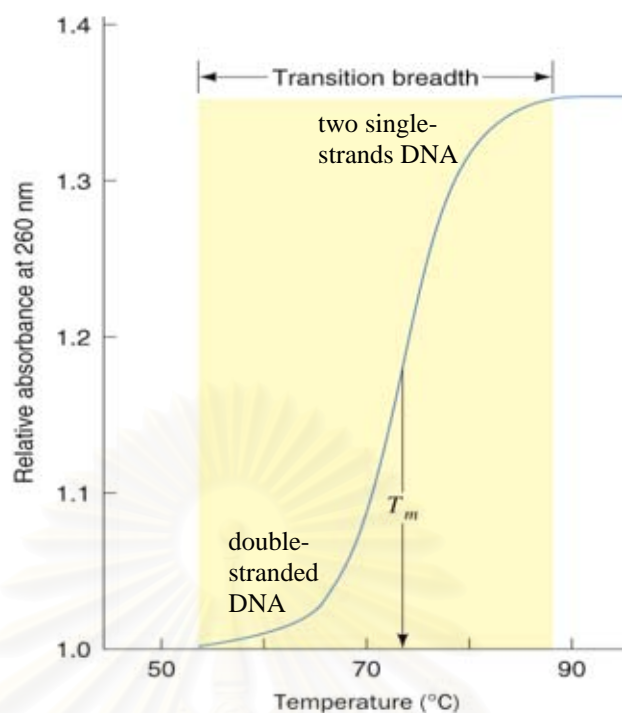


**Figure 3.17** The UV absorbance of  $T_m$  experiment.

Investigation of the binding properties of thiol-modified PNA nonamer HS(CH<sub>2</sub>)<sub>2</sub>CO-T<sub>9</sub>-LysNH<sub>2</sub> (**33**) with complementary DNA d(5'-AAAAAAAAA-3') or dA<sub>9</sub> in solution by  $T_m$  measurement was carried out to determine its applicability when self assembled on gold surface.

From the  $T_m$  experiments, melting of the PNA·DNA hybrid was observed at 260 nm. The  $T_m$  value was estimated to be 72 °C indicating that the HS(CH<sub>2</sub>)<sub>2</sub>CO-T<sub>9</sub>-LysNH<sub>2</sub> (**33**) formed stable hybrids with dA<sub>9</sub>. Repeating the  $T_m$  experiments between HS(CH<sub>2</sub>)<sub>2</sub>CO-T<sub>9</sub>-LysNH<sub>2</sub> (**33**) and different oligonucleotide nonamers containing one or two mismatch bases resulted in lowered  $T_m$  values of the complex by 20-27 °C per mismatch (**Figure 3.18** and **Table 3.5**, entry 1-7). Thus this thiol-modified PNA shows powerful discrimination for DNA in solution.

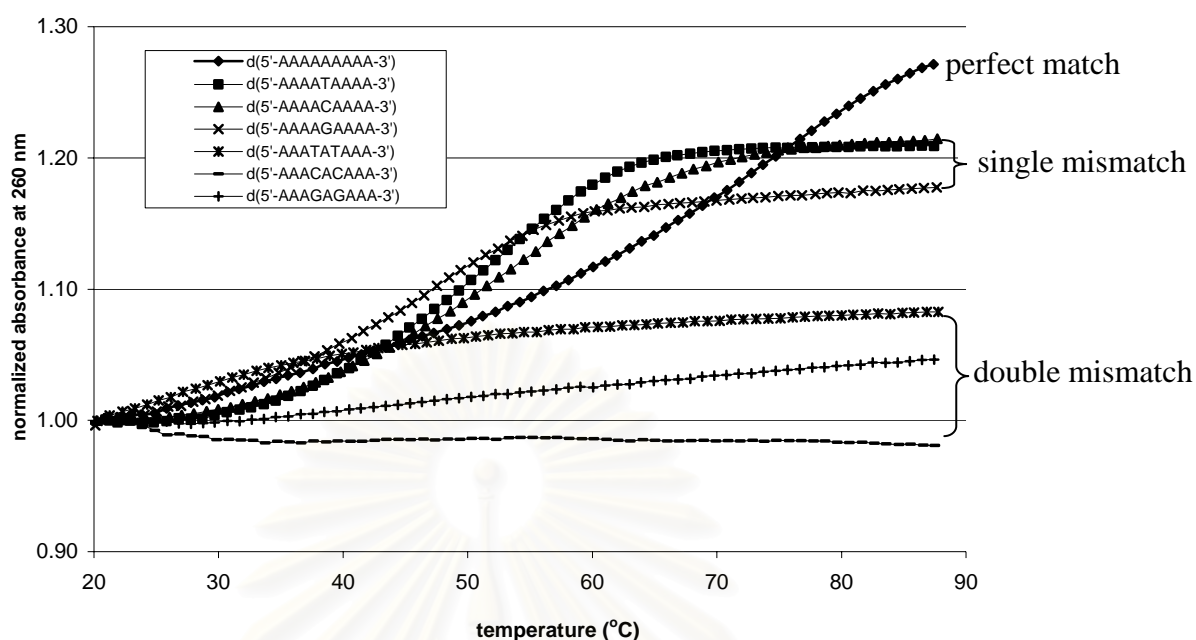


**Figure 3.18** Melting curves of HS(CH<sub>2</sub>)<sub>2</sub>CO-T<sub>9</sub>-LysNH<sub>2</sub> (**33**) with d(5'-AAAAAA AAA-3') or dA<sub>9</sub> (perfect match), d(5'-AAAAXAAA-3') (single mismatch, X = T, C and G) and d(5'-AAAXAXAAA-3') (double mismatch, X = T, C and G). The  $T_m$  was measured at molar ratio of PNA : DNA = 1:1; concentration of PNA strand = 1  $\mu$ M; 0.5 mM sodium phosphate buffer pH 7; heating rate 1  $^{\circ}$ C/min.

To investigate the effects of pH and ionic strength, the pH (6 and 8) of sodium phosphate buffer and salt concentration (1 and 10 mM NaCl) were changed in  $T_m$  experiments. In all cases, the binding experiments clearly indicate that the HS(CH<sub>2</sub>)<sub>2</sub>CO-T<sub>9</sub>-LysNH<sub>2</sub> (**33**) formed stable hybrids with dA<sub>9</sub> and gave high  $T_m$  (69-74  $^{\circ}$ C) (**Figure 3.19**, **3.20** and **Table 3.5**, entry 1 and 8-11). It appeared that the  $T_m$  of HS(CH<sub>2</sub>)<sub>2</sub>CO-T<sub>9</sub>-LysNH<sub>2</sub> (**33**) and dA<sub>9</sub> hybrid in solution changes only little at various pH and ionic strength.

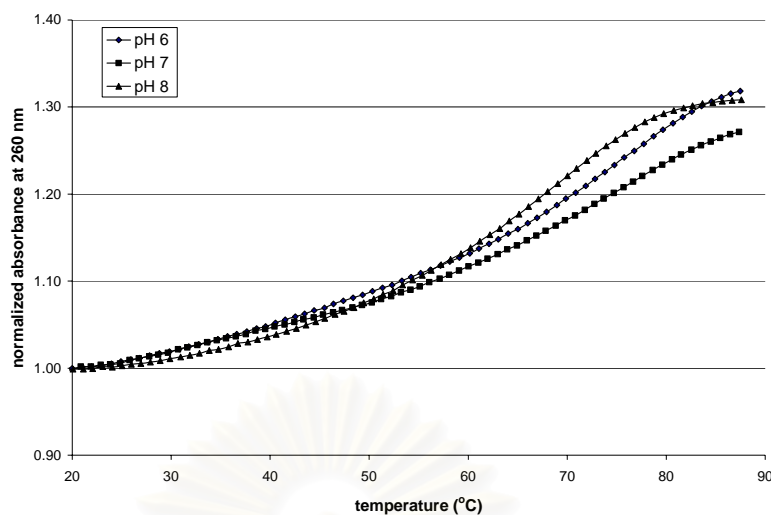


**Figure 3.19** Melting curves of  $\text{HS}(\text{CH}_2)_2\text{CO-T}_9\text{-LysNH}_2$  (**33**) with  $\text{dA}_9$  (perfect match). The  $T_m$  was measured at a ratio of PNA : DNA = 1:1; concentration of PNA strand =  $1 \mu\text{M}$ ;  $0.5 \text{ mM}$  sodium phosphate buffer pH 6, 7 and 8; heating rate  $1 \text{ }^\circ\text{C}/\text{min}$ .

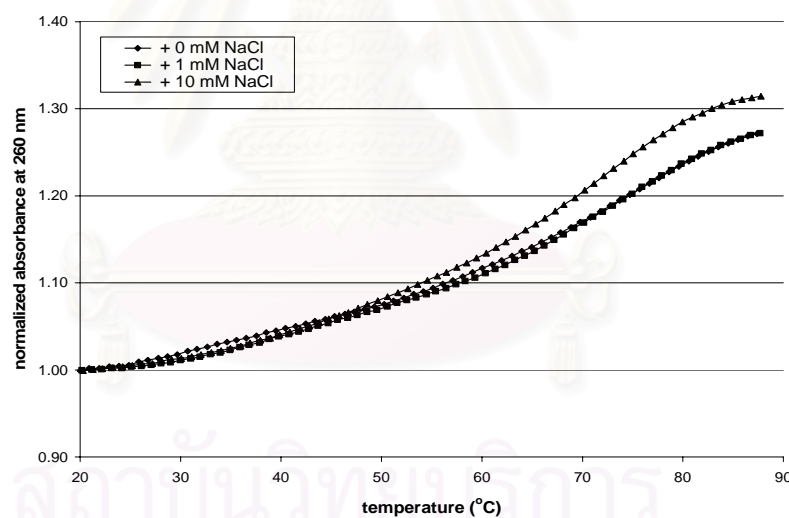


**Figure 3.20** Melting curves of  $\text{HS}(\text{CH}_2)_2\text{CO-T}_9\text{-LysNH}_2$  (**33**) with  $\text{dA}_9$  (perfect match). The  $T_m$  was measured at a ratio of PNA : DNA = 1:1; concentration of PNA strand =  $1 \mu\text{M}$ ;  $0.5 \text{ mM}$  sodium phosphate buffer pH 7 + 0, 1 and  $10 \text{ mM}$  NaCl; heating rate  $1 \text{ }^\circ\text{C}/\text{min}$ .



Moreover, the binding affinity of thiol-modified PNA nonamer having mixed nucleobases, HS(CH<sub>2</sub>)<sub>2</sub>CO-TTCTATGTT-LysNH<sub>2</sub> (**35**) with its anti parallel target DNA was investigated. The melting curve (**Figure 3.21**) indicates that the HS(CH<sub>2</sub>)<sub>2</sub>CO-TTCTATGTT-LysNH<sub>2</sub> (**35**) formed a stable hybrid with d(5'-AACATAGAA-3'). The mixture of HS(CH<sub>2</sub>)<sub>2</sub>CO-TTCTATGTT-LysNH<sub>2</sub> (**35**) and d(5'-AACATAGAA-3') has a slightly lower  $T_m$  value (54 °C) compared with the case of perfect match in HS(CH<sub>2</sub>)<sub>2</sub>CO-T<sub>9</sub>-LysNH<sub>2</sub> (**33**). On the other hand, HS(CH<sub>2</sub>)<sub>2</sub>CO-TTCTATGTT-LysNH<sub>2</sub> (**35**) failed to form hybrids with single mismatched DNAs (d(5'-AACAXAGAA-3'), X = G, A and C) and triple mismatched DNA (dA<sub>9</sub>) (**Figure 3.21** and **Table 3.5**, entry 13-16). It can be concluded that the binding affinity of PNA with DNA is dependent on the base sequences on PNA and DNA. Only PNA and DNA complementary base forms a stable hybrid which is the most desirable property for sensor applications.

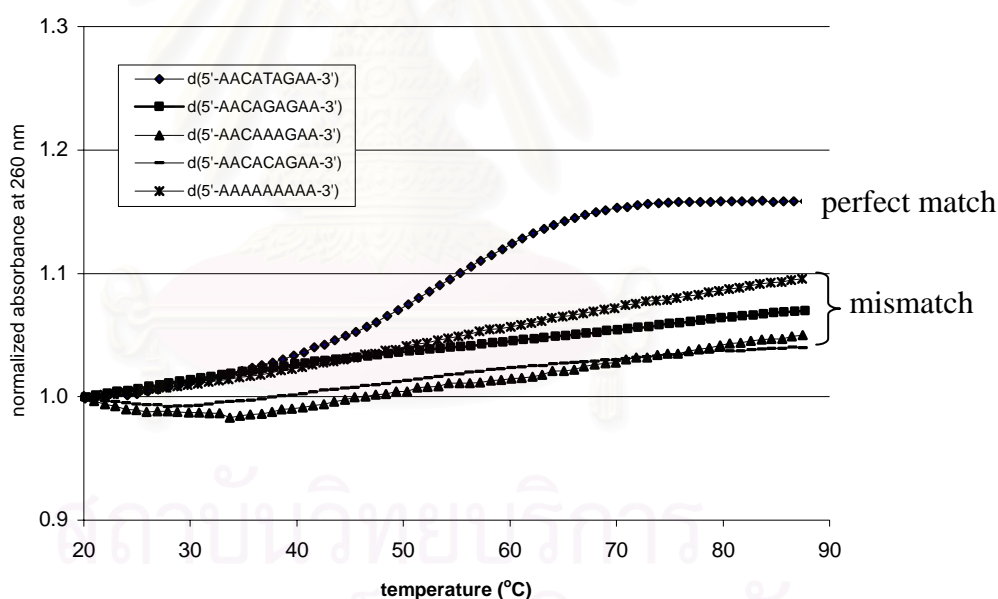


**Figure 3.21** Melting curves of HS(CH<sub>2</sub>)<sub>2</sub>CO-TTCTATGTT-LysNH<sub>2</sub> (**35**) with d(5'-AACATAGAA-3') (perfect match), d(5'-AACAXAGAA-3') (single mismatch, X = G, A and C) and dA<sub>9</sub> (triple mismatch). The  $T_m$  was measured at a ratio of PNA : DNA = 1:1; concentration of PNA strand = 1 μM; 0.5 mM sodium phosphate buffer pH 7; heating rate 1 °C/min.

**Table 3.5**  $T_m$  values of hybrids between thiol-modified PNA nonamer and oligo – nucleotides.

entry	PNA	oligonucleotide <sup>a</sup> (condition)	$T_m^b$ (°C)	note
1	(33)	d(5'-AAAAAAAAA-3') or dA <sub>9</sub>	72	perfect match
2	(33)	d(5'-AAAAT <u>T</u> AAAA-3')	52	single mismatch
3	(33)	d(5'-AAAAC <u>C</u> AAAA-3')	52	single mismatch
4	(33)	d(5'-AAAAG <u>G</u> AAAA-3')	48	single mismatch
5	(33)	d(5'-AAAT <u>T</u> A <u>T</u> AAA-3')	25	double mismatch
6	(33)	d(5'-AAAC <u>C</u> A <u>C</u> AAA-3')	<20	double mismatch
7	(33)	d(5'-AAAG <u>G</u> A <u>G</u> AAA-3')	<20	double mismatch
8	(33)	dA <sub>9</sub> (pH 6)	74	perfect match
9	(33)	dA <sub>9</sub> (pH 8)	69	perfect match
10	(33)	dA <sub>9</sub> (1 mM NaCl)	73	perfect match
11	(33)	dA <sub>9</sub> (10 mM NaCl)	71	perfect match
12	(35)	d(5'-AACATAGAA-3')	54	perfect match
13	(35)	d(5'-AACAG <u>G</u> AGAA-3')	<20	single mismatch
14	(35)	d(5'-AACAA <u>A</u> AGAA-3')	<20	single mismatch
15	(35)	d(5'-AACAC <u>C</u> AGAA-3')	<20	single mismatch
16	(35)	d(5'-AAA <u>A</u> AA <u>A</u> AAA-3') or dA <sub>9</sub>	<20	triple mismatch

<sup>a</sup>The  $T_m$  was measured at a ratio of PNA : DNA = 1:1; concentration of PNA strand = 1  $\mu$ M; 0.5 mM sodium phosphate buffer pH 7; heating rate 1 °C/min.

<sup>b</sup> $T_m$  was determined from first derivative plot.

### 3.6 Immobilization of thiol-modified PNA nonamer on gold surface

#### 3.6.1 QCM analysis

To study concentration-dependent SAM formation of HS(CH<sub>2</sub>)<sub>2</sub>CO-T<sub>9</sub>-LysNH<sub>2</sub> (33) on gold electrode, after F<sub>1</sub> of a cleaned gold electrode was obtained, the gold electrode was immersed in the thiol-modified PNA HS(CH<sub>2</sub>)<sub>2</sub>CO-T<sub>9</sub>-LysNH<sub>2</sub> (33) solution (1.5 mL) for 24 h using concentration of 0.5, 1.0, 2.0, 5.0 and 10.0  $\mu$ M in MilliQ water. After washing and drying, the frequency of immobilized PNA gold electrode was recorded until the equilibrium value (F<sub>2</sub>) was obtained. The frequency

difference between  $F_1$  and  $F_2$  ( $\Delta F_i$ ) indicated the amount of immobilized PNA on the gold electrode.

Results from **Figure 3.22** suggested that the coverage of the  $\text{HS}(\text{CH}_2)_2\text{CO-T}_9\text{-LysNH}_2$  (**33**) on the gold electrode increased with the PNA concentration and the optimal concentration for the SAM formation of  $\text{HS}(\text{CH}_2)_2\text{CO-T}_9\text{-Lys NH}_2$  (**33**) was approximately  $5.0 \mu\text{M}$ .

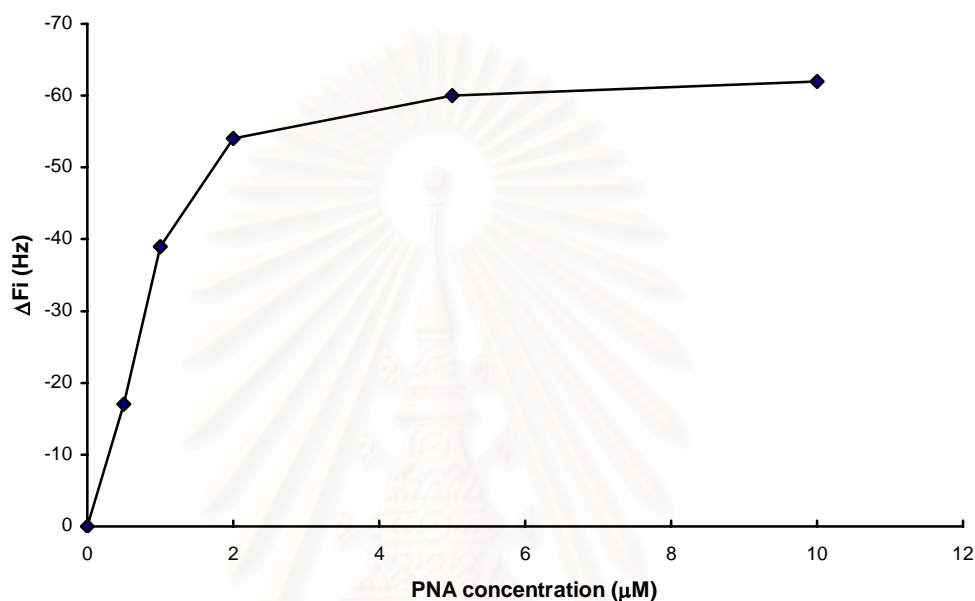


**Figure 3.22**  $\Delta F_i$  obtained upon increasing the PNA  $\text{HS}(\text{CH}_2)_2\text{CO-T}_9\text{-LysNH}_2$  (**33**) concentration.

### 3.6.2 AFM analysis

The surface coverage of the  $\text{HS}(\text{CH}_2)_2\text{CO-T}_9\text{-LysNH}_2$  (**33**) on the gold electrode was additionally assessed by comparing AFM images of the  $\text{HS}(\text{CH}_2)_2\text{CO-T}_9\text{-LysNH}_2$  (**33**) covered gold surface (**Figure 3.23(b)**) with the bare gold substrate (**Figure 3.23(a)**). As can be seen in **Figure 3.23**, the structure of the bare gold surface (rms roughness  $2.59 \text{ nm}$ ) is slightly roughened by the coverage of the thiol-modified PNA (rms roughness  $3.42 \text{ nm}$ ).

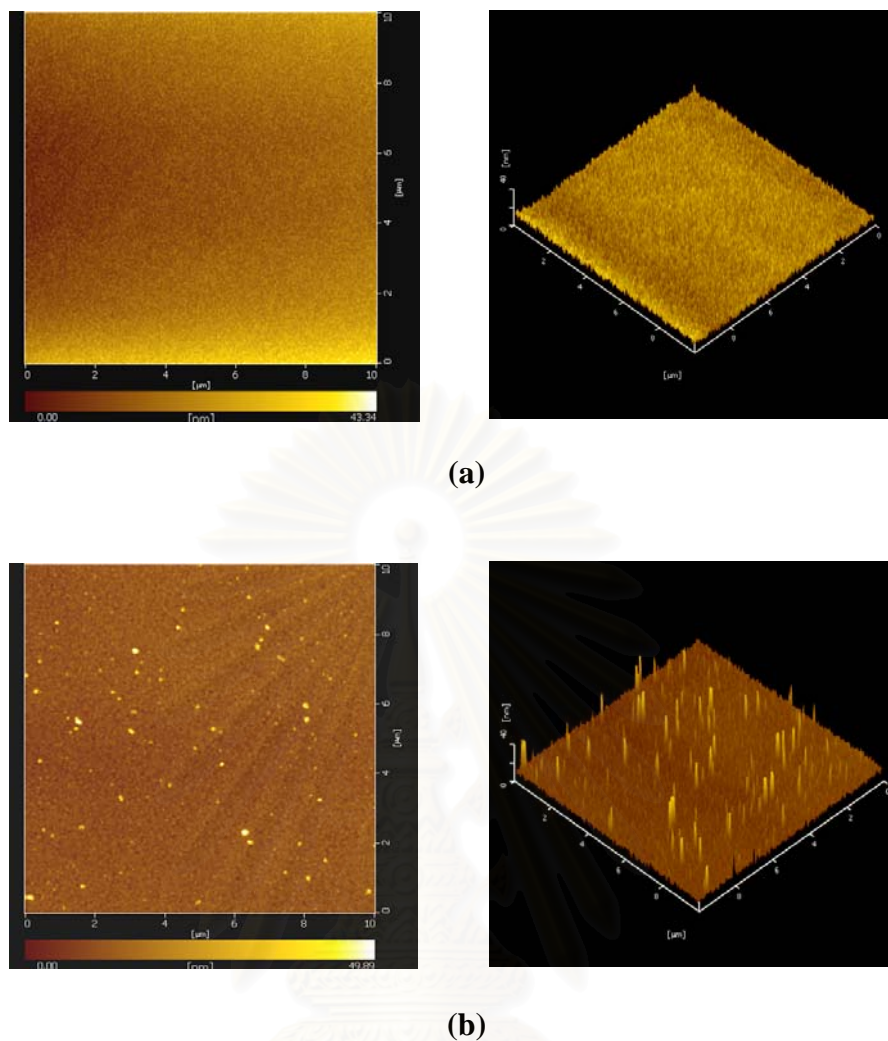


**Figure 3.23** AFM images of (a) bare gold surface (b) HS(CH<sub>2</sub>)<sub>2</sub>CO-T<sub>9</sub>-LysNH<sub>2</sub> (**33**) PNA immobilized on gold surface for 24 h using PNA concentration of 5.0 μM.

### 3.6.3 RAIRS analysis

The reflection absorption infrared spectroscopy (RAIRS) is a surface-sensitive technique which has been used for characterization of molecular orientation on surface. RAIRS is a reliable technique that can be used to confirm the presence of thiol-modified PNA immobilized on gold surface.[26]

The spectra of thiol-modified PNA on gold surface obtained from RAIRS technique (**Figure 3.25**) contained similar features as seen in the IR spectrum of free PNA (KBr method) (**Figure 3.24**). Moreover, the signal-to-noise ratio was improved upon increasing the PNA concentration from 1 to 5 μM suggesting that the greater

quantity and perhaps better packing of self-assembled PNA were achieved at higher concentration. This is in good agreement with the result obtained from QCM analysis.

The main absorption regions in the IR and RAIRS spectra which are fully consistent with the PNA structure could be identified. First, amide group (peptide bonds), the most important vibrations of which are the C=O stretching of the amide bond at  $\sim 1700$ - $1640\text{ cm}^{-1}$  (Amide I) and the combination of N-H deformation and C-N stretching (Amide II) at  $\sim 1550$ - $1530\text{ cm}^{-1}$ . Second, the C-H stretching vibrations of CH and CH<sub>2</sub> groups are expected in the  $2975$ - $2840\text{ cm}^{-1}$  region and the CH<sub>2</sub> scissor vibration band at  $\sim 1460$ - $1420\text{ cm}^{-1}$ .

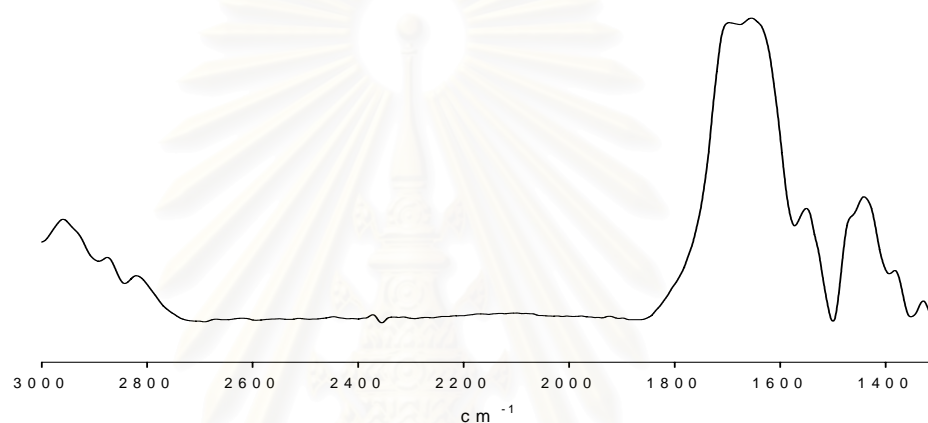


**Figure 3.24** IR (KBr method) spectrum of HS(CH<sub>2</sub>)<sub>2</sub>CO-T<sub>9</sub>-LysNH<sub>2</sub> (**33**) PNA.

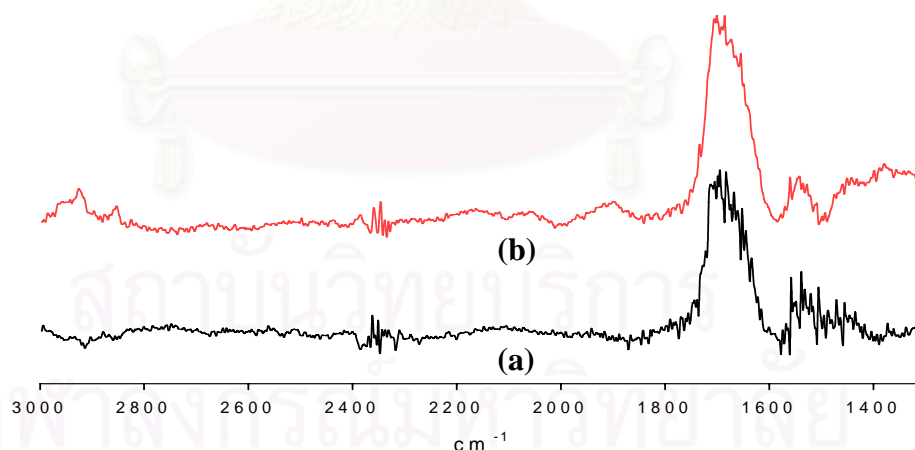


**Figure 3.25** RAIRS spectra of HS(CH<sub>2</sub>)<sub>2</sub>CO-T<sub>9</sub>-LysNH<sub>2</sub> (**33**) PNA on gold surface obtained by increasing PNA concentration: (a)  $1.0\ \mu\text{M}$  and (b)  $5.0\ \mu\text{M}$  at immobilization time of 24 h.

### 3.6.4 Water contact angle analysis

To examine the changes in surface polarity upon attachment of the HS(CH<sub>2</sub>)<sub>2</sub>CO-T<sub>9</sub>-LysNH<sub>2</sub> (**33**) PNA to the gold surface, the water contact angles on the bare gold surface and the thiol-modified PNA immobilized on gold surface were compared. The advancing contact angle was measured in these studies. For the bare gold surface a contact angle of  $97^\circ \pm 1.9^\circ$  was observed, which is higher than the reported value of  $92^\circ \pm 1.6^\circ$ . [58] The water contact angle on the thiol-modified PNA immobilized on gold surface at PNA concentration of 5.0  $\mu$ M and immobilization time of 24 h was found to be  $64^\circ \pm 1.2^\circ$ , which is very different from water contact angle observed for the bare gold surface. This result provided additional evidence that the gold surface is well covered with the hydrophilic thiol-modified PNA.

The results obtained from all techniques above confirmed that the direct immobilization of thiol-modified PNA on gold surface via the S atom of the thiol was successful.

After the immobilization step, the thiol-modified PNA SAMs on gold electrode were tested for hybridization reaction with target DNA. The results will be presented and discussed in the following sections.

## 3.7 Hybridization of thiol-modified PNA nonamer on gold surface with target DNA

### 3.7.1 QCM experiments

#### (a) Immobilization procedures

Three different procedures were employed for thiol-modified PNA HS(CH<sub>2</sub>)<sub>2</sub>CO-T<sub>9</sub>-LysNH<sub>2</sub> (**33**) immobilization based on the direct chemisorption of thiol on gold surface to investigate DNA hybridization reaction.

- I. Thiol-modified PNA procedure
- II. Thiol-modified PNA and blocking thiol procedure
- III. Mixed thiol-modified PNA and blocking thiol procedure

After the frequency at the equilibrium ( $F_2$ ) of the prepared gold electrode was recorded, the electrode was subsequent detected the hybridization reaction with 50  $\mu$ M DNA dA<sub>9</sub> in sodium phosphate buffer pH 7 (0.5 mM, 200  $\mu$ L) at room temperature (32 °C) for 1 h and the frequency ( $F_3$ ) was recorded. The  $\Delta F_h$  which is a difference between  $F_2$  and  $F_3$  indicated the extent of the hybridization reaction.

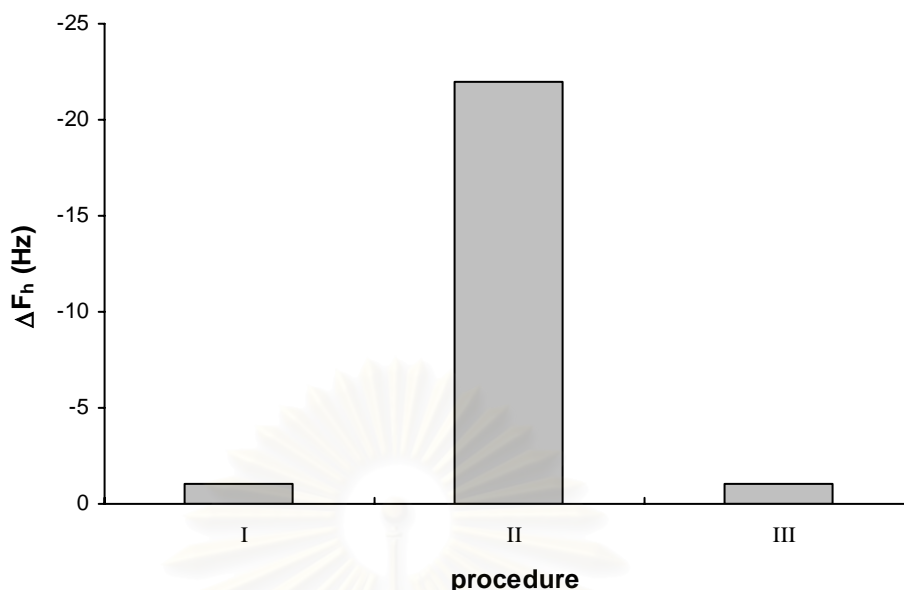


**Figure 3.26**  $\Delta F_h$  obtained from hybridization reaction between surface-immobilized HS(CH<sub>2</sub>)<sub>2</sub>CO-T<sub>9</sub>-LysNH<sub>2</sub> (**33**) PNA prepared by procedure I, II and III with complementary DNA (dA<sub>9</sub>).

From **Figure 3.26**, it can be demonstrated that the blocking step is critical to the success of subsequent DNA hybridization. As a result of non-specific adsorption of excess thiol-modified PNA in the absence of blocking step, the PNA immobilized on gold electrode prepared by procedure I failed to specifically bind with the complementary DNA (dA<sub>9</sub>). Also, the SAM obtained from procedure III was unable to show specific binding towards the complementary DNA (dA<sub>9</sub>). It is suspected that SAM formation from the smaller mercaptoethanol was more favorable than the one from thiol-modified PNA. The sequential SAM formation according to procedure II seemed to be the most effective way of generating SAM suitable for detection of DNA hybridization. For this reason, procedure II was selected for preparation of PNA-immobilized gold surface.

In procedure II, mercaptoethanol does not only prevent non-specific adsorption of the thiol-modified PNA immobilized on the gold surface, but also allows single-stranded PNA to adopt a more extended conformation and thus facilitating hybridization. Mercaptoethanol was selected as the spacer block agent because mercaptoethanol is soluble in aqueous solutions and the 2-carbon chain of

mercaptoethanol is the same length as the spacer group in thiol-modified PNA nonamer.

The reduction of non-specific adsorption of thiol-modified PNA on gold surface by the thiol blocking agent (mercaptoethanol) was confirmed by AFM images (**Figure 3.27**). Small protrusions possibly representing aggregates of PNA non-specifically adsorbed on gold surface were diminished and the surface became relatively smoother after the blocking step was applied.

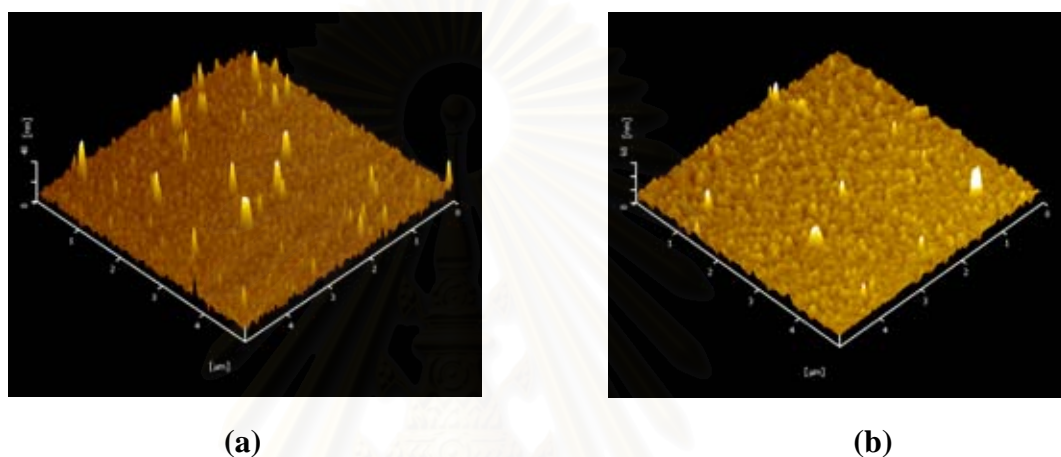


**Figure 3.27** AFM images of  $\text{HS}(\text{CH}_2)_2\text{CO-T}_9\text{-LysNH}_2$  (**33**) PNA immobilized on gold surface for 24 h using PNA concentration of  $5.0 \mu\text{M}$ : (a) before blocking step and (b) after blocking step with  $1.0 \text{ mM}$  mercaptoethanol.

### (b) Optimal hybridization condition

To find the optimal hybridization condition, the thiol-modified PNA (**33**) SAMs on gold electrode were prepared by procedure II and the PNA immobilization condition was fixed at  $5.0 \mu\text{M}$  of PNA concentration and 24 h of immobilization time. The DNA hybridization reaction was investigated under different conditions.

In the first set of experiments, the sodium phosphate buffer (pH 7) concentration (0, 0.05, 0.50, 5.0 and 50 mM) was varied, while the DNA concentration and hybridization time were kept constant at  $50 \mu\text{M}$  and 1 h, respectively.



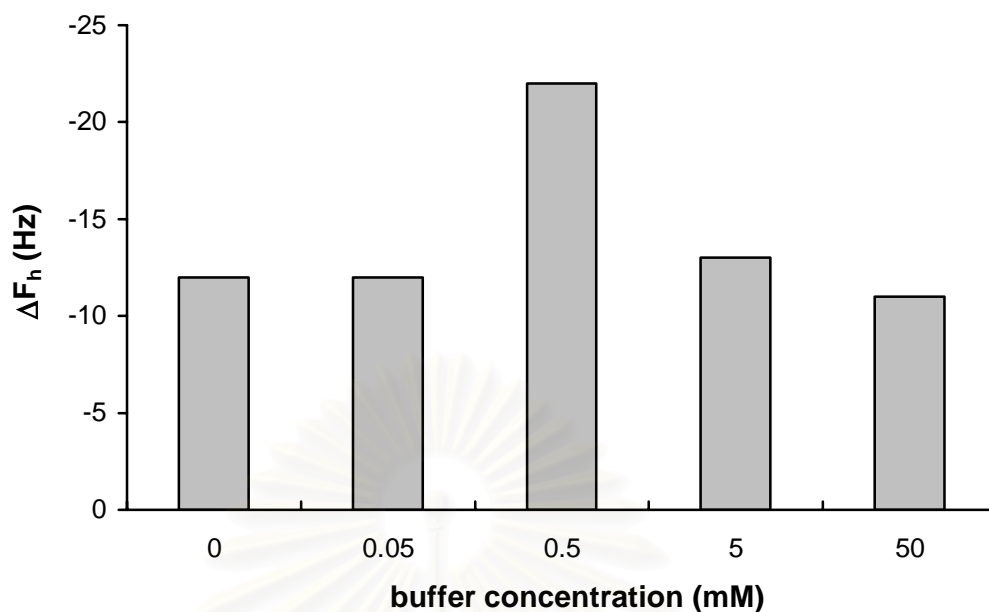


**Figure 3.28**  $\Delta F_h$  obtained from hybridization reaction between surface-immobilized HS(CH<sub>2</sub>)<sub>2</sub>CO-T<sub>9</sub>-LysNH<sub>2</sub> (**33**) PNA with complementary DNA (dA<sub>9</sub>) under different sodium phosphate buffer concentrations.

The data from **Figure 3.28** suggest that a maximum hybridization between immobilized PNA on gold surface with DNA in the solution was achieved when the concentration of sodium phosphate buffer is 0.5 mM. The extent of the hybridization reaction decreased when the concentration of buffer is lower or higher than 0.5 mM. It may be explained that intermolecular electrostatic repulsion between neighboring strands of DNA hybridized on gold surface is minimized under high ionic strength conditions, as the charged strands are better electrostatically shielded,[20] thus allowing higher extent of hybridization between PNA immobilized on gold surface and DNA. On the other hand, if the concentration of the buffer is too high, the counterion released upon PNA·DNA duplex formation on gold surface will cause a negative effect to the binding.[59] Therefore, sodium phosphate buffer concentration of 0.5 mM was selected as the optimal buffer concentration and applied in the later parts of the study.

In the second set of experiments, the hybridization reactions were carried out at 0.5 mM sodium phosphate buffer pH 7 and the hybridization time was kept constant at 1 h, while the DNA concentration (20, 50 and 100  $\mu\text{M}$ ) was changed. With increasing DNA concentration, the  $\Delta F_h$  increases and starts to reach saturation at a DNA concentration of 50  $\mu\text{M}$  (**Figure 3.29**). Although increasing the DNA concentration to 100  $\mu\text{M}$  yielded a slightly higher  $\Delta F_h$ , the improvement was not significant. Therefore, a DNA concentration of 50  $\mu\text{M}$  was selected as the optimal DNA concentration and used in the later parts of the study.

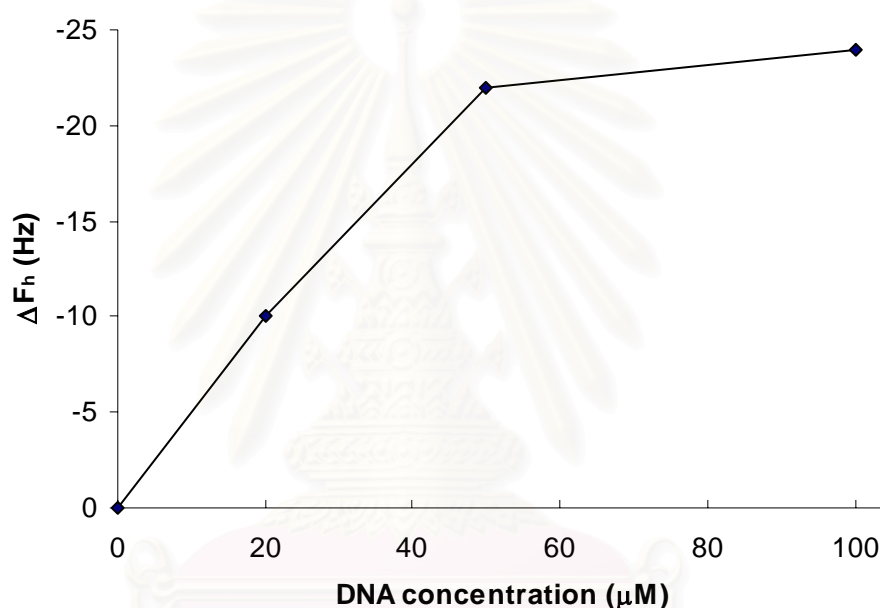


**Figure 3.29**  $\Delta F_h$  obtained from hybridization reaction between surface-immobilized  $\text{HS}(\text{CH}_2)_2\text{CO-T}_9\text{-LysNH}_2$  (**33**) PNA with complementary DNA ( $\text{dA}_9$ ) under different DNA concentrations.

Finally, in order to observe the effects of the hybridization time on the hybridization reaction, the thiol-modified PNA (**33**) SAMs on gold electrode were incubated with the solution of the 50  $\mu\text{M}$  complementary DNA ( $\text{dA}_9$ ) in 0.5 mM sodium phosphate buffer pH 7 for different periods of hybridization time (0.5, 1 and 3 h). With increasing the hybridization time, the  $\Delta F_h$  increases and starts to reach saturation at a hybridization time of 1 h (**Figure 3.30**). Therefore, this hybridization time (1h) was selected as the optimal hybridization time and used in the later parts of the study.

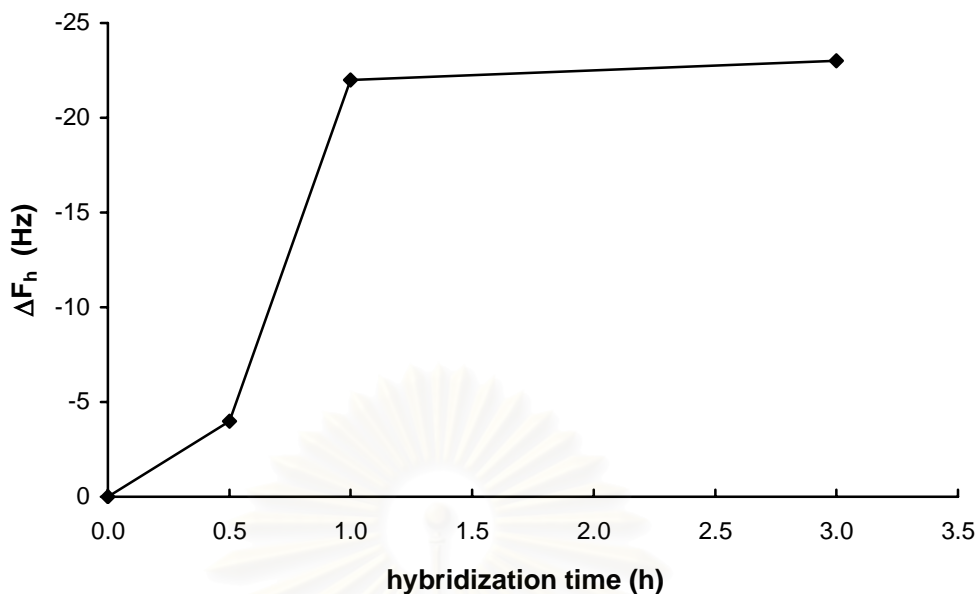


**Figure 3.30**  $\Delta F_h$  obtained from hybridization reaction between surface-immobilized HS(CH<sub>2</sub>)<sub>2</sub>CO-T<sub>9</sub>-LysNH<sub>2</sub> (**33**) PNA with complementary DNA (dA<sub>9</sub>) under different hybridization times.

From the results obtained from all above experiments, it can be concluded that the optimal hybridization condition is sodium phosphate buffer pH 7 concentration: 0.5 mM, DNA concentration: 50  $\mu$ M and hybridization time: 1 h. This optimal hybridization condition was used in later parts of the study.

### (c) Optimal immobilization condition

To find the optimal immobilization condition, the optimal hybridization condition obtained above was used, while the PNA concentration and immobilization time were varied.

In the first set of experiments, the PNA concentration (0.5, 1, 2 and 5  $\mu$ M) was changed, while the immobilization time was kept constant at 24 h. **Figure 3.31** shows a plot of the  $\Delta F_h$ , which represents the extent of the hybridization reaction, versus the PNA concentration. As expected, the PNA density on gold surface produced from a lower PNA concentration resulted in the attachment of fewer target DNA molecules. From **Figure 3.31**, it appears that the PNA concentration of 1.0  $\mu$ M yielded an optimal surface density for the acceptable hybridization efficiency.

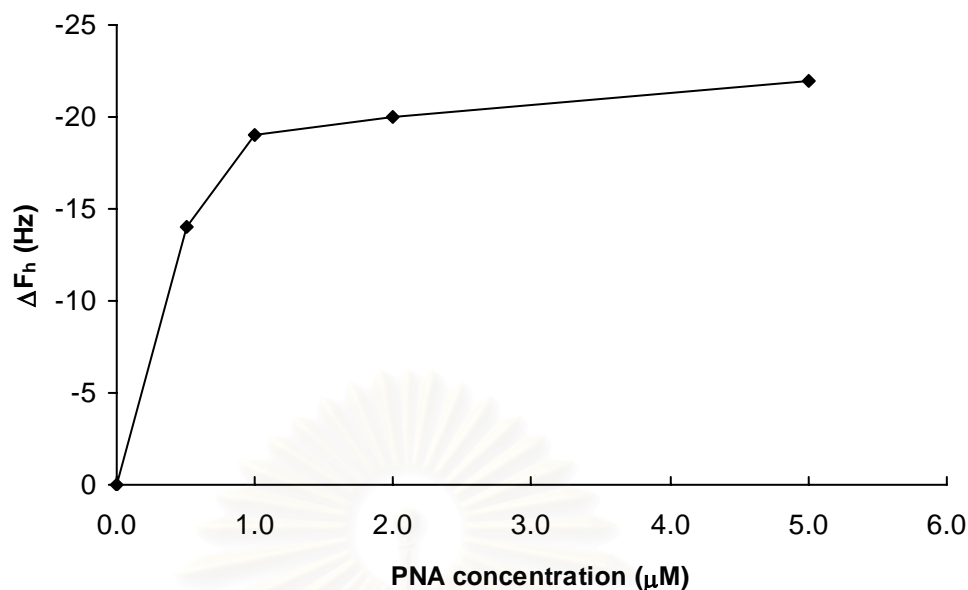


**Figure 3.31**  $\Delta F_h$  obtained from hybridization reaction between surface-immobilized  $\text{HS}(\text{CH}_2)_2\text{CO-T}_9\text{-LysNH}_2$  (**33**) PNA with complementary DNA ( $\text{dA}_9$ ) under different PNA concentration.

In the second set of experiments, the PNA concentration was kept constant at  $1.0 \mu\text{M}$  and the immobilization time (2, 3, 6, 24 and 48 h) was changed. **Figure 3.32** shows a plot of the  $\Delta F_h$  versus the immobilization times. Increasing the immobilization time caused a higher degree of  $\Delta F_h$  due to an increase in the amount of PNA immobilized on gold surface. The  $\Delta F_h$  starts to reach saturation at an immobilization time of 24 h. Although longer immobilization time yielded slightly higher  $\Delta F_h$ , the improvement was not significant. Therefore, an immobilization time of 24 h was selected as the optimal immobilization time.

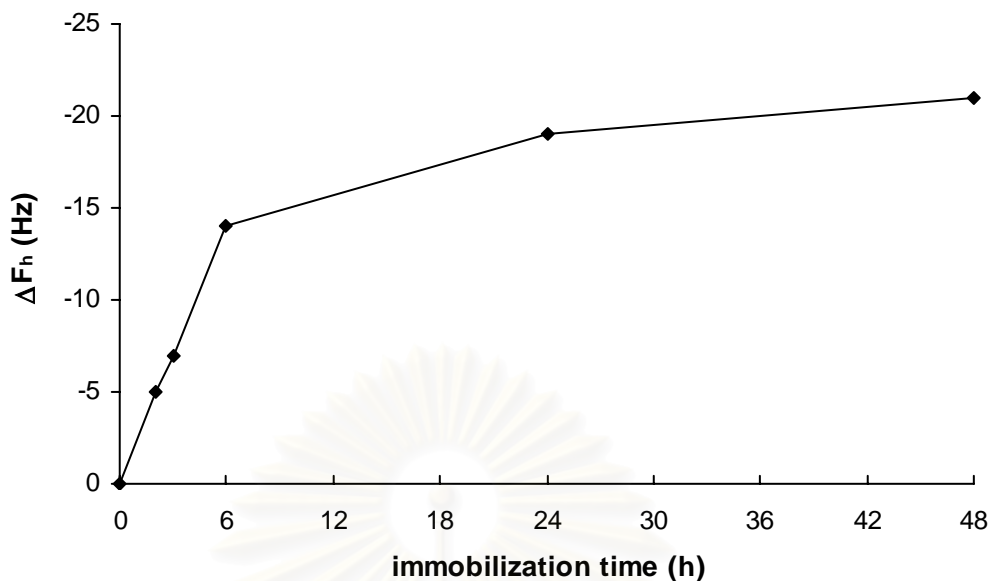


**Figure 3.32**  $\Delta F_h$  obtained from hybridization reaction between surface-immobilized HS(CH<sub>2</sub>)<sub>2</sub>CO-T<sub>9</sub>-LysNH<sub>2</sub> (**33**) PNA with complementary DNA (dA<sub>9</sub>) under different immobilization times.

From the results obtained from all above experiments in this section, it can be concluded that optimal immobilization condition is PNA concentration: 1.0  $\mu$ M and immobilization time: 24 h. This optimal immobilization condition was used in the next parts of the study.

#### (d) Effect of pH

To investigate the effect of pH, the thiol-modified PNA SAMs on gold electrode prepared under the optimal immobilization condition (PNA concentration: 1.0  $\mu$ M and immobilization time: 24 h) were hybridized with complementary DNA under the optimal hybridization condition (sodium phosphate buffer concentration: 0.5 mM, DNA concentration: 50  $\mu$ M and hybridization time: 1 h), while the pH (6, 7 and 8) of sodium phosphate buffer was varied. From **Figure 3.33**, it appears that the best hybridization efficiency was achieved at pH 7 in 0.5 mM sodium phosphate buffer. Therefore, this pH was selected and used in the later parts of the study.

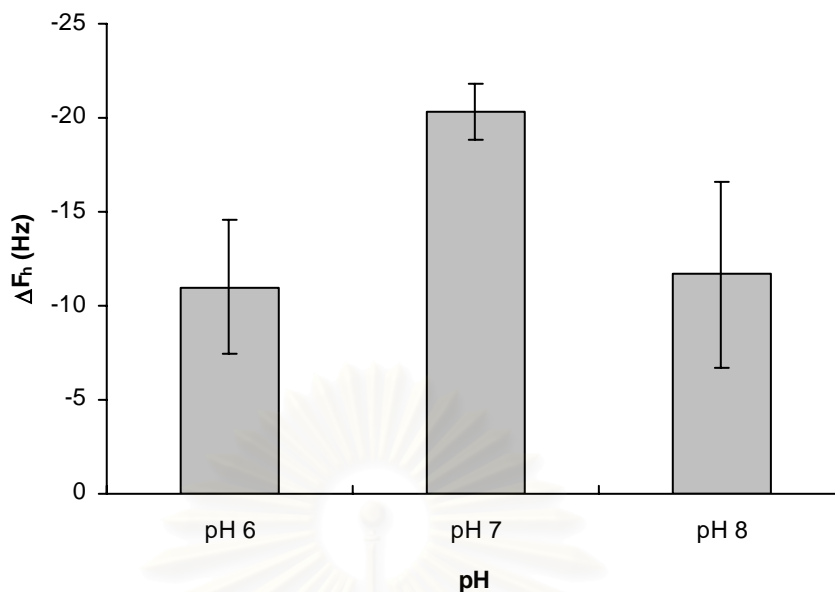


**Figure 3.33**  $\Delta F_h$  obtained from hybridization reaction between surface-immobilized HS(CH<sub>2</sub>)<sub>2</sub>CO-T<sub>9</sub>-LysNH<sub>2</sub> (**33**) PNA with complementary DNA (dA<sub>9</sub>) under different pH.

#### (e) Effect of ionic strength

To compare the frequency shifts due to hybridization under different ionic strength, the hybridization between the HS(CH<sub>2</sub>)<sub>2</sub>CO-T<sub>9</sub>-LysNH<sub>2</sub> (**33**) PNA immobilized on gold electrode and its complementary DNA (dA<sub>9</sub>) was studied at different NaCl concentration.

**Figure 3.34** shows that the best result was achieved without NaCl in the hybridization buffer and the apparent binding amount decreased with increasing ionic strength, but there is no significant difference in the  $\Delta F_h$  at NaCl concentrations of 1 and 10 mM. The decrease in  $\Delta F_h$  with increasing ionic strength is explained in terms of counterion release upon PNA·DNA duplex formation [59] on gold surface (section 3.7(a)(ii)).

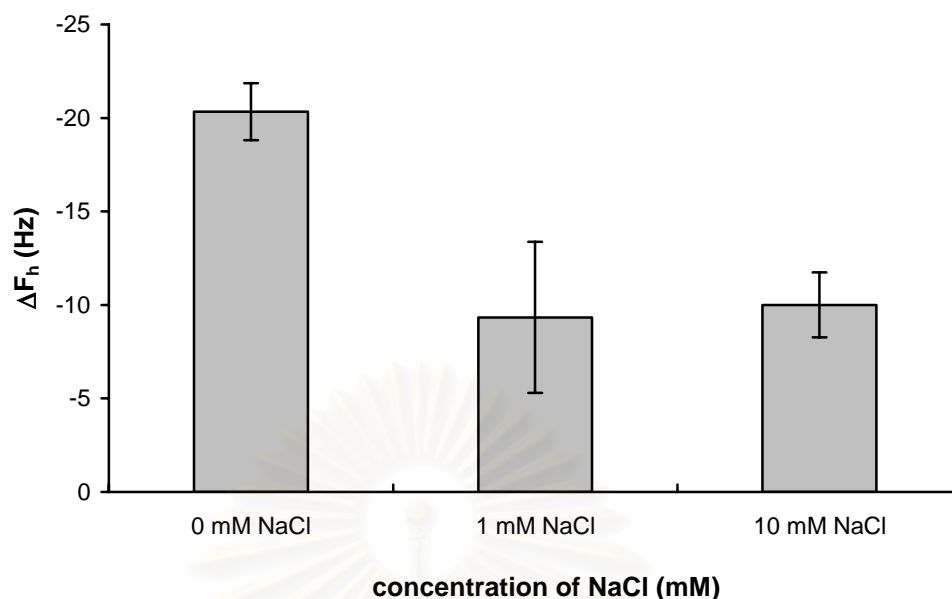


**Figure 3.34**  $\Delta F_h$  obtained from hybridization reaction between surface-immobilized HS(CH<sub>2</sub>)<sub>2</sub>CO-T<sub>9</sub>-LysNH<sub>2</sub> (**33**) PNA with complementary DNA (dA<sub>9</sub>) under different NaCl concentration.

#### (f) Specificity of DNA hybridization reaction

To investigate the specificity of DNA hybridization reaction, the thiol-modified PNA SAMs on gold electrode prepared by procedure II under the optimal immobilization condition were tested for hybridization specificity with different target DNA under the optimal DNA hybridization condition.

**Figure 3.35** demonstrates the  $\Delta F_h$  obtained from the hybridization of HS(CH<sub>2</sub>)<sub>2</sub>CO-T<sub>9</sub>-LysNH<sub>2</sub> (**33**) immobilized on gold electrode and perfect matched, single mismatched (thymine), double mismatched (thymine) and triple mismatched (thymine and mixed nucleobases) DNAs. Hybridization with a single mismatched DNA d(5'-AAAATTAAA-3') produced  $-20.3 \pm 2.5$  Hz frequency shift, which was comparable to that of the perfect matched DNA (dA<sub>9</sub>) ( $-20.3 \pm 1.5$  Hz). In contrast,  $\Delta F_h$  obtained from a double mismatched d(5'-AAATTATAAA-3') and a triple mismatched d(5'-AATATATATAA-3') DNA hybridization were progressively lowered (~10 Hz per mismatch). In the case of the triple mismatched DNA d(5'-AATATATATAA-3') and d(5'-AACATATAGAA-3'), there was very little frequency shift after the hybridization reaction indicating the absence of hybridization between these DNA and PNA on the gold surface.

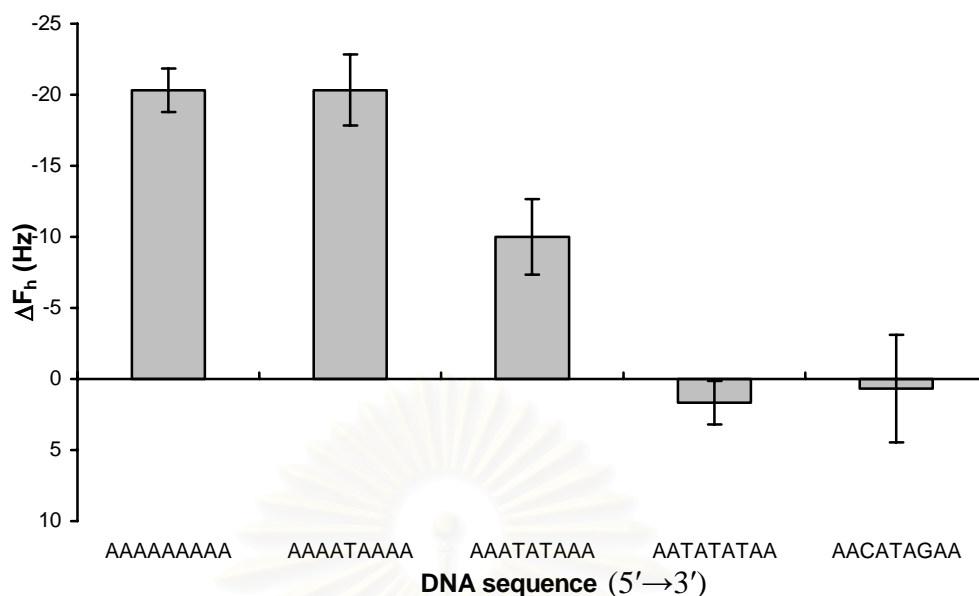


**Figure 3.35**  $\Delta F_h$  obtained from hybridization reaction between surface-immobilized HS(CH<sub>2</sub>)<sub>2</sub>CO-T<sub>9</sub>-LysNH<sub>2</sub> (**33**) PNA with dA<sub>9</sub> (perfect match), d(5'- AAA ATAAAA-3') (single mismatch), d(5'-AAATATAAA-3') (double mismatch), d(5'-AATATATAA-3') and d(5'-AACATAGAA-3') (triple mismatch).

To investigate the effect of DNA sequence on the binding affinity, HS(CH<sub>2</sub>)<sub>2</sub>CO-T<sub>9</sub>-LysNH<sub>2</sub> (**33**) SAMs on gold electrode were hybridized with different mismatched DNAs. **Figure 3.36** shows the  $\Delta F_h$  obtained from the hybridization of HS(CH<sub>2</sub>)<sub>2</sub>CO-T<sub>9</sub>-LysNH<sub>2</sub> (**33**) immobilized on gold electrode and single or double mismatched (thymine, cytosine and guanine) DNA.

When the mismatch nucleobases are cytosine and guanine, the  $\Delta F_h$  obtained from hybridization with single mismatched DNA were more pronounced than the thymine mismatch above. When the mismatch nucleobase is cytosine, the  $\Delta F_h$  values obtained from both single mismatched d(5'-AAAACAAA-3') and double mismatched d(5'-AAACACAAA-3') DNA hybridization were lower than the perfect matched and single mismatched thymine by 8-11 Hz. On the other hand, in the case of single and double mismatched guanine (d(5'-AAAAGAAA-3') and d(5'-AAAGAGAAA-3')) DNA, very little frequency shift was observed suggesting the absence of mismatched guanine DNA hybridization to PNA on the gold surface. It



can be concluded that the binding affinity of PNA immobilized on gold surface with the target DNA is extremely dependent on the type of nucleobases of DNA.

The results obtained from QCM which study the hybridization reaction on surface were not identical to those from  $T_m$  experiments which study the hybridization reaction in solution. In solution, the binding affinity of PNA and mismatched DNA is not dependent on the type of nucleobase mismatch but dependent on the number of mismatch in DNA chain. While the binding affinity on the surface is extremely dependent on both the type and number of mismatch nucleobases in the DNA.

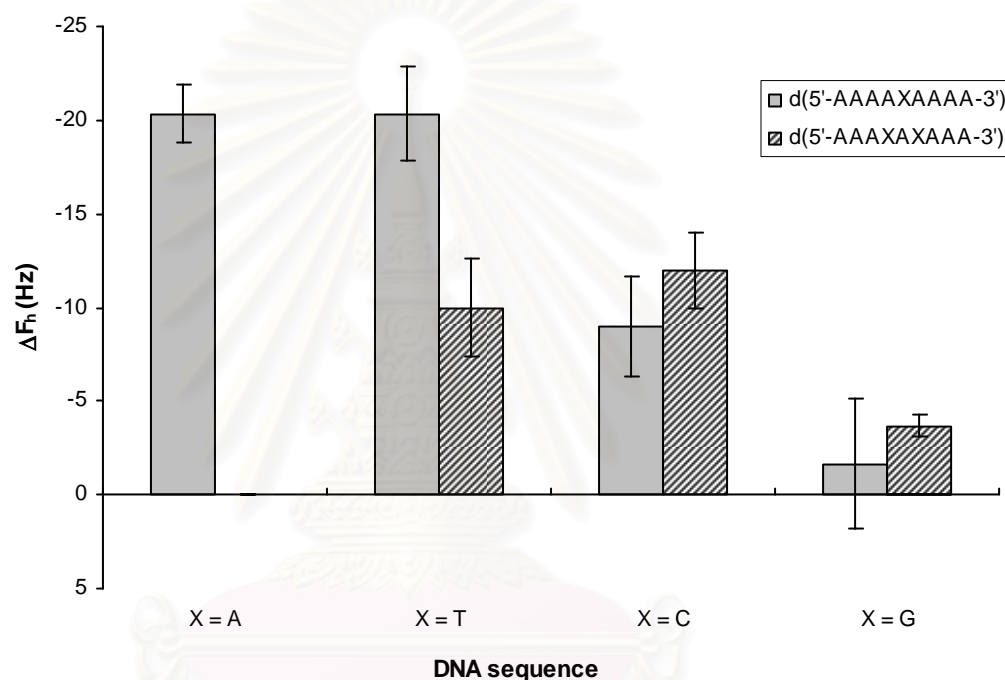


**Figure 3.36**  $\Delta F_h$  obtained from hybridization reaction between surface-immobilized  $\text{HS}(\text{CH}_2)_2\text{CO-T}_9\text{-LysNH}_2$  (**33**) PNA with  $\text{dA}_9$  (perfect match),  $\text{d}(5'\text{-AAAAXAAAA-3'})$  (single mismatch,  $X = \text{T, C}$  and  $\text{G}$ ) and  $\text{d}(5'\text{-AAAXAXAAA-3'})$  (double mismatch,  $X = \text{T, C}$  and  $\text{G}$ ).

Encouraged by the above results, the binding affinity of mixed nucleobases thiol-modified PNA nonamer  $\text{HS}(\text{CH}_2)_2\text{CO-TTCTATGTT-LysNH}_2$  (**35**) with perfect matched, single mismatched and triple mismatched DNA was next investigated (**Figure 3.37**). This should be a more realistic model for practical usage of PNA in DNA sequence detection. Hybridization with the perfect matched DNA  $\text{d}(5'\text{-AACATAGAA-3'})$  produced a frequency shift of  $\sim -13.3 \pm 2.1$  Hz, which was lower than that obtained from immobilized  $\text{HS}(\text{CH}_2)_2\text{CO-T}_9\text{-LysNH}_2$  (**33**) and its

complementary DNA. On the other hand, the immobilized PNA (**35**) failed to hybridize with all single mismatched DNAs (d(5'-AACAXAGAA-3'), X = A, C and G) and triple mismatched DNA (dA<sub>9</sub>). It can be concluded that the immobilized mixed base PNA on the gold surface forms a stable hybrid only with complementary DNA which is the most desirable property for sensor applications.

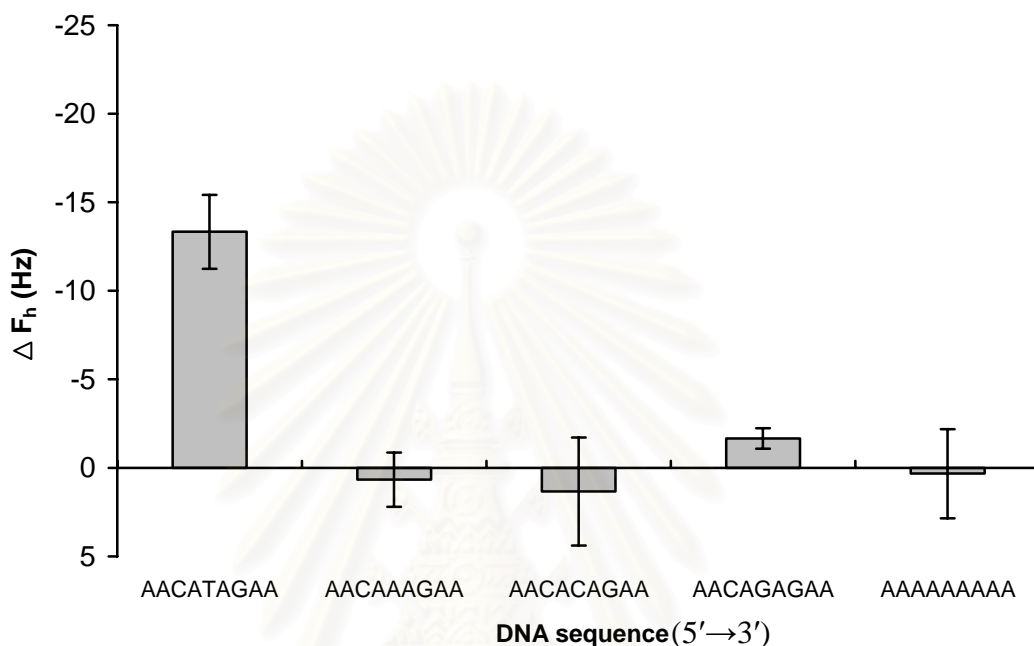


**Figure 3.37**  $\Delta F_h$  obtained from hybridization reaction between surface-immobilized HS(CH<sub>2</sub>)<sub>2</sub>CO-TTCTATGTT-LysNH<sub>2</sub> (**35**) PNA with d(5'-AACATAGAA-3') (perfect match), d(5'-AACAXAGAA-3') (single mismatch, X = A, C and G) and dA<sub>9</sub> (triple mismatch).

It should be noted that while dA<sub>9</sub> gave a  $\Delta F_h$  of -20 Hz with the immobilized HS(CH<sub>2</sub>)<sub>2</sub>CO-T<sub>9</sub>-LysNH<sub>2</sub> (**33**), the DNA d(5'-AACATAGAA-3') gave practically no frequency shift. In contrast, d(5'-AACATAGAA-3') gave a  $\Delta F_h$  of -13 Hz with immobilized HS(CH<sub>2</sub>)<sub>2</sub>CO-TTCTATGTT-LysNH<sub>2</sub> (**35**) while the dA<sub>9</sub> gave practically no frequency shift at all (**Figure 3.38**). This strongly suggests that the hybridization between the gold surface-immobilized PNA and DNA are highly sequence-specific.

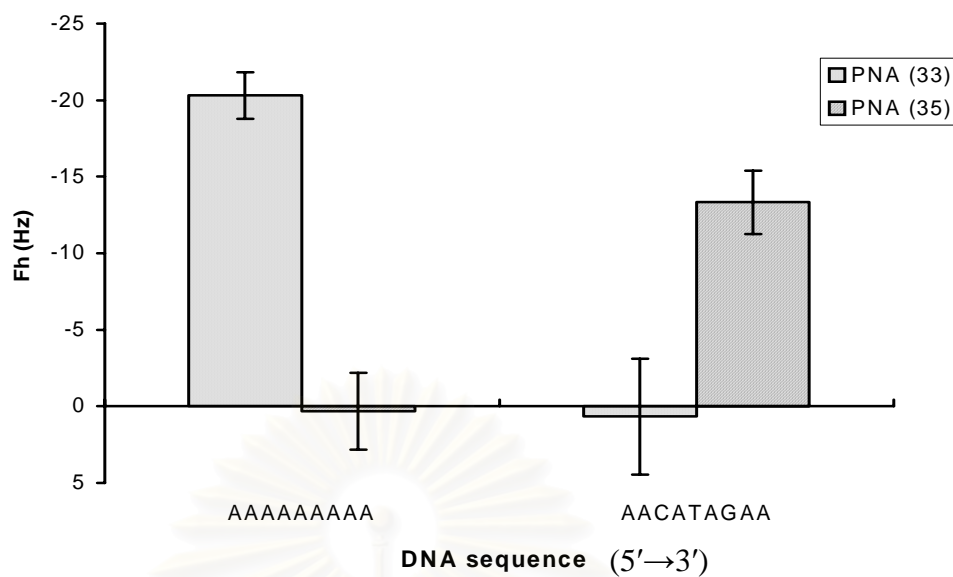


**Figure 3.38**  $\Delta F_h$  obtained from hybridization reaction between surface-immobilized  $\text{HS}(\text{CH}_2)_2\text{CO-T}_9\text{-LysNH}_2$  (**33**) PNA and  $\text{HS}(\text{CH}_2)_2\text{CO-TTCTATGTT-LysNH}_2$  (**35**) PNA with  $\text{dA}_9$  and  $\text{d}(5'\text{-AACATAGAA-}3')$

## CHAPTER IV

### CONCLUSION

In this research two novel thiol-modified polyamide nucleic acid (PNA) nonamers  $\text{HS}(\text{CH}_2)_2\text{CO-T}_9\text{-LysNH}_2$  (**33**) and  $\text{HS}(\text{CH}_2)_2\text{CO-TTCTATGTT-LysNH}_2$  (**35**) were synthesized by solid phase peptide synthesis and directly attached on gold-coated quartz crystals by self assembly monolayer (SAM) formation via S atom.

As monitored by quartz crystal microbalance (QCM) which is a very sensitive mass-measuring device, the amount of immobilized PNA on the gold electrode increased with the PNA concentration and the optimal concentration for the SAM formation of PNA was approximately  $5.0 \mu\text{M}$ .

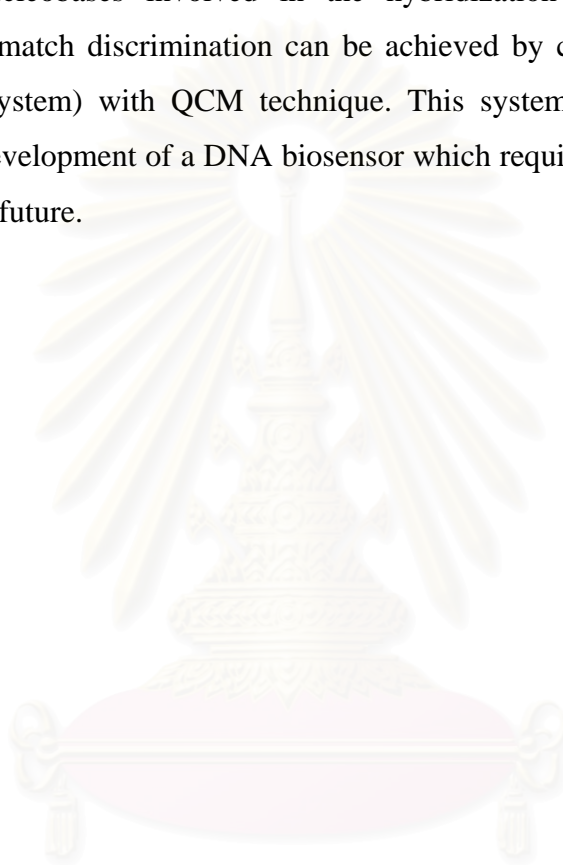
Three different procedures were employed for thiol-modified PNA immobilization considering the extent DNA hybridization using QCM. From the results, it can be demonstrated that the blocking step is critical to the success of subsequent DNA hybridization. The optimal immobilization condition obtained is PNA concentration:  $1.0 \mu\text{M}$  and immobilization time: 24 h and the optimal hybridization condition is DNA concentration:  $50 \mu\text{M}$ , sodium phosphate buffer pH 7 concentration:  $0.5 \text{ mM}$  and hybridization time: 1 h.

The effect of pH and ionic strength were also investigated, it appears that the best hybridization efficiency could be achieved at pH 7 of  $0.5 \text{ mM}$  sodium phosphate buffer without the addition of NaCl.

Two thiol-modified PNA SAMs on the gold electrode were hybridized with different DNA sequences to determine the specificity of hybridization.  $\text{HS}(\text{CH}_2)_2\text{CO-T}_9\text{-LysNH}_2$  (**33**) could bind excellently with perfect matched ( $\text{dA}_9$ ) and single mismatched thymine DNA ( $\text{d}(5'\text{-AAAAT}\underline{\text{T}}\text{AAAA-3'})$ ) which produced  $\sim -20 \text{ Hz}$  frequency shift and could bind moderately with double mismatched thymine DNA ( $\text{d}(5'\text{-AAAT}\underline{\text{T}}\underline{\text{A}}\text{AAA-3'})$ ) and mismatched cytosine DNAs ( $\text{d}(5'\text{-AAAAC}\underline{\text{C}}\text{AAA-3'})$ ) and  $\text{d}(5'\text{-AAAC}\underline{\text{C}}\underline{\text{A}}\text{AAA-3'})$ ) which produced  $\sim -9$  to  $-12 \text{ Hz}$  frequency shift but could not bind with mismatched guanine DNAs ( $\text{d}(5'\text{-AAAAG}\underline{\text{G}}\text{AAA-3'})$ ) and  $\text{d}(5'\text{-AAAG}\underline{\text{A}}\underline{\text{G}}\text{AAA-3'})$ ), triple mismatched thymine ( $\text{d}(5'\text{-AAT}\underline{\text{T}}\underline{\text{A}}\underline{\text{T}}\text{ATAA-3'})$ ) and triple mismatched mixed bases DNAs ( $\text{d}(5'\text{-AAC}\underline{\text{A}}\underline{\text{T}}\underline{\text{A}}\underline{\text{G}}\text{AA-3'})$ ). The immobilized  $\text{HS}(\text{CH}_2)_2\text{CO-TTCTATGTT-LysNH}_2$  (**35**) PNA could bind with its perfect matched

DNA (d(5'-AACATAGAA-3')) producing a frequency shift of  $\sim -13$  Hz but could not bind with all three single mismatched DNAs (d(5'-AACAAAAGAA-3'), d(5'-AACACAGAA-3') and d(5'-AACAGAGAA-3')) and the triple mismatched DNA (dA<sub>9</sub>).

It can be concluded that the binding affinity of PNA immobilized on the gold surface with target DNA is extremely dependent on the type and number of mismatched nucleobases involved in the hybridization of PNA and DNA. A remarkable mismatch discrimination can be achieved by combination of Vilaivan's PNA (ACPC system) with QCM technique. This system should be an important prototype for development of a DNA biosensor which requires no external labeling of the DNA in the future.



สถาบันวิทยบริการ  
จุฬาลงกรณ์มหาวิทยาลัย

## REFERENCES

1. Egholm, M., Nielsen, P. E., Buchardt, O., and Berg, R. H. Recognition of guanine and adenine in DNA by cytosine and thymine containing peptide nucleic acid (PNA). J. Am. Chem. Soc. 114 (1992) : 9677-9678.
2. Hyrup, B., Egholm, M., Nielsen, P. E., Wittung, P., Norden, B., and Buchardt, O. Structure-activity studies of the binding of modified peptide nucleic acid (PNAs) to DNA. J. Am. Chem. Soc. 116 (1994) : 7964-7970.
3. Hamilton, S. E., Simmons, C. G., Kathiriya, I. S., and Corey, D. R. Cellular delivery of peptide nucleic acids and inhibition of human telomerase. Chem. Biol. 6 (1999) : 343.
4. Nielsen, P. E. Peptide nucleic acid: a versatile tool in genetic diagnostics and molecular biology. Curr. Opin. Biol. 12 (2001) : 16.
5. Suparpprom, C., Srisuwannaket, C., Sangvanich, P., and Vilaivan, T. Synthesis and oligodeoxynucleotide binding properties of pyrrolidinyl peptide nucleic acids bearing prolyl-2-aminocyclopentanecarboxylic acid (ACPC) backbones. Tetrahedron Lett. 46 (2005) : 2833-2837.
6. Schoenenberger, C., Jorritsma, J., Sondag-Huethorst, J. A. M., and Fokkink, L. G. J. Domain structure of self-assembled alkanethiol monolayers on gold. J. Phys. Chem. 99 (1995) : 3259-3271.
7. Kajikawa, K. Molecular Electronics and Bioelectronics. 7 (1996) : 2.
8. Schessle, H. M., Karpovich, D. S., and Blanchard, G. J. Quantitating the balance between enthalpic and entropic forces in alkanethiol/gold monolayer self assembly. J. Am. Chem. Soc. 118 (1996) : 9645.
9. Sato, Y., Ye, S., Haba, T., and Uosaki, K. Potential dependent orientation and oxidative decomposition of mercaptoalkanenitrile monolayers on gold. An in situ fourier transform infrared spectroscopy study. Langmuir. 12 (1996) : 2726-2736.
10. Wilbur, J. L., Biebuyck, H., MacDonald, J. C., and Whitesides, G. M. Scanning force microscopies can image patterned self-assembled monolayers. Langmuir. 13 (1995) : 825-831.
11. Bain, C. D., and Whitesides, G. M. Correlations between wettability and structure in monolayers of alkanethiols adsorbed on gold. J. Am. Chem. Soc. 110, (1988) : 3665-3666.

12. Laibinis, P. E., Bain, C. D., and Whitesides, G. M. Attenuation of photoelectrons in monolayers of n-alkanethiols adsorbed on copper, silver, and gold. J. Phys. Chem. 95 (1991) : 7017-7021.
13. Widrig, C. A., Chung, C., and Porter, M. D. The electrochemical desorption of n-alkanethiol monolayers from polycrystalline Au and Ag electrodes. J. Electroanal. Chem. 310 (1991) : 335-359.
14. Bryant, M. A., and Pemberton, J. E. Surface raman scattering of self-assembled monolayers formed from 1-alkanethiols: behavior of films at gold and comparison to films at silver. J. Am. Chem. Soc. 113 (1991) : 8284-8293.
15. Chidsey, C. E. D., and Loiacono, D. N. Chemical functionality in self-assembled monolayers: structural and electrochemical properties. Langmuir. 6 (1990) : 682-691.
16. Ohtsuka, T., Sato, Y., and Uosaki, K. Dynamic ellipsometry of a self-assembled monolayer of a ferrocenylalkanethiol during oxidation-reduction cycles. Langmuir. 10 (1994) : 3658-3662.
17. Shimazu, K., Yagi, I., Sato, Y., and Uosaki, K. In situ and dynamic monitoring of the self-assembling and redox processes of a ferrocenylundecanethiol monolayer by electrochemical quartz crystal microbalance. Langmuir. 8 (1992) : 1385-1387.
18. Schneider, T. W., and Buttry, D. A. Electrochemical quartz crystal microbalance studies of adsorption and desorption of self-assembled monolayers of alkyl thiols on gold. J. Am. Chem. Soc. 115 (1993) : 12391-12397.
19. Tombelli, S., Mascini, M., and Turner, A. P. F. Improved procedures for immobilization of oligonucleotides on gold-coated piezoelectric quartz crystals. Biosens. Bioelectron. 17 (2002) : 929-936.
20. Levicky, R., Herne, T. M., Tarlov, M. J., and Satija, S. K. Using self-assembly to control the structure of DNA monolayers on gold: a neutron reflectivity study. J. Am. Chem. Soc. 120 (1998) : 9787-9792.
21. Herne, T. M., and Tarlov, M. J. Characterization of DNA probes immobilized on gold surface. J. Am. Chem. Soc. 119 (1997) : 8916-8920.
22. Petrovykh, D. Y., Kimura-Suda, H., Whitman, L. J., and Tarlov, M. J. Quantitative analysis and characterization of DNA immobilized on gold. J. Am. Chem. Soc. 125 (2003) : 5219-5226.

23. Mannelli, I., Minunni, M., Tombelli, S., Wang, R., Spiriti, M. M., and Mascini, M. Direct immobilization of DNA probes for the development of affinity biosensors. Bioelectrochemistry. 66 (2005) : 129-138.
24. Feldner, J. C., Ostrop, M., Friedrichs, O., Sohn, S., Lipinsky, D., Gunst, U. and Arlinghaus, H. F. TOF-SIMS investigation of the immobilization process of peptide nucleic acids. Appl. Surf. Sci. 203-204 (2003) : 722-725.
25. Arlinghaus, H. F., Schroder, M., Feldner, J. C., Brandt, O., Hoheisel, J. D. and Lipinsky, D. Development of PNA microarrays for gene diagnostics with TOF-SIMS. Appl. Surf. Sci. 231-232 (2004) : 392-396.
26. Mateo-Marti, E., Briones, C., Roman, E., Briand, E., Pradier, C. M., and Martin-Gago, J. A. Self-assembled monolayers of peptide nucleic acids on gold surfaces: A spectroscopic study. Langmuir. 21 (2005) : 9510-9517.
27. Kumar, A. Biosensors based on piezoelectric crystal detectors: theory and application.
28. Downs, M. E. A. Prospects for nucleic-acid biosensor. Biochem. Soc. Trans. 19 (1991) : 39-43.
29. Palecek, E. New trends in electrochemical analysis of nucleic acids. Bioelectrochem. Bioenerg. 20 (1988) : 179-194.
30. Jost, J. P., Munch, O., and Andersson, T. Study of protein-DNA interactions by surface-plasmon resonance (real-time kinetics). Nucleic Acids Res. 19 (1991) : 2788.
31. Piscevic, D., Lawall, R., Veiyh, M., Liley, M., Okahata, Y., and Knoll, W. Oligonucleotide hybridization observed by surface-plasmon-optical techniques. Appl. Surf. Sci. 90 (1995) : 425-436.
32. Bardea, A., Dagan, A., Ben-Dov, I., Amit, B., and Willner, I. Amplified microgravimetric quartz-crystal-microbalance analysis of oligonucleotide complexes: a route to a Tay-Sachs sensor. Chem. Commun. 7 (1998) : 839-840.
33. Caruso, F., Rodda, H., Furlong, D. F., Niikura, K., and Okahata, Y. Quartz crystal microbalance study of DNA immobilization and hybridization for nucleic acid sensor development. Anal. Chem. 69 (1997) : 2043-2049.
34. Yamagushi, S., Shimomura, T., Tatsuma, T., and Oyama, N. Adsorption, immobilization, and hybridization of DNA studied by the use of quartz-crystal oscillators. Anal. Chem. 65 (1993) : 1925-1927.



35. Zhou, X. C., Huang, L. Q., and Li, S. F. Y. Microgravimetric DNA sensor based on quartz crystal microbalance: comparison of oligonucleotide immobilization methods and the application in genetic diagnosis. Biosens. Bioelectron. 16 (2001) : 85-95.
36. Curie, J., and Curie, P. Comp Rend. 91 (1880) : 294.
37. Sauerbrey, G. Z. Z Physik. 155 (1959) : 206.
38. Su, H., Sandra, C., and Thompson, M. Kinetic of hybridization of interfacial RNA homopolymers studies by thickness-shear mode acoustic wave sensor. Biosens. Bioelectron. 12 (1997) : 161-173.
39. Okahata, Y., Niikura, K., Sugiura, Y., Sawada, M., and Morri, T. Kinetic studies of sequence-specific binding of GCN4-bZIP peptide to DNA strands immobilized on 27-MHz quartz crystal microbalance. Biochemistry. 37 (1998) : 5666-5672.
40. Niikura, K., Matsuno, H., Ohatake, H., Furasama, H., and Ebara, Y. Direct monitoring of DNA polymerase reaction on a quartz crystal microbalance. J. Am. Chem. Soc. 120 (1998) : 8537-8538.
41. Cho, Y. K., Kim, S., Kim, Y. A., Lim, H. K., Lee, K., Yoon, D. S., Lim, G., Pak, Y. E., Ha, T. H., and Kim, K. Characterization of DNA immobilization and subsequent hybridization using in situ quartz crystal microbalance, fluorescence spectroscopy, and surface plasmon resonance. J. Colloid Interface Sci. 278 (2004) : 44-52.
42. Duman, M., Saber, R., and Piskin, E. A new approach for immobilization of oligonucleotides onto piezoelectric quartz crystal for preparation of a nucleic acid sensor for following hybridization. Biosens. Bioelectron. 18 (2003) : 1355-1363.
43. Su, X., Wu, Y. J., and Knoll, W. Comparison of surface plasmon resonance spectroscopy and quartz crystal microbalance techniques for studying DNA assembly and hybridization. Biosens. Bioelectron. 21 (2005) : 719-726.
44. Wang, J., Nielsen, P. E., Jiang, M., Cai, X., Fernandes, J. R., Grant, D. H., Ozsoz, M., Beglieter, A., and Mowat, M. Mismatch-sensitivity hybridization detection by peptide nucleic acids immobilized on a quartz crystal microbalance. Anal. Chem. 69 (1997) : 5200-5202.

45. Stafshede, P. W., Rodahl, M., Kasemo, B., Nielsen, P., and Norden, B. Detection of point mutations in DNA by PNA-based quartz-crystal biosensor. Colloids Surf, A. 174 (2000) : 269-273.
46. Lowe, G., and Vilaivan, T. Amino acid bearing nucleobases for the synthesis of novel peptide nucleic acid. J. Chem. Soc., Perkin Trans I. (1997) : 539-546.
47. Lowe, G., and Vilaivan, T. Amino acid bearing nucleobases for the synthesis of novel peptide nucleic acid. J. Chem. Soc., Perkin Trans I. (1997) : 547-554.
48. Lowe, G., and Vilaivan, T. Solid phase synthesis of novel peptide nucleic acid. J. Chem. Soc., Perkin Trans I. (1997) : 555-560.
49. LaPlae, P. R., Umezawa, N., Lee, H. S., and Gellman, S. H. An efficient route to either enantiomer of *trans*-2-aminocyclopentanecarboxylic acid. J. Org. Chem. 66 (2001) : 5629-5632.
50. Srisuwannaket, C. "Synthesis and DNA-binding properties of pyrrolidinyl peptide nucleic acids bearing (1S, 2S)-2-aminocyclopentane carboxylic acids spacer," (Doctoral dissertation, Graduate School, Chulalongkorn University, 2005).
51. Vilaivan, T., and Lowe, G. A novel pyrrolidinyl PNA showing high sequence specificity and preferential binding to DNA over RNA. J. Am. Chem. Soc. 124 (2002) : 9326-9327.
52. Merrifield, R. D. Solid phase peptide synthesis. I. The synthesis of a tetrapeptide. J. Am. Chem. Soc. 85 (1963) : 2149-2154.
53. Nielsen, P. E., Egholm, M., Berg, R. H., and Buchardt, O. Sequence-selective recognition of DNA by strand displacement with a thymine-substituted polyamide. Science 254 (1991) : 1497-1500.
54. Egholm, M., Buchardt, O., Nielsen, P. E., and Berg, R. H. Peptide nucleic acid (PNA): oligonucleotide analogues with an achiral peptide backbone. J. Am. Chem. Soc. 114 (1992) : 1845-1847.
55. Egholm, M., Buchardt, O., Christensen, L., Behrens, C., Freier, S., Driver, D. A., Berg, R. H., Kim, S. K., Norden, B., and Nielsen, P. E. PNA hybridizes to complementary oligonucleotides obeying the Watson-Crick hydrogen bonding rules. Nature. 365 (1993) : 566-568.
56. Ngamviriyavong, P. "Synthesis of peptide nucleic acid containing aminoethyl linkers," (Master's thesis, Graduate School, Chulalongkorn University, 2004), p. 80.

57. Adam, R. L. P., Knowler, J. T., and Leader, D. P. The biochemistry of the nucleic acids. 11<sup>th</sup> ed. Chapman & Hall : London, 1992.
58. Cho, E. C., Kim, Y. D., and Cho, K. Thermally responsive poly (N-isopropylacrylamide) monolayer on gold: synthesis, surface characterization, and protein interaction adsorption studies. Polymer. 45 (2004) : 3195-3204.
59. Tomac, S., Sarkar, M., Ratilainen, T., Wittung, P., Nielsen, P. E., Norden, B., and Graslund, A. Ionic effects on the stability and conformation of peptide nucleic acid complexes. J. Am. Chem. Soc. 118 (1996) : 5544-5552.



สถาบันวิทยบริการ  
จุฬาลงกรณ์มหาวิทยาลัย



## **APPENDIX A**

สถาบันวิทยบริการ  
จุฬาลงกรณ์มหาวิทยาลัย

**Example of data from UV analysis in  $T_m$  experiments**

**Table A1** Data from UV analysis of HS(CH<sub>2</sub>)<sub>2</sub>CO-T<sub>9</sub>-LysNH<sub>2</sub> (**33**) & dA<sub>9</sub> at 20.0-90.0 °C

Entry	Temperature (°C)	Absorbance	Correct Temp.* (°C)	Normalized Abs.
1	19.9	0.1373	18.9	1.0000
2	20.9	0.1370	19.9	0.9978
3	21.9	0.1376	20.8	1.0017
4	23.0	0.1376	21.9	1.0017
5	24.0	0.1378	22.8	1.0037
6	25.0	0.1379	23.8	1.0045
7	26.0	0.1381	24.8	1.0055
8	27.0	0.1386	25.8	1.0092
9	27.9	0.1389	26.7	1.0112
10	29.0	0.1392	27.7	1.0136
11	29.9	0.1394	28.6	1.0154
12	30.9	0.1398	29.6	1.0177
13	32.0	0.1403	30.7	1.0216
14	32.9	0.1406	31.6	1.0238
15	34.0	0.1410	32.6	1.0266
16	35.0	0.1414	33.6	1.0296
17	36.0	0.1417	34.6	1.0318
18	36.9	0.1420	35.5	1.0343
19	37.9	0.1423	36.5	1.0364
20	39.0	0.1427	37.5	1.0392
21	40.0	0.1432	38.5	1.0430
22	41.0	0.1435	39.5	1.0448
23	41.9	0.1439	40.4	1.0479
24	43.0	0.1442	41.4	1.0501
25	44.0	0.1446	42.4	1.0532
26	44.9	0.1450	43.3	1.0558
27	46.0	0.1453	44.4	1.0581
28	46.9	0.1458	45.3	1.0615

Entry	Temperature (°C)	Absorbance	Correct Temp.* (°C)	Normalized Abs.
29	48.0	0.1461	46.3	1.0641
30	48.9	0.1465	47.2	1.0666
31	50.0	0.1469	48.3	1.0695
32	51.0	0.1473	49.2	1.0724
33	52.0	0.1477	50.2	1.0756
34	52.9	0.1482	51.1	1.0794
35	54.0	0.1487	52.2	1.0825
36	55.0	0.1493	53.2	1.0869
37	56.0	0.1497	54.1	1.0901
38	56.9	0.1502	55.1	1.0940
39	57.9	0.1509	56.0	1.0986
40	59.0	0.1514	57.1	1.1025
41	60.0	0.1520	58.0	1.1071
42	61.0	0.1527	59.0	1.1122
43	62.0	0.1534	60.0	1.1169
44	63.0	0.1539	61.0	1.1210
45	63.9	0.1546	61.9	1.1257
46	65.0	0.1553	62.9	1.1310
47	66.0	0.1561	63.9	1.1364
48	67.0	0.1567	64.9	1.1409
49	68.0	0.1575	65.9	1.1468
50	69.0	0.1583	66.8	1.1524
51	69.9	0.1590	67.8	1.1576
52	71.0	0.1598	68.8	1.1636
53	71.9	0.1606	69.7	1.1697
54	73.0	0.1614	70.8	1.1754
55	74.0	0.1623	71.7	1.1818
56	75.0	0.1632	72.7	1.1886
57	75.9	0.1641	73.6	1.1948
58	77.0	0.1650	74.7	1.2013
59	78.0	0.1658	75.6	1.2077

Entry	Temperature (°C)	Absorbance	Correct Temp.* (°C)	Normalized Abs.
60	79.0	0.1668	76.6	1.2143
61	79.9	0.1676	77.6	1.2207
62	81.0	0.1686	78.6	1.2276
63	82.0	0.1694	79.6	1.2335
64	83.0	0.1702	80.5	1.2397
65	83.9	0.1710	81.5	1.2452
66	85.0	0.1718	82.5	1.2507
67	86.0	0.1725	83.5	1.2559
68	87.0	0.1730	84.4	1.2601
69	88.0	0.1736	85.4	1.2645
70	89.0	0.1742	86.4	1.2687
71	89.9	0.1746	87.3	1.2713

\* The equation for determining the corrected temp was obtained by measuring the actual temp in the cuvette using a temperature probe and plotting against the set temperature ( $T_{\text{block}}$ ) from 20-90 °C. A linear relationship was obtained with  $T_{\text{actual}} = 0.978T_{\text{block}} - 0.6068$  and  $r^2 > 0.99$ . ( $T_{\text{actual}}$  = Actual temperature as measured by the built-in temperature probe,  $T_{\text{block}}$  = Temperature of the heating block)

Correct temperature and normalized absorbance are defined as follows.

$$\text{Correct Temp.} = (0.978 \times T_{\text{block}}) - 0.6068$$

$$\text{Normalized Abs.} = \text{Abs}_{\text{obs}} / \text{Abs}_{\text{init}}$$

In entry 1;  $T_{\text{obs}} = 19.9$  °C,  $\text{Abs}_{\text{init}} = 0.1373$ ,  $\text{Abs}_{\text{obs}} = 0.1373$ ;

$$\text{Correct Temp.} = (0.978 \times T_{\text{obs}}) - 0.6068$$

$$\text{Correct Temp.} = (0.978 \times 19.9) - 0.6068$$

$$= 18.9 \text{ °C}$$

$$\text{Normalized Abs.} = \text{Abs}_{\text{obs}} / \text{Abs}_{\text{init}}$$

$$= 0.1373 / 0.1373$$

$$= 1.0000$$

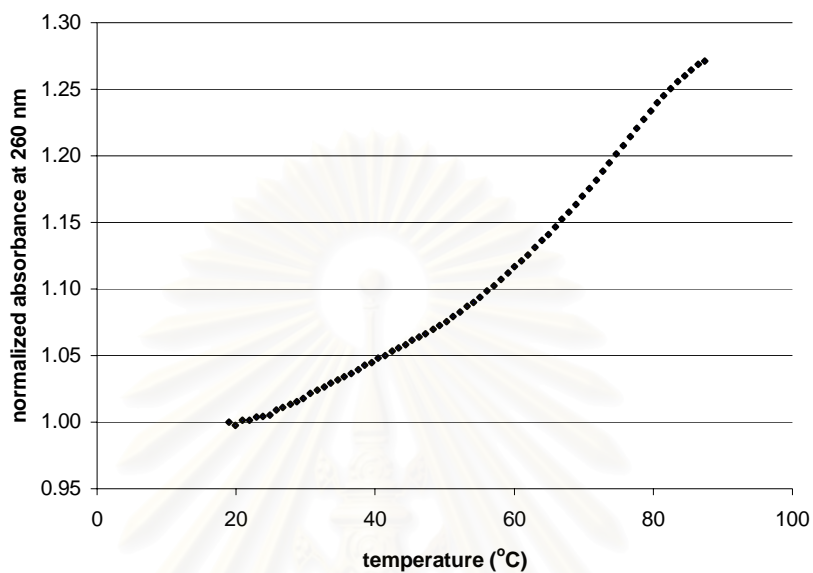
In entry 25;  $T_{\text{obs}} = 44.0$  °C,  $\text{Abs}_{\text{init}} = 0.1373$ ,  $\text{Abs}_{\text{obs}} = 0.1446$ ;

$$\text{Correct Temp.} = (0.978 \times T_{\text{obs}}) - 0.6068$$

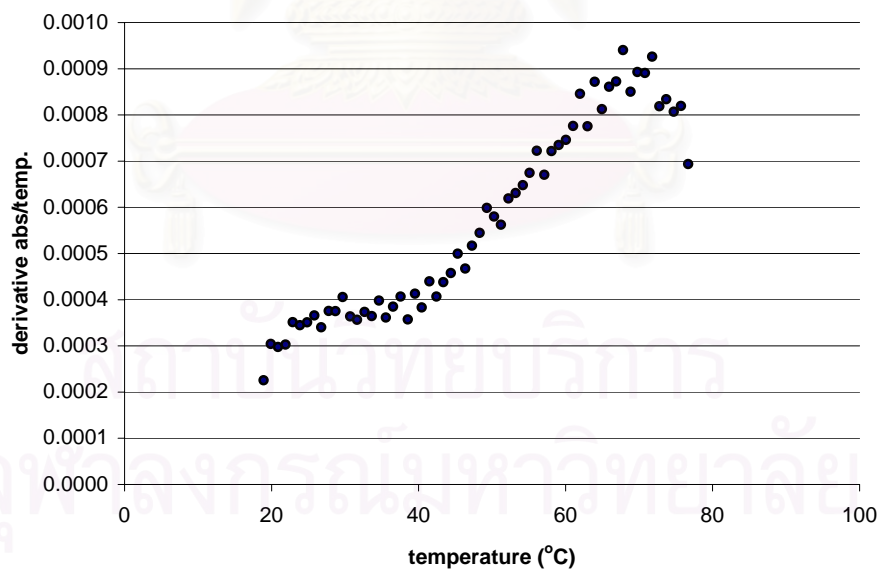
$$\text{Correct Temp.} = (0.978 \times 44.0) - 0.6068$$

$$= 42.4 \text{ °C}$$

$$\begin{aligned} \text{Normalized Abs.} &= \text{Abs}_{\text{obs}}/\text{Abs}_{\text{Sinit}} \\ &= 0.1446/0.1373 \\ &= 1.0532 \end{aligned}$$



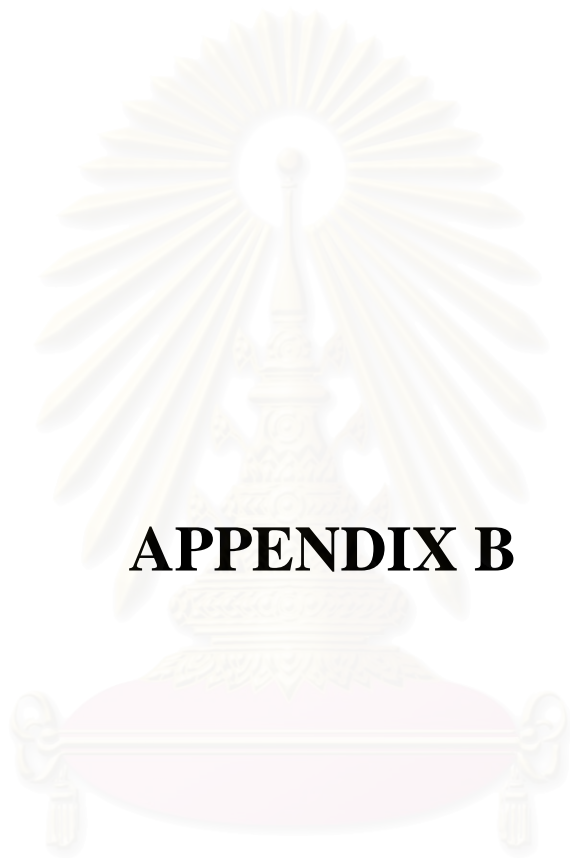
(a)



(b)

**Figure A1** (a) Melting curve and (b) UV- $T_m$  first derivative curve of HS(CH<sub>2</sub>)<sub>2</sub>CO-T<sub>9</sub>-LysNH<sub>2</sub> (**33**) with dA<sub>9</sub>. Condition: 0.5 mM sodium phosphate buffer pH 7.0 and molar ratio of PNA : DNA = 1:1





## **APPENDIX B**

สถาบันวิทยบริการ  
จุฬาลงกรณ์มหาวิทยาลัย

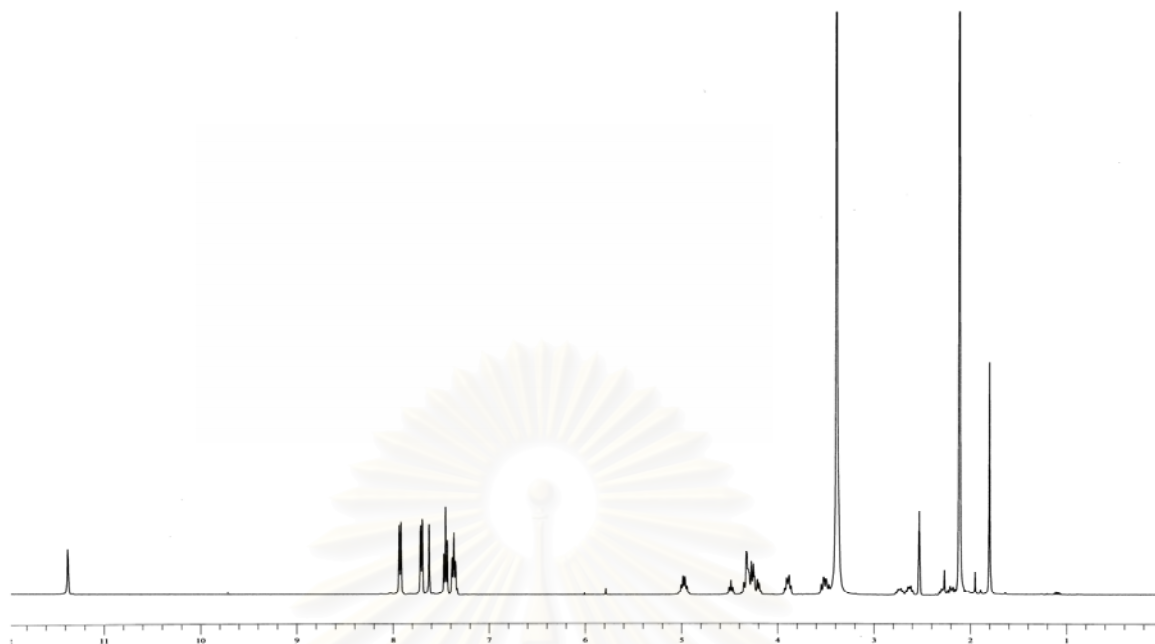


**Figure B1** <sup>1</sup>H NMR spectrum (400 MHz, DMSO-*d*<sub>6</sub>) of *N*-fluorenylmethoxy-carbonylamino-*cis*-4-(thymine-1-yl)-D-proline (**11**)

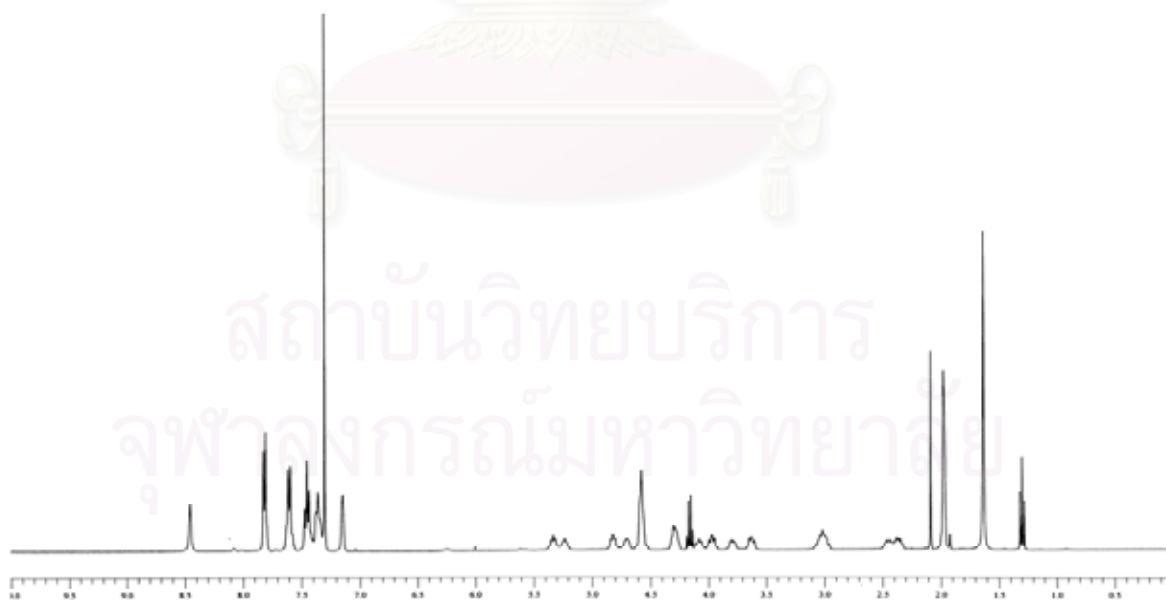


**Figure B2** <sup>1</sup>H NMR spectrum (400 MHz, DMSO-*d*<sub>6</sub>) of *N*-fluorenylmethoxy-carbonylamino-*cis*-4-(thymine-1-yl)-D-proline pentafluorophenyl ester (**12**)

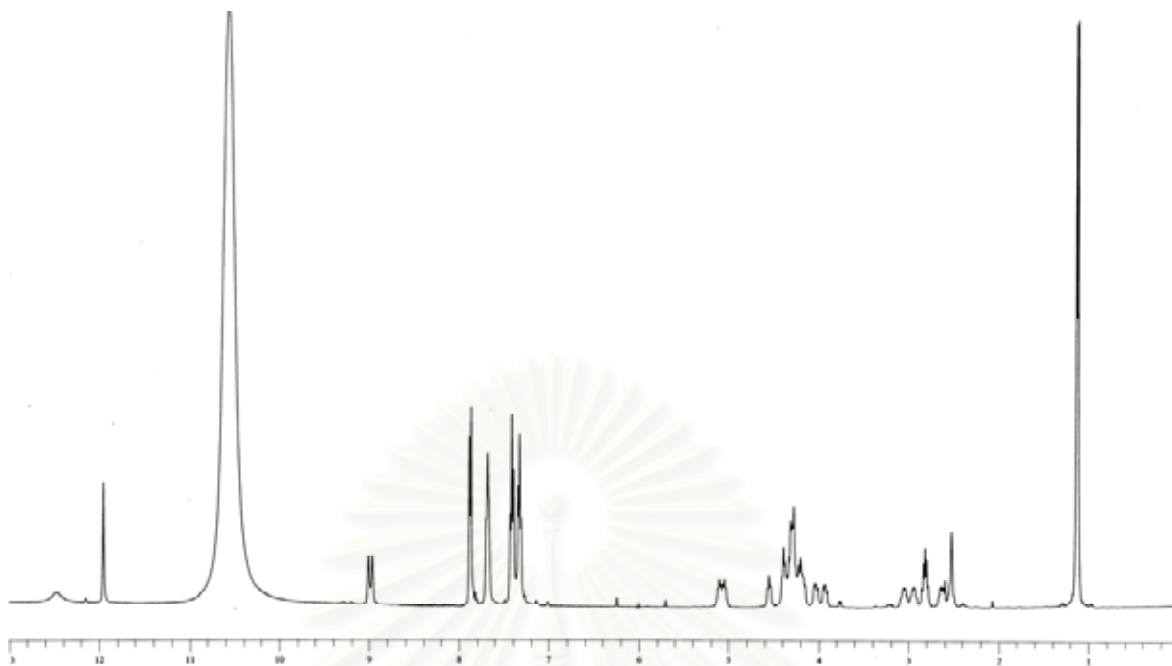


**Figure B3**  $^1\text{H}$  NMR spectrum (400 MHz,  $\text{DMSO-}d_6$  + 1 drop TFA) of *N*-fluoren-9-ylmethoxycarbonylamino-*cis*-4-( $N^2$ -isobutyrylguanin-9-yl)-D-proline (**14**)

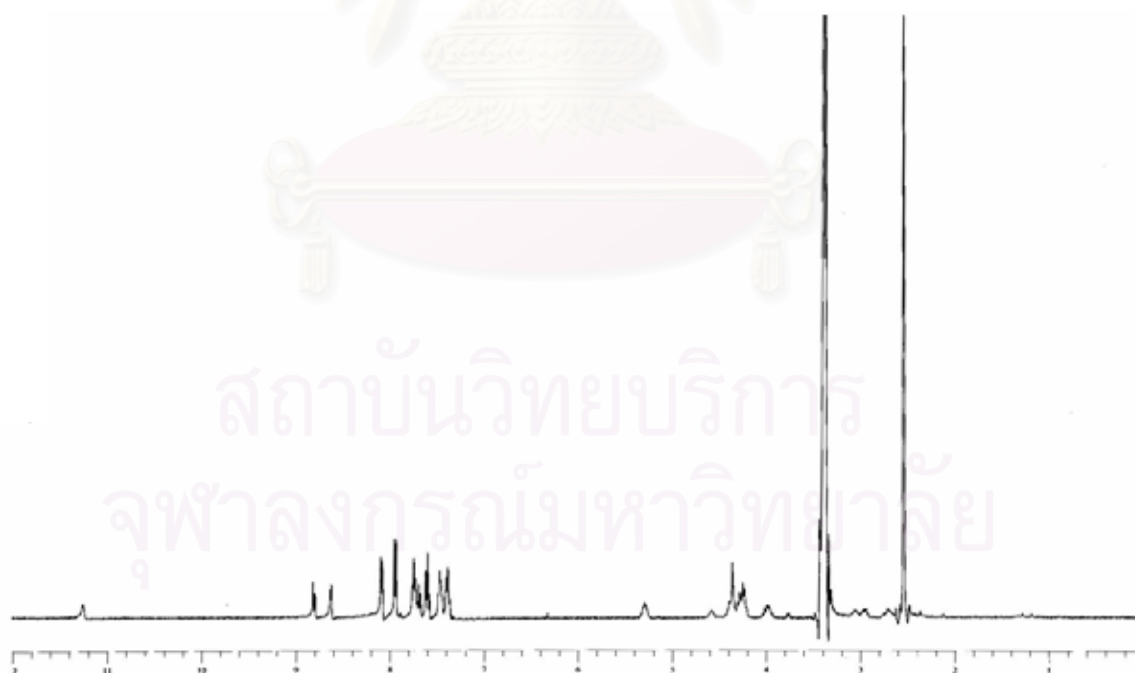


**Figure B4**  $^1\text{H}$  NMR spectrum (400 MHz,  $\text{DMSO-}d_6$ ) of *N*-fluoren-9-ylmethoxycarbonylamino-*cis*-4-( $N^4$ -benzoyladenin-9-yl)-D-proline (**17**)

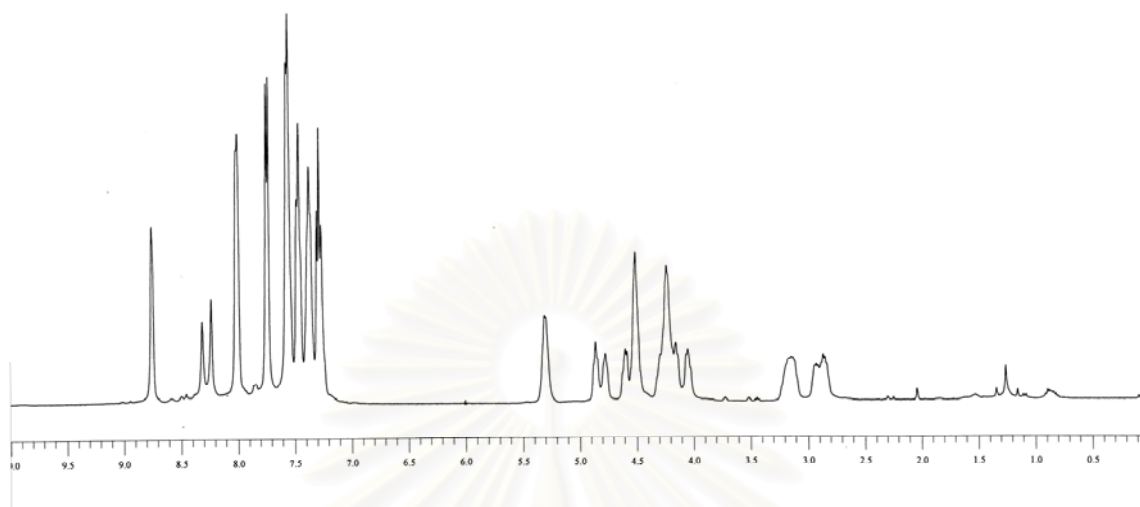


**Figure B5** <sup>1</sup>H NMR spectrum (400 MHz, CDCl<sub>3</sub>) of *N*-fluoren-9-*cis*-4-(*N*<sup>4</sup>-benzoyl-adenin-9-yl)-D-proline pentafluorophenyl ester (**18**)

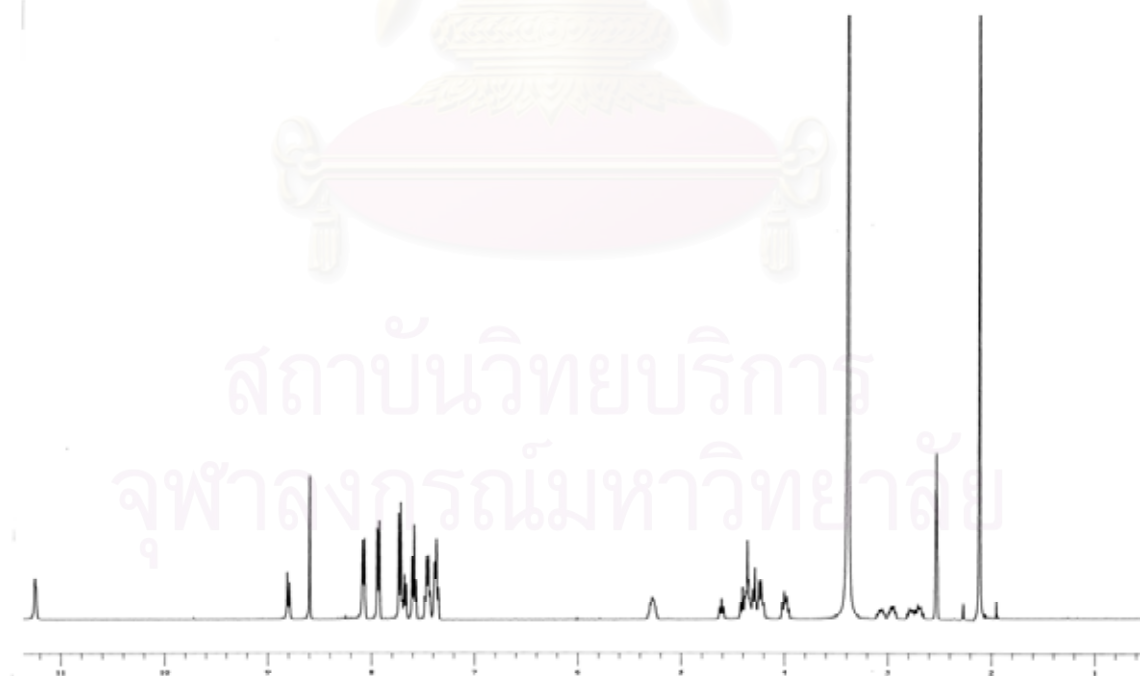


**Figure B6** <sup>1</sup>H NMR spectrum (400 MHz, DMSO-*d*<sub>6</sub>) of *N*-fluoren-9-ylmethoxy-carbonylamino-*cis*-4-(*N*<sup>4</sup>-benzocyctosin-1-yl)-D-proline (**20**)

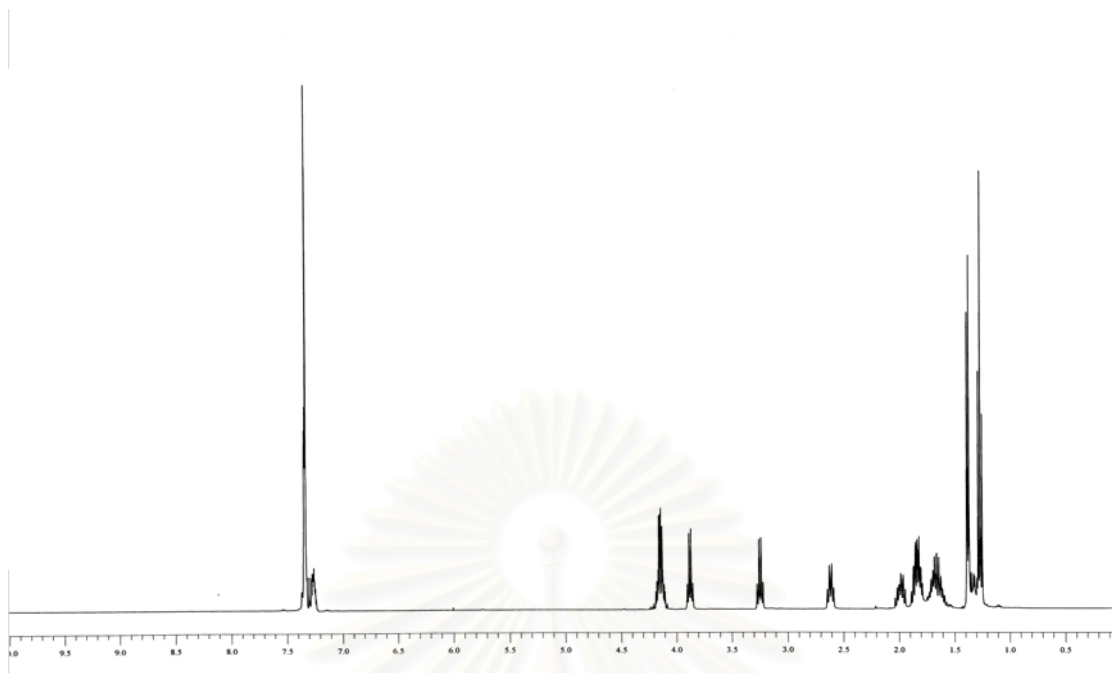


**Figure B7** <sup>1</sup>H NMR spectrum (400 MHz, CDCl<sub>3</sub>) of ethyl (1*S*, 2*S*)-2-[(1'*S*)-phenylethyl]-aminocyclopentanecarboxylate (**24**)

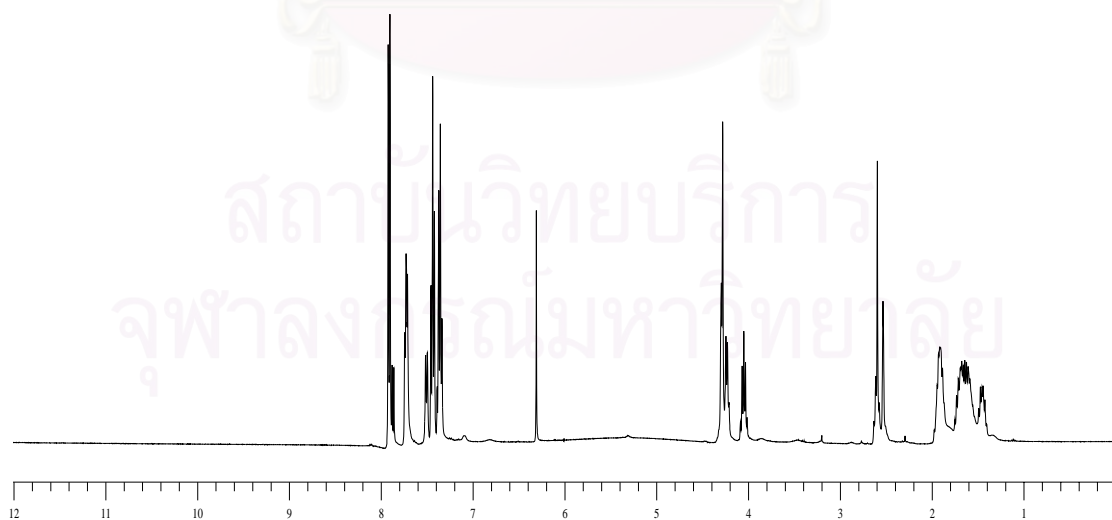


**Figure B8** <sup>1</sup>H NMR spectrum (400 MHz, DMSO-*d*<sub>6</sub>) of *N*-fluoren-9-ylmethoxy-carbonyl-2-amino-cyclopentanecarboxylic acid (**27**)

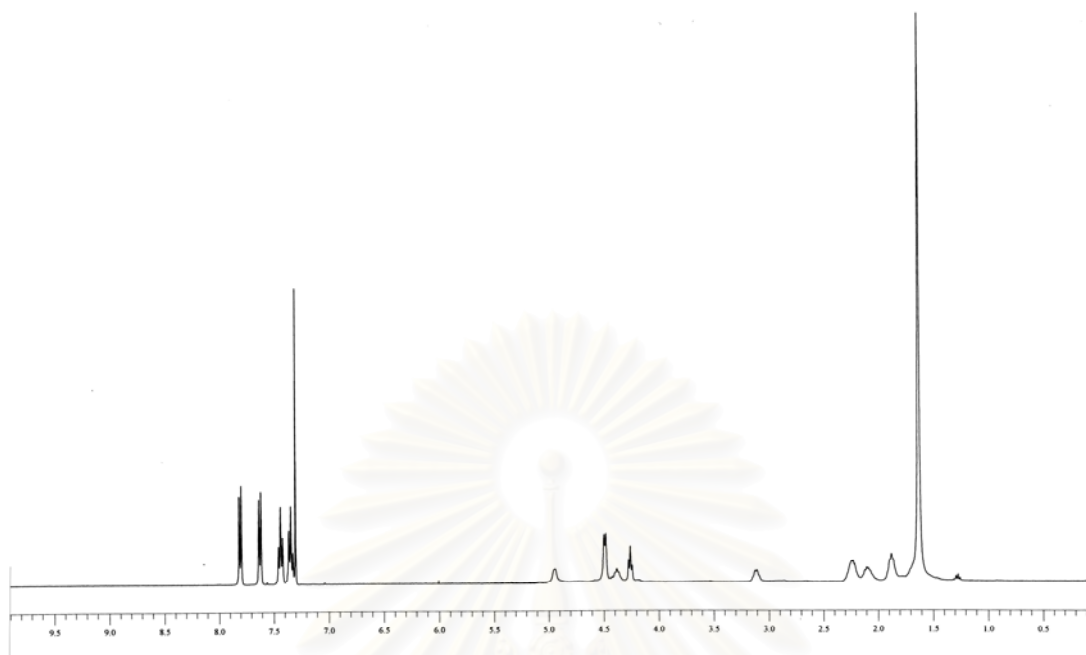


**Figure B9** <sup>1</sup>H NMR spectrum (400 MHz, CDCl<sub>3</sub>) of *N*-fluoren-9-ylmethoxycarbonyl-2-aminocyclopentane carboxylic acid pentafluorophenyl ester (**28**)

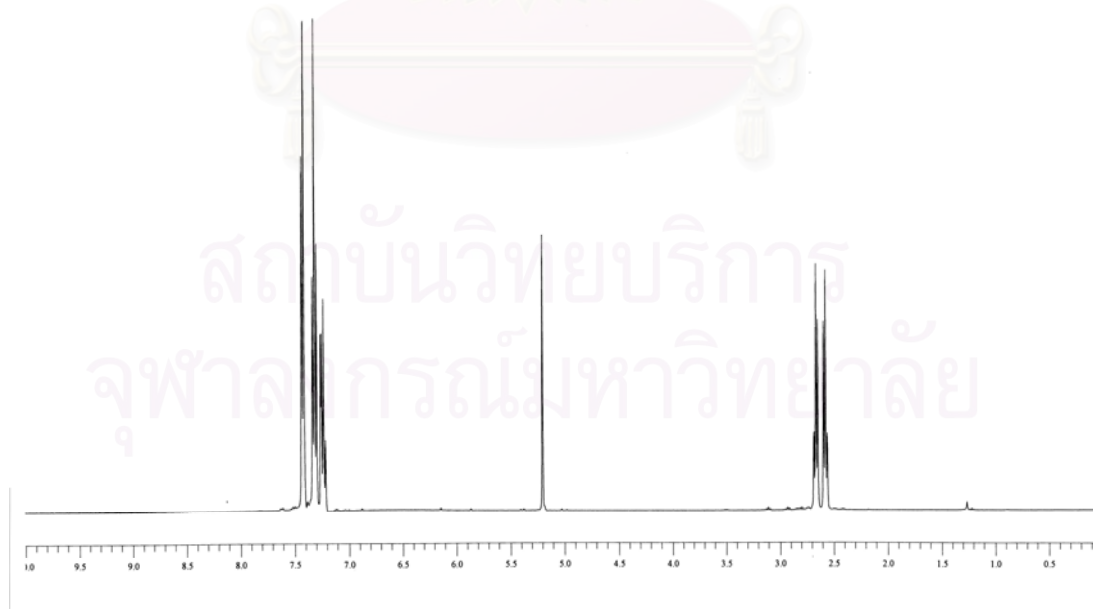


**Figure B10** <sup>1</sup>H NMR spectrum (400 MHz, CDCl<sub>3</sub>) of 3-benzhydrylthio-propionic acid (**30**)

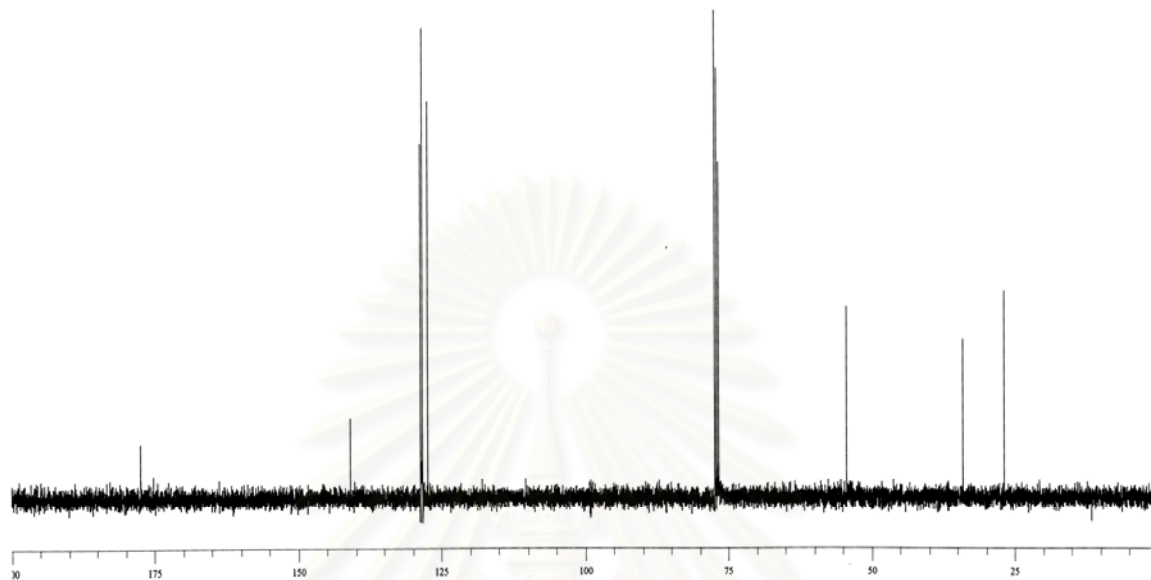


**Figure B11**  $^{13}\text{C}$  NMR spectrum (100 MHz,  $\text{CDCl}_3$ ) of 3-benzhydrylthio-propionic acid (**30**)

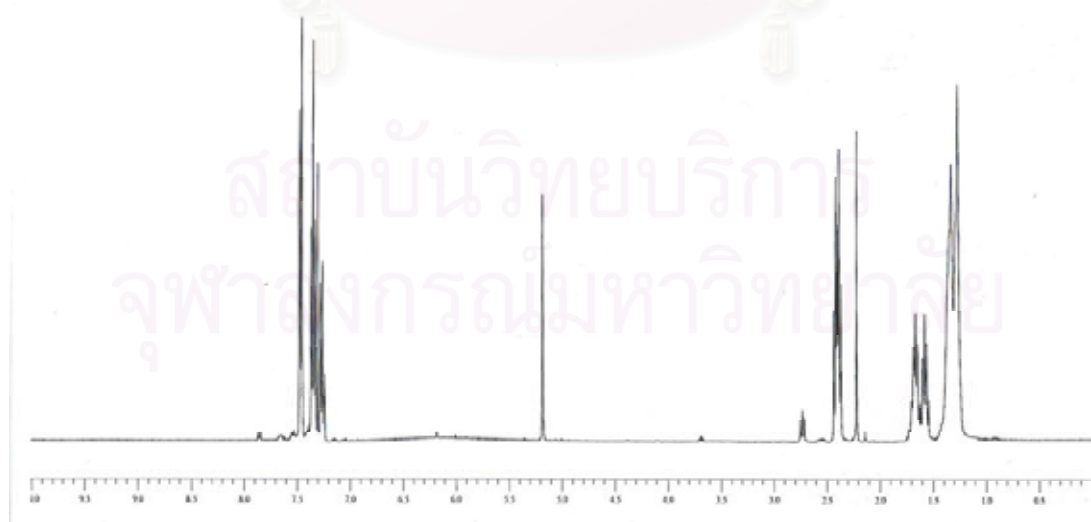


**Figure B12**  $^1\text{H}$  NMR spectrum (400 MHz,  $\text{CDCl}_3$ ) of 11-benzhydrylthio-undecanoic acid (**32**)

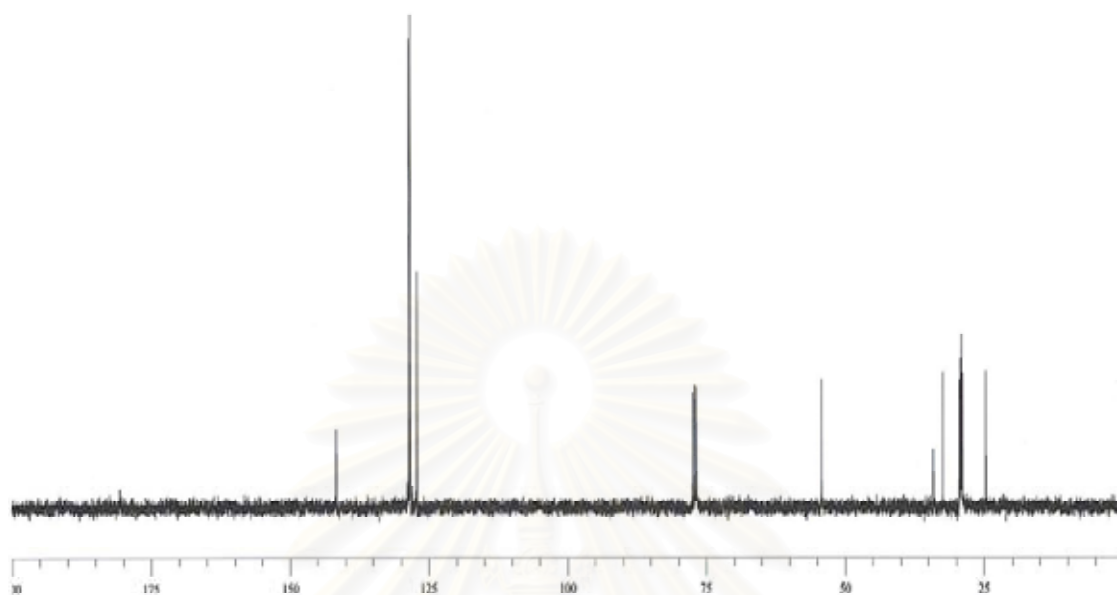


**Figure B13**  $^{13}\text{C}$  NMR spectrum (100 MHz,  $\text{CDCl}_3$ ) of 11-benzhydrylthio-undecanoic acid (**32**)

สถาบันวิทยบริการ  
จุฬาลงกรณ์มหาวิทยาลัย



**VITAE**

Miss Cheeraporn Ananthanawat was born on May 11<sup>th</sup>, 1982 in Chonburi, Thailand. She received a Bachelor Degree of Science (2<sup>nd</sup> class honor), majoring in Chemistry from Chulalongkorn University in 2004. In the same year, she was admitted to the Master's degree of Science, program in Petrochemistry and Polymer Science, at Chulalongkorn University.



สถาบันวิทยบริการ  
จุฬาลงกรณ์มหาวิทยาลัย